DEL-SG-09-17

EXPERIMENTAL AND NUMERICAL STUDY ON ROCK SEAWALL IN SWASH ZONE TO REDUCE WAVE OVERTOPPING AND OVERWASH OF SAND BEACH

Hyun Dong Kim, Nobuhisa Kobayashi and Xavier Chávez Cárdenas

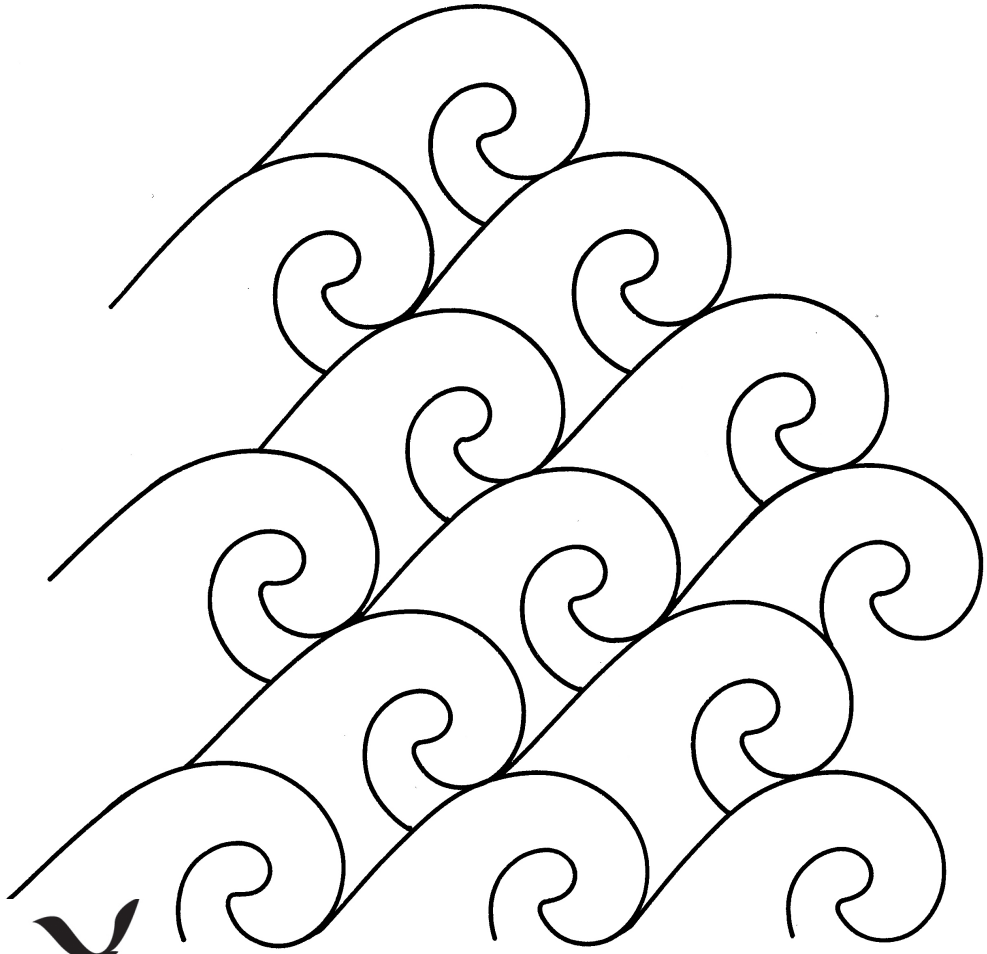

Sea Grant Delaware

Delaware Sea Grant College Program
Newark, Delaware 19716

EXPERIMENTAL AND NUMERICAL STUDY ON ROCK SEAWALL IN SWASH ZONE TO REDUCE WAVE OVERTOPPING AND OVERWASH OF SAND BEACH

by

HYUN DONG KIM, NOBUHISA KOBAYASHI,
and XAVIER CHÁVEZ CÁRDENAS

RESEARCH REPORT NO. CACR-17-02
FEBRUARY, 2017

CENTER FOR APPLIED COASTAL RESEARCH

Ocean Engineering Laboratory
University of Delaware
Newark, Delaware 19716

ACKNOWLEDGMENTS

This study was partially supported by the U.S Army Corps of Engineers under Cooperative Agreement No. W912HZ-15-2-0028 and by the Delaware Sea Grant under Grant No. NOAA SG2016-18 R/RCE-9.

TABLE OF CONTENTS

LIST OF TABLES

LIST OF FIGURES

ABSTRACT

Hydraulic model tests were conducted in a wave flume to reduce storm induced damage to backshore areas. Because no such methods were available to design structures to reduce the storm damage, four test series: sand beach with a berm, sand beach with a dune, a rock seawall and a sand-covered rock seawall with 14 tests and 140 runs were conducted in the small-scale experiment to compare the effectiveness in reducing storm wave overtopping and sand overwash. Using almost same incident irregular waves, water level was raised to increase the wave overtopping and sand overwash. It was found that the dune was effective to reduce wave overtopping compared to the berm without the dune. However, when the still water level (SWL) was increased, the narrow dune was easily eroded. The stone seawall eliminated the erosion problem of the dune; however, the buried seawall combined the aesthetics of the dune and the robustness of the stone seawall. The stone seawall buried inside the dune functioned like the dune initially and like the seawall after the sand on and inside the porous seawall was eroded by overtopping waves. Both stone seawall and buried stone seawall were deformed but reduced wave overtopping. The existing numerical model, CSHORE is extended to predict sand transport on and inside the porous structure in the swash zone. The hydraulic model tests and the numerical model are compared to evaluate the effectiveness of coastal storm protection techniques.

Chapter 1

INTRODUCTION

Among many natural hazards, hurricanes are considered as one of the most powerful and dangerous natural phenomena that can cause coastal damage including property damages. In 2012, Hurricane Sandy caused extensive damage in New York and New Jersey. Irish et al. (2013) and Walling et al. (2014) compared the impacts of Hurricane Sandy on New Jersey Coast. They compared the three communities: Sea Girt, Bay Head, and Mantoloking north of Atlantic City due to the vast difference in damage within an alongshore distance of 12 km. A wide beach and a large dune protected Sea Girt which suffered the least damage of the three towns. The beach of Bay Head was narrow but a relic rock seawall was buried underneath its dune and the seaward side of the dune was eroded as shown in Figure 1.1. The 1,260 m long seawall reduced damage to the area landward of the seawall but increased erosion seaward of it (Walling et al. 2016). Mantoloking is located on a barrier spit and its narrow dune almost vanished. Three major breaches were formed across the barrier spit. The post-storm surveys show the consequences of the specific storm, but do not reveal the actual processes of beach and dune erosion with and without a rock seawall. Wave absorbing breakwaters have been constructed on eroding beaches to reduce wave overtopping and beach erosion. An example of such breakwaters is shown in Figure 1.2. The quantitative understanding of the interaction processes between the rock structure and sand beach is essential for the prediction of the consequences of various storms.

To elucidate the interaction processes, an experiment was conducted as explained in detail in Chapter 2. Chapter 3 describes the experimental results of four test series: no protection, dune only, rock seawall and buried rock seawall. The experiment consisted of 14 tests with 140 runs in a wave flume to examine stone damage and compare the effectiveness of each test series by increasing the water level in each test series (Kim et al. (2016)). This small-scale experiment was conducted to measure wave overtopping and overwash, and sand mobility inside the stone seawall. Wolters and van Gent (2012) investigated sand transport inside granular (stone) open filters on a horizontal sand bed under wave and current loading. Wolters et al. (2014) extended their experiment to sloped granular open filters under wave loading. Their experimental results may not be applicable to stone seawalls in the swash zone.

Chapter 4 introduces cross-shore numerical model, CSHORE (Kobayashi 2016) and extends to predict sand transport on and inside the porous structures in the swash zone and simulate sand and stone interactions in the swash zone on a sand beach. In Chapter 5, comparison between the extended numerical model results and the experimental results in Chapter 2 is presented for wave hydrodynamics, wave overtopping and overwash, beach profile changes and stone damage.

Figure 1.1: Partially exposed relic rock seawall after Hurricane Sandy (Irish et al. 2013)

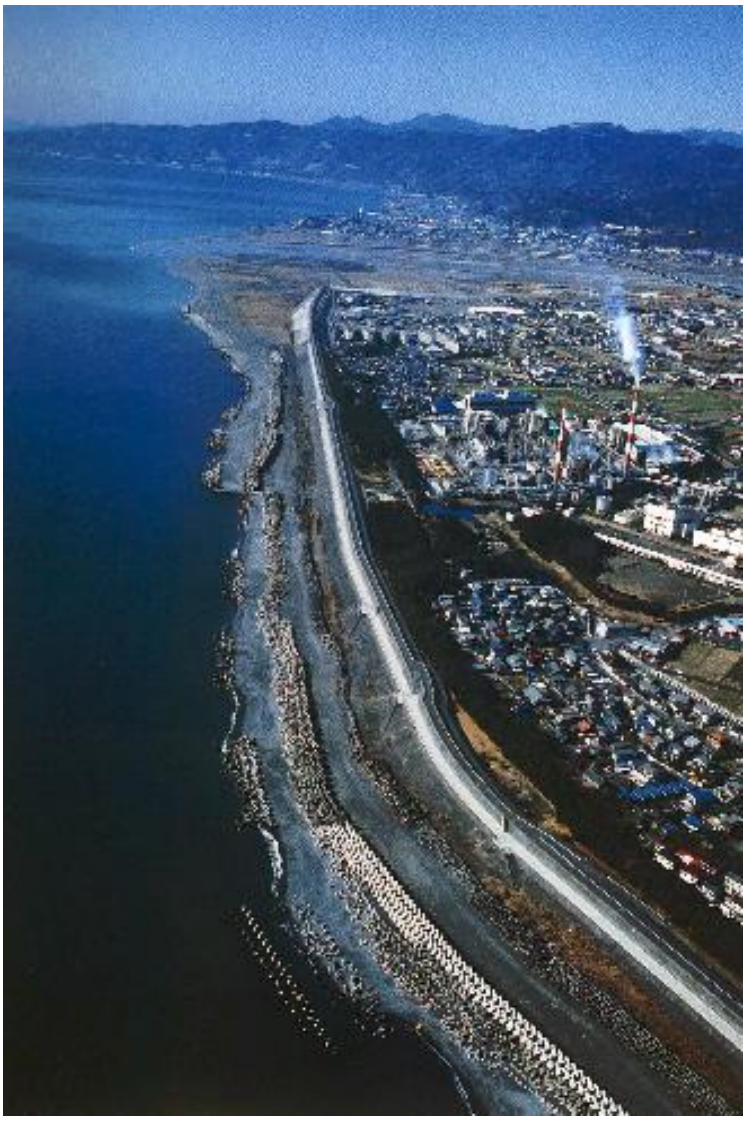

Figure 1.2: Several rows of wave absorbing breakwaters in front of seawall (17 m above sea level) constructed on Fuji Coast in Japan to reduce wave overtopping and beach erosion (Japan Society of Civil Engineers, Committee on Coastal Engineering 1994)

Chapter 2

EXPERIMENT

This Chapter provides an overview of the hydraulic model experiment (Kim et al. 2016) which was conducted in University of Delaware wave flume located in basement of the Dupont Hall. Overview of experiment setup, sand profiles and characteristics of stones used are explained in the following where the details of this experimental setup were given by Figlus et al. (2011).

2.1 Experimental Setup

Wave flume used in this experiment is 30 m long, 1.15m wide and 1.5m high as shown in Figure 2.1. Wooden boards were placed along the center of the wave flume to divide it into two sections in longshore direction to reduce amount of fine sand and water level change due to wave overtopping, and to minimize seiching in the flume. A 400 s irregular wave train with a Texel, Marsen and Arsloe (TMA) spectral shape was generated by the paddle of the piston-type wave maker in a water depth of 92, 94, 96 or 98 cm. The spectral significant wave height and peak period were approximately 17 cm and 2.6 s. Nine wave gauges were placed in the flume. Wave gauges 1 to 8 (WG1-WG8) were used to measure the free surface elevation outside and inside the surf zone and in the swash zone and WG9 was used to measure the wave level in the basin after each run to collect the volume of overtopped water. The wave overtopping rate q_o and sand overwash rate q_{bs} were measured by collecting overtopped water and sand in water collection basin and sand trap during each 400 s

run. To measure fluid velocities in the surf zone, three velocimeters: Acoustic Doppler Velocimeter (ADV) sensors were co-located at WG4, WG5, and WG6 (WG4 with 2D ADV and WG5-WG6 with Red and Blue Vectrinos). Sand used in the experiment consisted of well-sorted fine sand with a median diameter of 0.18 mm, a fall velocity of 2.0 cm/s, density of 2.6 g/cm^3, and porosity of 0.4, respectively. For this experiment, measurements of beach profile changes were necessary to compare the difference of each test series. Acuity AR4000- LIR laser line scanner system was used to obtain accurate three dimensional profile data after each 10 runs (4,000 s) with constant SWL. For two tests series with no rock seawall, the beach profile was also measured after 5 runs because of relatively rapid profile changes (Kim et al. 2016). The three dimensional bathymetry data were averaged alongshore after confirmation of alongshore uniformity.

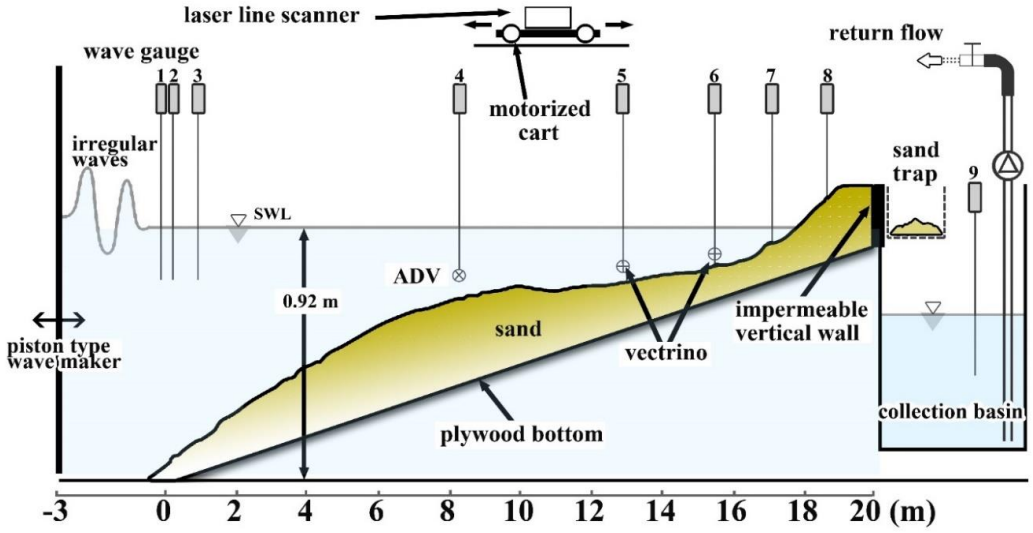

Figure 2.1: Schematic view of experimental setup for no dune (N) series with no rock seawall and no dune: wave paddle, beach profile on top of plywood bottom; collection basin including sand trap; water recirculation system; laser line scanner mounted to a motorized cart; and locations of the instruments measuring hydrodynamics

2.2 Four Test Series

Total four test series with increasing still water level (SWL) by 2 cm increment in each series in the wave flume were conducted to examine the damage of each test (Table 2.1). The initial profiles for each of four test series are depicted in Figure 2.2.

Table 2.1: Sequence of 4 test series with Still Water Level (SWL) = 0, 2, 4 or 6 cm consisting of 140 runs (400 s duration for each run)

Series	Description	SWL (cm)	No. of runs (s)
N	No protection	0, 2, and 4	30
D	Dune only	0, 2, and 4	30
R	Rock seawall	0, 2, 4 and 6	40
B	Buried rock seawall	0, 2, 4 and 6	40

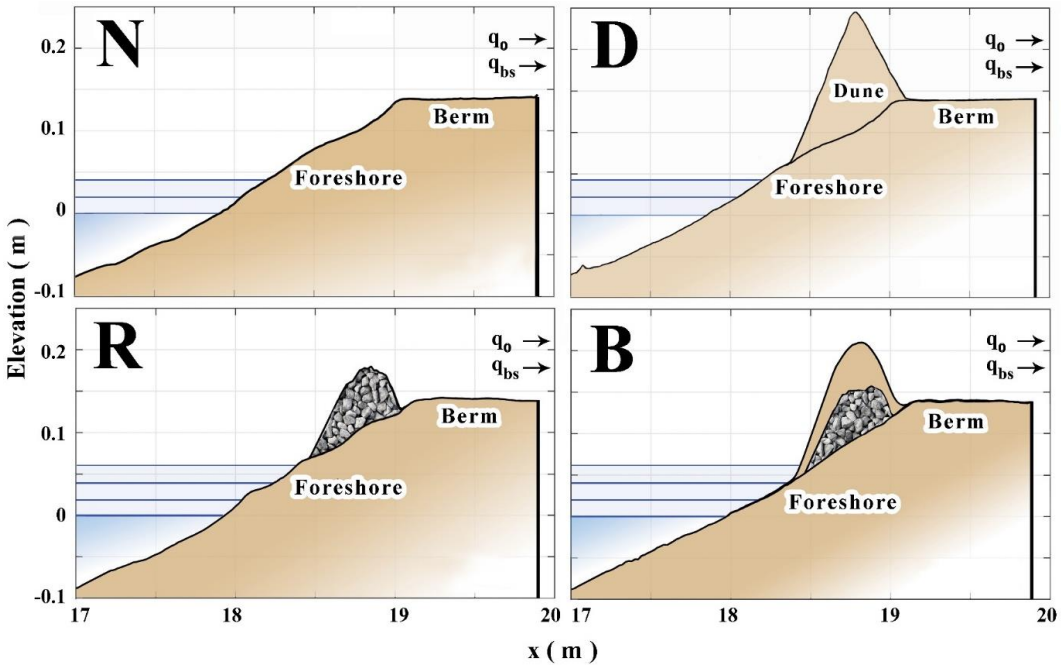

Figure 2.2: Four test series initial profiles (N, D, R, and B) where SWL increased by 2 cm after 10 runs

The first test series with a berm and a foreshore slope of approximately 0.1 correspond to no protection, N test series, without dune or rock seawall as shown in Figure 2.3. The berm was exposed to ten 400 s runs, SWL was increased by 2 cm and the eroded foreshore was exposed to 10 runs. When SWL was increased to 4 cm, accreted berm was exposed to 10 runs and caused rapid berm erosion. The vertical wall was not exposed to direct wave action at the end of the N test series with 12,000 s (30 runs total) wave action.

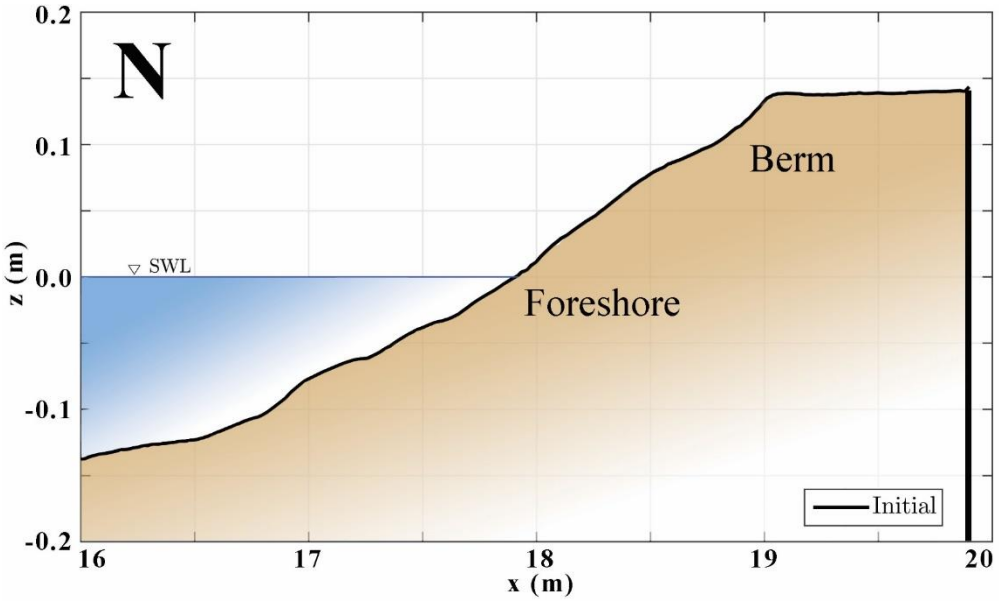

Figure 2.3: Test series no protection (N) initial profile

For the test series D, dune only test series, shown in Figure 2.4, the initial berm profile was rebuilt on the initial profile for series N and a sand dune with a crest elevation of 10 cm above the berm crest was built on the foreshore. The cross sectional area of the dune above the foreshore was 526 cm^2, and seaward dune slope

started to erode during 10 runs with SWL at z = 0. Decrease of the dune crest occurred during 10 runs with 2 cm SWL increase. By increasing to 4 cm SWL, Destruction of the dune was occurred after 10 runs at the end of series D (t = 12,000 s).

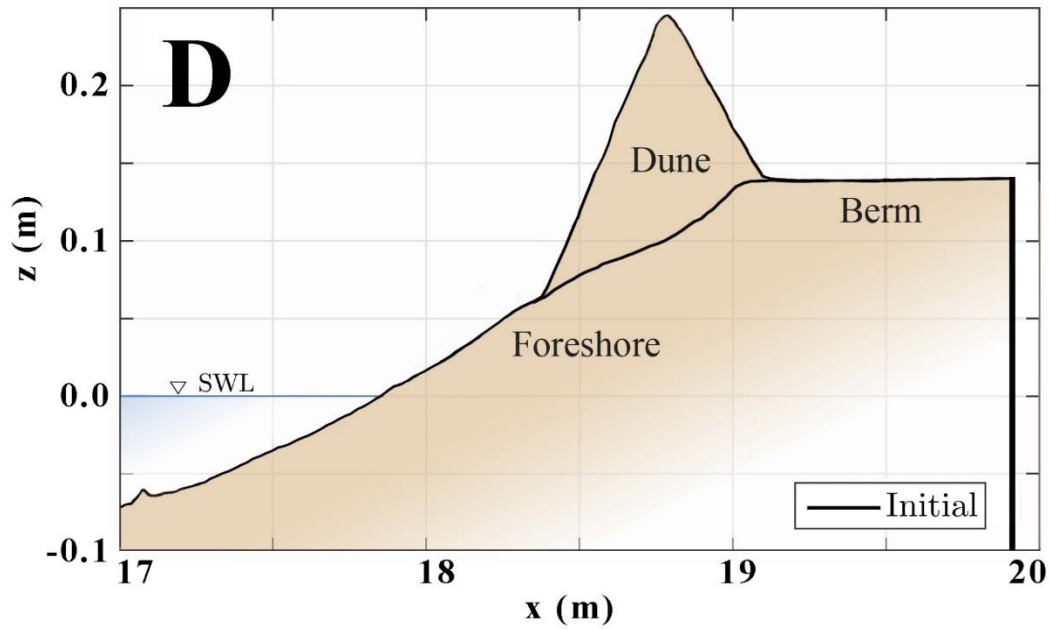

Figure 2.4: Test series dune only (D) initial profile

Series R, rock seawall test series, was rebuilt after D test series with replacing the dune of D test series with the stone seawall with a crest height of 8 cm and horizontal width of 56 cm as shown in Figure 2.5. Polyester fabric mesh shown in Figure 2.6 with 0.074 mm opening was placed under the stone seawall with rebuilt foreshore. The cross-sectional area of the structure was 253 cm^2 and the side slopes were about 1/2. During first two 10 runs with SWL at z= 0 and 2 cm, no wave overtopping occurred and profile change was relatively small; however minor

overtopping and slight sand beach erosion occurred during 10 runs with SWL at z = 4 cm. When SWL was increased (z = 6 cm), both wave overtopping and overwash significantly increased during the last 10 runs.

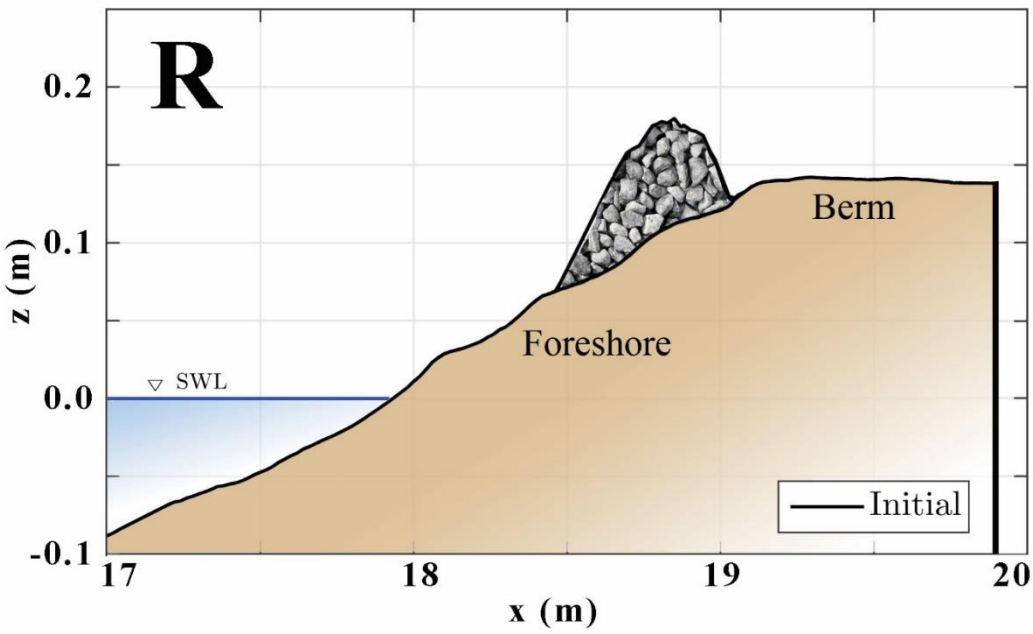

Figure 2.5: Test series rock seawall (R) initial profile

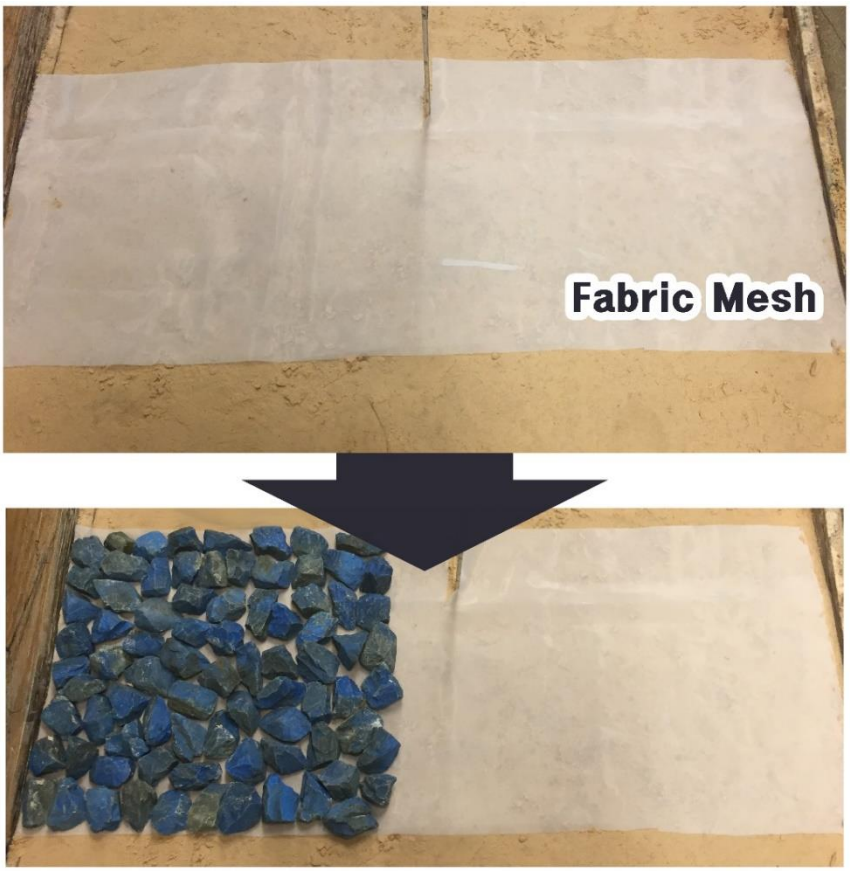

Figure 2.6: Polyester fabric mesh used in both R and D test series on the berm, under the stone structures

The buried seawall test series (B) has a concept of combining both test series D and R where the seawall in R test series is covered with sand to look like dune but rock seawall buried inside as shown in Figure 2.7. After rebuilding the berm profile, seawall was built on the rebuilt profile on top of the fabric mesh. Cross-sectional area of the seawall is 224 cm^2 which is similar to that of R test series. Mixture of sand and water was poured into the seawall to cover the structure and fill its voids. Sand dune was built to cover the entire seawall. Dune profile was measured afterwards, and the cross-sectional area of the initial profile of series B shown in Figure 2.8 including the

seawall was 469 cm^2. This buried seawall was exposed to wave action of 10 runs for each of the SWL at z = 0, 2, 4 and 6 cm to compare the R and B test series.

Figure 2.7: Process of building buried seawall (B) initial profile

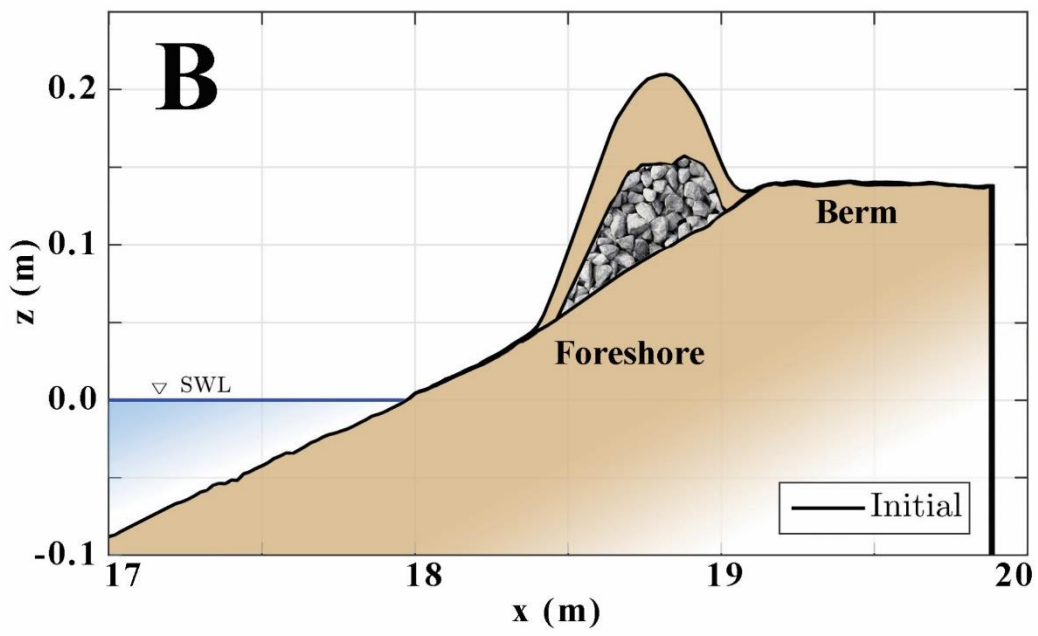

Figure 2.8: Test series buried seawall (B) initial profile

2.3 Sand and Stone Characteristics

Fine sand in Table 2.1 was placed across the 115 cm wide flume in this experiment. For R and B test series, two different characteristics of stones (green and blue colored) as listed in Table 2.1 were used for the seawall. Across the 115 cm wide flume, green stones were placed 62 cm wide, and blue stones were placed 53 cm wide as shown in Figure 2.9. The nominal stone diameters, $D_{n50} = (M_{50} / \rho_s)^{1/3}$ of the green and blue stones were 3.52 and 3.81 cm, respectively, where M_{50} = median stone mass and ρ_s = stone density. Empirical formulas are available to predict stone damage inside the surf zone (Melby and Kobayashi 2011) but no formula exists to estimate stone damage on seawalls located on the foreshore in the swash zone. A previous experiment conducted in same wave flume used the same stones to measure damage initiation on a submerged breakwater located in 12 cm water depth inside the surf zone

on a sand beach with similar wave conditions. These stones on the submerged breakwater in the surf zone were found to be stable (Garcia and Kobayashi 2015)

Table 2.2: Characteristics of sand and two stones

Parameter	Sand	Blue Stone	Green Stone
Diameter (cm)	0.018	3.81	3.52
Density (g/cm^3)	2.60	3.06	2.94
Porosity	0.40	0.44	0.44
Width (cm)	115	53	62

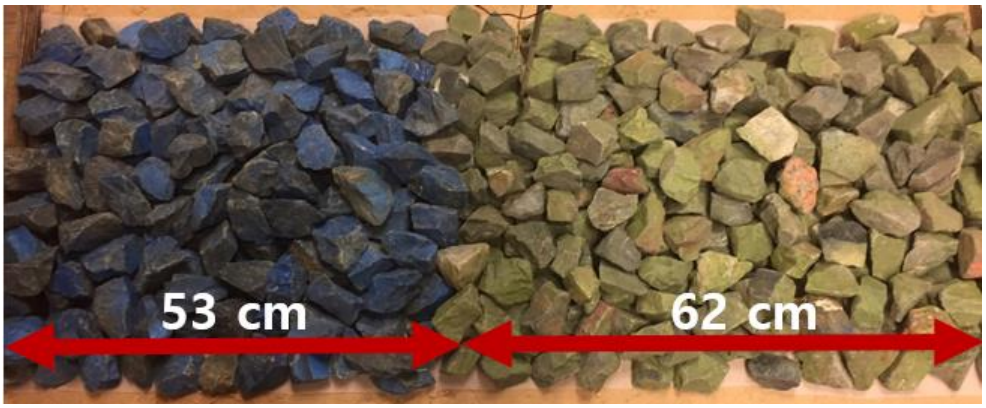

Figure 2.9: Green and blue stones used in R and B test series

2.4 Block Locations

Wooden blocks were used in the previous experiment conducted by Xavier and Kobayashi (2015). In both series N and D, the wooden blocks slid due to major wave overtopping. For series R and B, blocks were placed landward of the seawall. The blocks became wet but did not slid much because the seawall reduced wave overtopping and wave action on the berm. These blocks were also placed on the berm as shown in Figure 2.10 where four wooden blocks were used as model houses (idealized wooden houses). Each block was 8.3 cm long, 3.8 cm high and 118 g in weight.

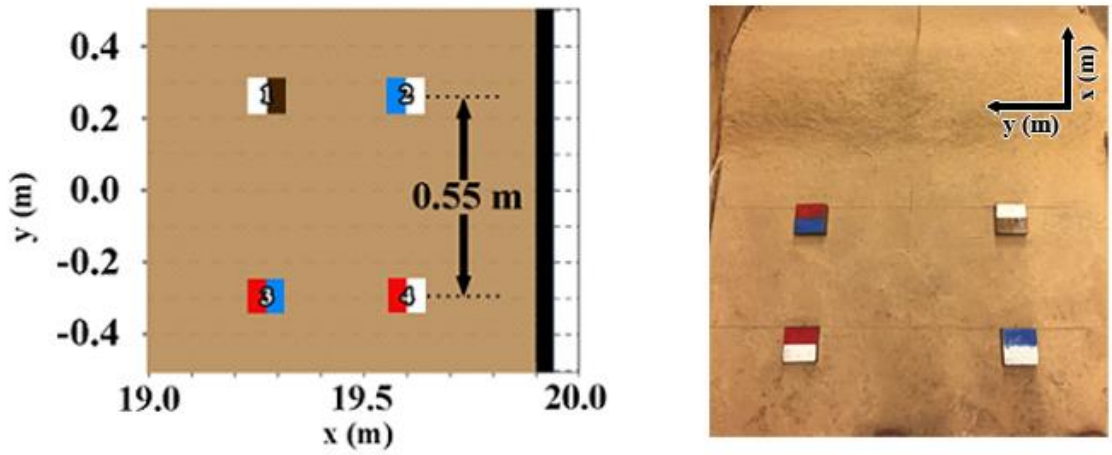

Figure 2.10: Top view of initial block locations

Chapter 3

DATA ANALYSIS

In this chapter, analyzed data are presented in order of hydrodynamics, overtopping and overwash rates, and morphological evolutions.

3.1 Free Surface and Velocity Statistics

Tables 3.1 – 3.14 list the incident wave characteristics at the location x = 0 of WG1 for 14 tests in series N, D, R and B. Incident wave characteristics of N test series at the location x = 0 of WG1 are listed in Tables 3.1- 3.3 and those of D test series are listed in Tables 3.4 – 3.6. R test series are listed in Tables 3.7 – 3.10 and B test series are listed in Tables 3.11- 3.14. The time series from wave gauges (WG1: x = 0.0, WG2: x= 0.25, and WG3: x = 0.95 m) for each run were used to separate incident and reflected waves at the location x = 0 of WG1. The spectral significant wave height H_{mo} was approximately 17 cm and the peak period T_p of incident waves was about 2.6 s. In these tables, H_{rms} = root-mean-square wave height, H_s = significant wave height, T_s = significant wave period, and R = wave reflection coefficient.

To examine the cross-shore wave transformation, the mean $\bar{\eta}$ and standard deviation (SD) σ_η of the free surface elevation η above SWL at the eight wave gauges for each run were calculated. The measured values for $\bar{\eta}$ were negative (wave setdown) at WG1 to WG3 outside the surf zone and WG4 at x= 8.3 m near the breaker zone. The measured values for $\bar{\eta}$ were positive (wave setup) at WG5 to WG7 at x = 12.9, 15.5, and 17.1 m in the inner surf zone. Tables 3.15-3.17 list the mean free-surface elevation $\bar{\eta}$ at 7 wave gauge locations for N test series. Likewise, Tables 3.18-3.20 for D test series, Tables 3.21-3.24 for R test series, and Tables 3.25-3.28 for B test series.

Moreover, Tables 3.29-3.31 list the free-surface standard deviation σ_η at 7 wave gauge locations for N test series. Likewise, Tables 3.31-3.33 for D test series, Tables 3.34-3.37 for R test series, and Tables 3.38-3.41 for B test series. The cross-shore variation of the local significant wave height $H_{mo} = 4\ \sigma_\eta$ was related to the wave height decay due to irregular wave breaking.

For convenience, use is made of time t = 0 – 4,000 s with SWL = 0 cm for Low (L) water level, t = 4,000 – 8,000 s with SWL = 2 cm for Medium (M) water level, t = 8,000 – 12,000 s with SWL = 4 cm for High (H) water level, and t = 12,000 – 16,000 s with SWL = 6 cm for Extreme (E) water level in Tables 3.1-3.81. The letters of L, M, H, and E are attached next to series N, D, R, and B. The run number (1 to 10) indicates the temporal sequence of runs (400 s for each run) starting from run 1 for each test denoted by the two letters (series and SWL).

Table 3.1: Incident wave characteristics for N test series, SWL = 0 cm

Run	H_{mo} (cm)	H_{rms} (cm)	H_s (cm)	T_p (s)	T_s (s)	R
NL1	16.16	11.43	15.57	2.62	2.03	0.13
NL2	16.23	11.48	15.58	2.62	2.02	0.12
NL3	17.39	12.29	16.74	2.62	1.99	0.13
NL4	17.40	12.30	16.72	2.62	2.03	0.13
NL5	17.31	12.24	16.60	2.62	2.01	0.14
NL6	17.04	12.05	16.31	2.62	2.04	0.14
NL7	17.19	12.16	16.47	2.62	2.01	0.14
NL8	17.25	12.19	16.53	2.62	2.01	0.14
NL9	17.00	12.02	16.35	2.62	2.01	0.14
NL10	16.66	11.78	16.04	2.62	2.04	0.15
Average	**16.96**	**11.99**	**16.29**	**2.62**	**2.02**	**0.14**

Table 3.2: Incident wave characteristics for N test series, SWL = 2 cm

Run	H_{mo} (cm)	H_{rms} (cm)	H_s (cm)	T_p (s)	T_s (s)	R
NM1	16.41	11.61	15.89	2.64	2.13	0.18
NM2	16.48	11.65	15.95	2.64	2.15	0.18
NM3	16.60	11.74	16.07	2.64	2.14	0.19
NM4	16.65	11.77	16.10	2.64	2.11	0.20
NM5	16.60	11.74	16.03	2.64	2.14	0.21
NM6	16.24	11.48	15.71	2.64	2.13	0.21
NM7	16.40	11.60	15.85	2.64	2.15	0.21
NM8	16.47	11.65	16.00	2.64	2.17	0.21
NM9	16.51	11.68	15.89	2.64	2.13	0.21
NM10	16.57	11.72	15.99	2.64	2.12	0.21
Average	**16.49**	**11.66**	**15.95**	**2.64**	**2.14**	**0.20**

Table 3.3: Incident wave characteristics for N test series, SWL = 4 cm

Run	H_{mo} (cm)	H_{rms} (cm)	H_s (cm)	T_p (s)	T_s (s)	R
NH1	16.28	11.51	15.52	2.42	2.13	0.17
NH2	16.50	11.67	15.78	2.42	2.11	0.17
NH3	16.70	11.81	16.00	2.57	2.11	0.17
NH4	16.70	11.81	15.99	2.57	2.12	0.16
NH5	16.76	11.85	16.14	2.57	2.13	0.15
NH6	16.41	11.61	15.78	2.57	2.12	0.15
NH7	16.57	11.72	15.80	2.57	2.12	0.14
NH8	16.66	11.78	15.90	2.57	2.11	0.14
NH9	16.72	11.83	15.96	2.57	2.13	0.14
NH10	16.70	11.81	15.95	2.57	2.15	0.13
Average	**16.60**	**11.74**	**15.88**	**2.54**	**2.12**	**0.15**

Table 3.4: Incident wave characteristics for D test series, SWL = 0 cm

Run	H_{mo} (cm)	H_{rms} (cm)	H_s (cm)	T_p (s)	T_s (s)	R
DL1	16.49	11.66	15.81	2.62	2.03	0.16
DL2	16.74	11.84	16.03	2.62	2.04	0.17
DL3	16.77	11.86	16.03	2.62	2.02	0.17
DL4	16.87	11.93	16.09	2.62	2.04	0.17
DL5	16.85	11.91	16.09	2.62	2.03	0.16
DL6	16.59	11.73	15.91	2.62	2.03	0.17
DL7	16.71	11.82	16.00	2.62	2.02	0.17
DL8	16.76	11.85	16.11	2.62	2.04	0.17
DL9	16.79	11.87	16.07	2.62	2.01	0.17
DL10	16.78	11.87	16.08	2.62	2.01	0.16
Average	**16.73**	**11.83**	**16.02**	**2.62**	**2.03**	**0.17**

Table 3.5: Incident wave characteristics for D test series, SWL = 2 cm

Run	H_{mo} (cm)	H_{rms} (cm)	H_s (cm)	T_p (s)	T_s (s)	R
DM1	16.41	11.60	15.79	2.64	2.13	0.20
DM2	16.66	11.78	16.13	2.64	2.16	0.19
DM3	16.76	11.85	16.24	2.64	2.15	0.19
DM4	16.80	11.88	16.32	2.64	2.14	0.19
DM5	16.93	11.97	16.40	2.64	2.15	0.18
DM6	16.61	11.74	16.17	2.64	2.16	0.19
DM7	16.81	11.89	16.28	2.64	2.12	0.19
DM8	16.80	11.88	16.27	2.64	2.14	0.19
DM9	16.90	11.95	16.38	2.64	2.14	0.19
DM10	16.97	12.00	16.46	2.64	2.14	0.19
Average	**16.76**	**11.85**	**16.24**	**2.64**	**2.14**	**0.19**

Table 3.6: Incident wave characteristics for D test series, SWL = 4 cm

Run	H_{mo} (cm)	H_{rms} (cm)	H_s (cm)	T_p (s)	T_s (s)	R
DH1	16.39	11.59	15.69	2.57	2.12	0.20
DH2	16.63	11.76	15.84	2.57	2.10	0.19
DH3	16.64	11.77	15.91	2.42	2.10	0.18
DH4	16.69	11.80	15.80	2.42	2.08	0.17
DH5	16.68	11.79	15.85	2.57	2.11	0.17
DH6	16.70	11.81	15.90	2.57	2.13	0.18
DH7	16.83	11.90	16.09	2.57	2.07	0.18
DH8	16.89	11.94	16.10	2.57	2.12	0.18
DH9	17.00	12.02	16.36	2.57	2.12	0.18
DH10	17.00	12.02	16.24	2.57	2.10	0.17
Average	**16.74**	**11.84**	**15.98**	**2.54**	**2.10**	**0.18**

Table 3.7: Incident wave characteristics for R test series, SWL = 0 cm

Run	H_{mo} (cm)	H_{rms} (cm)	H_s (cm)	T_p (s)	T_s (s)	R
RL1	16.30	11.52	15.58	2.62	1.99	0.14
RL2	16.64	11.77	16.21	2.41	2.05	0.14
RL3	16.80	11.88	16.29	2.41	2.07	0.13
RL4	16.87	11.93	16.29	2.41	2.05	0.14
RL5	16.82	11.90	16.27	2.41	2.04	0.14
RL6	17.00	12.00	16.36	2.41	2.05	0.15
RL7	16.95	11.98	16.35	2.41	2.03	0.14
RL8	17.00	12.02	16.31	2.41	2.06	0.15
RL9	16.91	11.96	16.44	2.41	2.04	0.14
RL10	16.83	11.90	16.14	2.41	2.03	0.14
Average	**16.81**	**11.89**	**16.22**	**2.43**	**2.04**	**0.14**

Table 3.8: Incident wave characteristics for R test series, SWL = 2 cm

Run	H_{mo} (cm)	H_{rms} (cm)	H_s (cm)	T_p (s)	T_s (s)	R
RM1	16.20	11.45	15.71	2.64	2.15	0.17
RM2	16.47	11.65	16.05	2.64	2.18	0.18
RM3	16.53	11.69	16.02	2.64	2.16	0.17
RM4	16.60	11.74	16.05	2.64	2.12	0.17
RM5	16.51	11.67	15.88	2.64	2.15	0.17
RM6	16.55	11.70	16.09	2.64	2.15	0.17
RM7	16.55	11.70	16.08	2.64	2.15	0.17
RM8	16.53	11.69	16.12	2.64	2.14	0.17
RM9	16.51	11.68	15.96	2.64	2.13	0.17
RM10	16.46	11.64	16.00	2.64	2.13	0.18
Average	**16.49**	**11.66**	**16.00**	**2.64**	**2.15**	**0.17**

Table 3.9: Incident wave characteristics for R test series, SWL = 4 cm

Run	H_{mo} (cm)	H_{rms} (cm)	H_s (cm)	T_p (s)	T_s (s)	R
RH1	18.24	12.90	17.49	2.57	2.21	0.23
RH2	16.63	11.76	15.77	2.42	2.13	0.18
RH3	16.69	11.80	15.92	2.42	2.13	0.17
RH4	16.75	11.85	16.06	2.42	2.11	0.18
RH5	16.80	11.88	16.00	2.42	2.13	0.18
RH6	16.78	11.86	16.07	2.42	2.13	0.18
RH7	16.74	11.84	15.96	2.42	2.11	0.18
RH8	16.73	11.83	16.04	2.42	2.13	0.18
RH9	16.41	11.61	15.64	2.42	2.10	0.18
RH10	16.41	11.61	15.64	2.42	2.10	0.18
Average	**16.82**	**11.89**	**16.06**	**2.44**	**2.13**	**0.18**

Table 3.10: Incident wave characteristics for R test series, SWL = 6 cm

Run	H_{mo} (cm)	H_{rms} (cm)	H_s (cm)	T_p (s)	T_s (s)	R
RE1	16.60	11.74	16.16	2.50	2.09	0.20
RE2	17.38	12.29	16.40	2.35	2.13	0.20
RE3	17.49	12.36	16.50	2.35	2.12	0.19
RE4	17.05	12.06	16.67	2.50	2.09	0.19
RE5	16.92	11.96	16.48	2.50	2.08	0.19
RE6	17.51	12.38	16.45	2.35	2.10	0.19
RE7	17.05	12.06	16.63	2.50	2.09	0.19
RE8	17.55	12.41	16.58	2.35	2.11	0.19
RE9	17.52	12.39	15.57	2.35	2.08	0.19
RE10	17.57	12.43	16.61	2.35	2.12	0.19
Average	**17.26**	**12.21**	**16.41**	**2.41**	**2.10**	**0.19**

Table 3.11: Incident wave characteristics for B test series, SWL = 0 cm

Run	H_{mo} (cm)	H_{rms} (cm)	H_s (cm)	T_p (s)	T_s (s)	R
BL1	17.68	12.50	17.14	2.62	2.20	0.22
BL2	18.50	13.08	17.80	2.62	2.17	0.22
BL3	18.19	12.86	17.45	2.62	2.13	0.22
BL4	18.43	13.03	17.62	2.62	2.11	0.22
BL5	18.28	12.92	17.50	2.62	2.15	0.22
BL6	18.20	12.87	17.44	2.62	2.13	0.22
BL7	18.33	12.96	17.62	2.62	2.13	0.22
BL8	18.37	12.99	17.68	2.62	2.13	0.22
BL9	18.28	12.93	17.34	2.62	2.15	0.22
BL10	18.33	12.96	17.69	2.62	2.14	0.22
Average	**18.26**	**12.91**	**17.53**	**2.62**	**2.14**	**0.22**

Table 3.12: Incident wave characteristics for B test series, SWL = 2 cm

Run	H_{mo} (cm)	H_{rms} (cm)	H_s (cm)	T_p (s)	T_s (s)	R
BM1	18.01	12.73	17.89	2.59	2.18	0.23
BM2	18.07	12.79	17.66	2.64	2.29	0.23
BM3	18.10	12.80	17.66	2.64	2.29	0.23
BM4	18.16	12.84	17.76	2.64	2.28	0.23
BM5	18.16	12.84	17.71	2.64	2.26	0.23
BM6	18.16	12.85	17.68	2.64	2.28	0.23
BM7	18.20	12.87	17.89	2.64	2.30	0.23
BM8	18.17	12.85	17.79	2.64	2.28	0.23
BM9	18.11	12.80	17.60	2.64	2.30	0.23
BM10	18.09	12.79	17.71	2.64	2.30	0.23
Average	**18.12**	**12.82**	**17.74**	**2.64**	**2.28**	**0.23**

Table 3.13: Incident wave characteristics for B test series, SWL = 4 cm

Run	H_{mo} (cm)	H_{rms} (cm)	H_s (cm)	T_p (s)	T_s (s)	R
BH1	17.43	12.32	17.00	2.57	2.25	0.24
BH2	17.51	12.38	16.81	2.57	2.24	0.23
BH3	17.70	12.52	16.97	2.57	2.22	0.23
BH4	17.88	12.64	17.17	2.57	2.23	0.23
BH5	17.89	12.65	17.16	2.57	2.23	0.23
BH6	17.90	12.66	17.22	2.57	2.24	0.23
BH7	17.88	12.64	17.20	2.57	2.22	0.23
BH8	17.89	12.65	17.28	2.57	2.25	0.23
BH9	17.88	12.64	17.17	2.57	2.22	0.23
BH10	17.92	12.67	17.16	2.57	2.22	0.23
Average	**17.79**	**12.58**	**17.11**	**2.57**	**2.23**	**0.23**

Table 3.14: Incident wave characteristics for B test series, SWL = 6 cm

Run	H_{mo} (cm)	H_{rms} (cm)	H_s (cm)	T_p (s)	T_s (s)	R
BE1	18.79	13.29	17.94	2.35	2.23	0.24
BE2	18.95	13.40	18.11	2.35	2.22	0.24
BE3	19.09	13.50	18.24	2.35	2.22	0.24
BE4	19.15	13.54	18.44	2.35	2.22	0.24
BE5	19.15	13.54	18.43	2.35	2.22	0.24
BE6	19.17	13.55	18.49	2.35	2.21	0.24
BE7	19.16	13.55	18.26	2.35	2.22	0.24
BE8	19.09	13.50	18.31	2.35	2.23	0.24
BE9	19.11	13.51	18.38	2.35	2.23	0.24
BE10	19.11	13.51	18.43	2.35	2.23	0.24
Average	**19.08**	**13.49**	**18.30**	**2.35**	**2.22**	**0.24**

Table 3.15: Mean free-surface elevation $\bar{\eta}$ (cm) at 7 wave gauge locations for N test series, SWL = 0 cm

Run	WG1	WG2	WG3	WG4	WG5	WG6	WG7
NL1	-0.06	-0.09	-0.06	-0.16	0.19	0.58	0.22
NL2	-0.09	-0.10	-0.07	-0.16	0.15	0.17	0.15
NL3	-0.11	-0.14	-0.08	-0.15	0.22	0.29	0.29
NL4	-0.11	-0.17	-0.08	-0.15	0.23	0.29	0.28
NL5	-0.10	-0.14	-0.07	-0.14	0.22	0.26	0.27
NL6	-0.07	-0.11	-0.05	-0.16	0.19	0.18	0.20
NL7	-0.11	-0.11	-0.07	-0.14	0.18	0.34	0.26
NL8	-0.11	-0.12	-0.07	-0.15	0.20	0.26	0.24
NL9	-0.09	-0.10	-0.07	-0.15	0.21	0.28	0.29
NL10	-0.10	-0.12	-0.06	-0.21	0.06	0.16	0.21
Average	**-0.10**	**-0.12**	**-0.07**	**-0.16**	**0.19**	**0.28**	**0.24**

Table 3.16: Mean free-surface elevation $\bar{\eta}$ (cm) at 7 wave gauge locations for N test series, SWL = 2 cm

Run	WG1	WG2	WG3	WG4	WG5	WG6	WG7
NM1	-0.11	-0.12	-0.12	-0.25	0.05	0.09	0.07
NM2	-0.16	-0.11	-0.13	-0.17	0.06	0.14	0.11
NM3	-0.10	-0.10	-0.17	-0.18	0.01	0.15	0.11
NM4	-0.06	-0.05	-0.11	-0.14	0.09	0.18	0.14
NM5	-0.10	-0.08	-0.12	-0.16	0.08	0.15	0.10
NM6	-0.05	-0.08	-0.10	-0.17	0.09	0.17	0.07
NM7	-0.04	-0.10	-0.12	-0.15	0.07	0.17	0.08
NM8	-0.09	-0.09	-0.11	-0.16	0.09	0.17	0.11
NM9	-0.06	-0.09	-0.11	-0.14	0.05	0.13	0.12
NM10	-0.09	-0.08	-0.10	-0.13	0.09	0.16	0.11
Average	**-0.09**	**-0.09**	**-0.12**	**-0.17**	**0.07**	**0.15**	**0.10**

Table 3.17: Mean free-surface elevation $\bar{\eta}$ (cm) at 7 wave gauge locations for N test series, SWL = 4 cm

Run	WG1	WG2	WG3	WG4	WG5	WG6	WG7
NH1	-0.13	-0.18	-0.15	-0.25	-0.03	-0.03	-0.09
NH2	-0.16	-0.15	-0.15	-0.23	-0.01	0.09	-0.04
NH3	-0.16	-0.18	-0.19	-0.19	-0.02	0.07	0.00
NH4	-0.15	-0.17	-0.15	-0.23	-0.02	0.07	-0.02
NH5	-0.16	-0.19	-0.15	-0.22	-0.02	0.08	0.04
NH6	-0.21	-0.26	-0.19	-0.33	-0.09	0.00	-0.05
NH7	-0.15	-0.21	-0.15	-0.24	-0.02	0.02	-0.05
NH8	-0.15	-0.19	-0.16	-0.23	-0.02	0.04	-0.01
NH9	-0.15	-0.18	-0.16	-0.24	-0.01	0.05	0.04
NH10	-0.16	-0.20	-0.16	-0.24	0.01	0.05	0.04
Average	**-0.16**	**-0.19**	**-0.16**	**-0.24**	**-0.02**	**0.04**	**-0.01**

Table 3.18: Mean free-surface elevation $\bar{\eta}$ (cm) at 7 wave gauge locations for D test series, SWL = 0 cm

Run	WG1	WG2	WG3	WG4	WG5	WG6	WG7
DL1	-0.18	-0.16	-0.05	-0.19	0.14	0.16	0.30
DL2	-0.10	-0.11	-0.07	-0.17	0.16	0.21	0.27
DL3	-0.11	-0.10	-0.04	-0.17	0.17	0.22	0.26
DL4	-0.10	-0.14	-0.06	-0.15	0.19	0.25	0.27
DL5	-0.09	-0.10	-0.06	-0.20	0.19	0.24	0.27
DL6	-0.08	-0.08	-0.05	-0.17	0.19	0.21	0.24
DL7	-0.09	-0.08	-0.05	-0.18	0.20	0.21	0.27
DL8	-0.12	-0.10	-0.05	-0.16	0.22	0.25	0.27
DL9	-0.09	-0.10	-0.05	-0.18	0.20	0.23	0.21
DL10	-0.09	-0.08	-0.05	-0.19	0.20	0.25	0.24
Average	**-0.11**	**-0.11**	**-0.05**	**-0.18**	**0.19**	**0.22**	**0.26**

Table 3.19: Mean free-surface elevation $\bar{\eta}$ (cm) at 7 wave gauge locations for D test series, SWL = 2 cm

Run	WG1	WG2	WG3	WG4	WG5	WG6	WG7
DM1	-0.09	-0.12	-0.10	-0.15	0.14	0.15	0.03
DM2	-0.06	-0.09	-0.09	-0.16	0.14	0.16	0.04
DM3	-0.04	-0.07	-0.14	-0.17	0.12	0.19	0.04
DM4	-0.05	-0.07	-0.09	-0.17	0.15	0.19	0.07
DM5	-0.04	-0.08	-0.08	-0.18	0.16	0.19	0.09
DM6	-0.04	-0.06	-0.06	-0.18	0.16	0.15	0.00
DM7	-0.04	-0.08	-0.08	-0.15	0.14	0.18	0.04
DM8	-0.03	-0.05	-0.09	-0.18	0.14	0.19	0.13
DM9	-0.04	-0.06	-0.09	-0.14	0.16	0.19	0.01
DM10	-0.03	-0.06	-0.09	-0.16	0.15	0.20	0.06
Average	**-0.05**	**-0.07**	**-0.09**	**-0.16**	**0.15**	**0.18**	**0.05**

Table 3.20: Mean free-surface elevation $\bar{\eta}$ (cm) at 7 wave gauge locations for D test series, SWL = 4 cm

Run	WG1	WG2	WG3	WG4	WG5	WG6	WG7
DH1	-0.30	-0.24	-0.13	-0.23	0.01	0.00	-0.07
DH2	-0.19	-0.22	-0.15	-0.26	-0.01	-0.01	-0.08
DH3	-0.16	-0.19	-0.13	-0.23	0.01	0.05	-0.11
DH4	-0.17	-0.18	-0.13	-0.22	0.01	0.09	-0.10
DH5	-0.15	-0.18	-0.13	-0.22	0.02	0.06	-0.12
DH6	-0.10	-0.12	-0.11	-0.21	0.04	0.10	-0.20
DH7	-0.12	-0.13	-0.10	-0.22	0.03	0.05	-0.18
DH8	-0.13	-0.13	-0.11	-0.22	0.02	0.06	-0.17
DH9	-0.12	-0.15	-0.11	-0.22	0.02	0.08	-0.16
DH10	-0.12	-0.14	-0.11	-0.17	0.02	0.08	-0.16
Average	**-0.16**	**-0.17**	**-0.12**	**-0.22**	**0.02**	**0.06**	**-0.14**

Table 3.21: Mean free-surface elevation $\bar{\eta}$ (cm) at 7 wave gauge locations for R test series, SWL = 0 cm

Run	WG1	WG2	WG3	WG4	WG5	WG6	WG7
RL1	-0.15	-0.16	-0.12	-0.22	0.12	0.13	0.19
RL2	-0.12	-0.13	-0.13	-0.16	0.26	0.33	0.27
RL3	-0.11	-0.10	-0.08	-0.20	0.27	0.33	0.32
RL4	-0.08	-0.12	-0.07	-0.17	0.28	0.33	0.34
RL5	-0.07	-0.11	-0.08	-0.14	0.28	0.32	0.33
RL6	-0.03	-0.08	-0.13	-0.15	0.29	0.36	0.35
RL7	-0.08	-0.12	-0.09	-0.13	0.28	0.36	0.35
RL8	-0.10	-0.14	-0.08	-0.17	0.27	0.34	0.38
RL9	-0.09	-0.12	-0.07	-0.18	0.28	0.32	0.38
RL10	-0.12	-0.15	-0.06	-0.18	0.26	0.33	0.37
Average	**-0.10**	**-0.12**	**-0.09**	**-0.17**	**0.26**	**0.32**	**0.33**

Table 3.22: Mean free-surface elevation $\bar{\eta}$ (cm) at 7 wave gauge locations for R test series, SWL = 2 cm

Run	WG1	WG2	WG3	WG4	WG5	WG6	WG7
RM1	NR	NR	NR	NR	NR	NR	NR
RM2	-0.08	-0.10	-0.10	-0.16	0.14	0.21	0.23
RM3	-0.08	-0.09	-0.11	-0.15	0.15	0.18	0.19
RM4	-0.08	-0.10	-0.08	-0.17	0.17	0.20	0.13
RM5	-0.09	-0.08	-0.08	-0.18	0.16	0.20	0.08
RM6	-0.08	-0.10	-0.08	-0.16	0.18	0.22	0.19
RM7	-0.09	-0.08	-0.09	-0.14	0.16	0.21	0.22
RM8	-0.08	-0.06	-0.10	-0.13	0.16	0.20	0.16
RM9	-0.09	-0.09	-0.08	-0.15	0.16	0.20	0.23
RM10	-0.08	-0.09	-0.08	-0.17	0.15	0.20	0.24
Average	**-0.08**	**-0.09**	**-0.09**	**-0.16**	**0.16**	**0.20**	**0.19**

Table 3.23: Mean free-surface elevation $\bar{\eta}$ (cm) at 7 wave gauge locations for R test series, SWL = 4 cm

Run	WG1	WG2	WG3	WG4	WG5	WG6	WG7
RH1	-0.10	-0.12	-0.08	-0.15	0.08	0.15	0.12
RH2	-0.07	-0.09	-0.09	-0.17	0.09	0.14	0.08
RH3	-0.06	-0.10	-0.10	-0.16	0.06	0.13	0.11
RH4	-0.06	-0.09	-0.11	-0.16	0.09	0.15	0.17
RH5	-0.09	-0.08	-0.08	-0.17	0.11	0.13	0.13
RH6	-0.07	-0.09	-0.08	-0.17	0.11	0.12	0.12
RH7	-0.04	-0.08	-0.10	-0.19	0.11	0.13	0.12
RH8	-0.09	-0.10	-0.08	-0.13	0.12	0.17	0.14
RH9	-0.07	-0.10	-0.08	-0.17	0.12	0.15	0.16
RH10	-0.07	-0.09	-0.08	-0.17	0.10	0.15	-0.02
Average	**-0.07**	**-0.09**	**-0.09**	**-0.16**	**0.10**	**0.14**	**0.11**

Table 3.24: Mean free-surface elevation $\bar{\eta}$ (cm) at 7 wave gauge locations for R test series, SWL = 6 cm

Run	WG1	WG2	WG3	WG4	WG5	WG6	WG7
RE1	-0.16	-0.18	-0.12	-0.23	0.02	0.08	0.04
RE2	-0.18	-0.17	-0.08	-0.18	0.02	0.11	0.02
RE3	-0.10	-0.09	-0.10	-0.21	0.00	0.09	-0.03
RE4	-0.09	-0.10	-0.09	-0.17	0.06	0.09	0.07
RE5	-0.09	-0.11	-0.08	-0.17	0.04	0.07	0.01
RE6	-0.10	-0.11	-0.11	-0.18	0.01	0.11	0.06
RE7	-0.08	-0.11	-0.07	-0.17	0.03	0.05	0.04
RE8	-0.10	-0.11	-0.10	-0.18	0.04	0.08	0.03
RE9	-0.08	-0.09	-0.07	-0.18	0.01	0.10	0.06
RE10	-0.11	-0.11	-0.08	-0.16	0.02	0.12	0.04
Average	**-0.11**	**-0.12**	**-0.09**	**-0.18**	**0.03**	**0.09**	**0.03**

Table 3.25: Mean free-surface elevation $\bar{\eta}$ (cm) at 7 wave gauge locations for B test series, SWL = 0 cm

Run	WG1	WG2	WG3	WG4	WG5	WG6	WG7
BL1	-0.18	-0.24	-0.13	-0.21	0.16	0.26	0.17
BL2	-0.13	-0.15	-0.07	-0.16	0.18	0.25	0.25
BL3	-0.07	-0.12	-0.08	-0.18	0.19	0.19	0.25
BL4	-0.10	-0.14	-0.07	-0.16	0.19	0.27	0.30
BL5	-0.12	-0.12	-0.07	-0.15	0.21	0.23	0.28
BL6	-0.08	-0.11	-0.08	-0.15	0.22	0.26	0.28
BL7	-0.09	-0.14	-0.08	-0.12	0.20	0.25	0.31
BL8	-0.08	-0.11	-0.07	-0.14	0.22	0.23	0.31
BL9	-0.07	-0.10	-0.07	-0.13	0.21	0.27	0.30
BL10	-0.06	-0.14	-0.07	-0.12	0.22	0.28	0.30
Average	**-0.10**	**-0.14**	**-0.08**	**-0.15**	**0.20**	**0.25**	**0.28**

Table 3.26: Mean free-surface elevation $\bar{\eta}$ (cm) at 7 wave gauge locations for B test series, SWL = 2 cm

Run	WG1	WG2	WG3	WG4	WG5	WG6	WG7
BM1	-0.19	-0.20	-0.09	-0.19	0.16	0.18	0.23
BM2	-0.09	-0.19	-0.07	-0.18	0.13	0.23	0.22
BM3	-0.10	-0.15	-0.09	-0.18	0.17	0.24	0.26
BM4	-0.07	-0.09	-0.08	-0.18	0.18	0.24	0.25
BM5	-0.08	-0.12	-0.06	-0.16	0.19	0.26	0.24
BM6	-0.09	-0.11	-0.05	-0.19	0.19	0.25	0.28
BM7	-0.09	-0.12	-0.07	-0.18	0.19	0.22	0.29
BM8	-0.08	-0.12	-0.06	-0.19	0.17	0.22	0.29
BM9	-0.09	-0.12	-0.06	-0.18	0.17	0.19	0.29
BM10	-0.08	-0.11	-0.06	-0.18	0.18	0.19	0.28
Average	**-0.10**	**-0.13**	**-0.07**	**-0.18**	**0.17**	**0.22**	**0.26**

Table 3.27: Mean free-surface elevation $\bar{\eta}$ (cm) at 7 wave gauge locations for B test series, SWL = 4 cm

Run	WG1	WG2	WG3	WG4	WG5	WG6	WG7
BH1	-0.12	-0.19	-0.12	-0.23	0.06	0.09	0.06
BH2	-0.08	-0.15	-0.13	-0.22	0.03	0.14	0.13
BH3	-0.12	-0.12	-0.09	-0.18	0.06	0.15	0.16
BH4	-0.10	-0.12	-0.09	-0.17	0.11	0.17	0.19
BH5	-0.08	-0.10	-0.09	-0.14	0.11	0.14	0.16
BH6	-0.08	-0.10	-0.11	-0.19	0.11	0.16	0.19
BH7	-0.11	-0.11	-0.09	-0.18	0.10	0.14	0.18
BH8	-0.11	-0.11	-0.09	-0.17	0.10	0.16	0.20
BH9	-0.10	-0.12	-0.10	-0.17	0.10	0.16	0.19
BH10	-0.11	-0.11	-0.11	-0.18	0.12	0.14	0.20
Average	**-0.10**	**-0.12**	**-0.10**	**-0.18**	**0.09**	**0.15**	**0.17**

Table 3.28: Mean free-surface elevation $\bar{\eta}$ (cm) at 7 wave gauge locations for B test series, SWL = 6 cm

Run	WG1	WG2	WG3	WG4	WG5	WG6	WG7
BE1	-0.17	-0.16	-0.11	-0.28	0.15	0.04	-0.07
BE2	-0.16	-0.14	-0.08	-0.20	0.01	0.09	0.02
BE3	-0.12	-0.12	-0.09	-0.17	0.05	0.11	0.03
BE4	-0.13	-0.11	-0.08	-0.20	0.07	0.10	0.08
BE5	-0.09	-0.12	-0.08	-0.20	0.09	0.10	0.06
BE6	-0.11	-0.11	-0.07	-0.20	0.03	0.10	0.07
BE7	-0.10	-0.12	-0.07	-0.20	0.12	0.15	0.07
BE8	-0.10	-0.12	-0.07	-0.18	0.08	0.13	0.04
BE9	-0.09	-0.11	-0.08	-0.19	0.05	0.10	0.00
BE10	-0.11	-0.11	-0.06	-0.20	0.17	0.11	0.07
Average	**-0.12**	**-0.12**	**-0.08**	**-0.20**	**0.08**	**0.10**	**0.04**

Table 3.29: Free-surface standard deviation σ_η (cm) at 7 wave gauge locations for N test series, SWL = 0 cm

Run	WG1	WG2	WG3	WG4	WG5	WG6	WG7
NL1	4.00	3.99	4.07	3.83	2.84	2.55	2.33
NL2	4.01	4.01	4.10	3.85	2.82	2.56	2.37
NL3	4.31	4.30	4.39	4.03	2.91	2.61	2.42
NL4	4.31	4.31	4.41	4.03	2.91	2.61	2.44
NL5	4.29	4.28	4.38	4.03	2.92	2.62	2.45
NL6	4.20	4.20	4.34	3.97	2.95	2.63	2.42
NL7	4.24	4.24	4.36	3.98	2.95	2.64	2.43
NL8	4.26	4.26	4.39	3.97	2.96	2.65	2.44
NL9	4.21	4.20	4.34	3.96	2.95	2.68	2.47
NL10	4.10	4.12	4.24	3.92	2.92	2.65	2.47
Average	**4.19**	**4.19**	**4.30**	**3.96**	**2.91**	**2.62**	**2.42**

Table 3.30: Free-surface standard deviation σ_η (cm) at 7 wave gauge locations for N test series, SWL = 2 cm

Run	WG1	WG2	WG3	WG4	WG5	WG6	WG7
NM1	4.07	4.10	4.23	4.02	3.21	3.07	2.91
NM2	4.13	4.12	4.27	4.05	3.21	3.07	2.88
NM3	4.16	4.15	4.28	4.07	3.22	3.09	2.88
NM4	4.21	4.16	4.32	4.09	3.21	3.07	2.85
NM5	4.24	4.16	4.31	4.07	3.20	3.07	2.87
NM6	4.10	4.05	4.21	3.96	3.15	3.03	2.80
NM7	4.13	4.09	4.28	3.99	3.16	3.04	2.81
NM8	4.16	4.12	4.27	4.00	3.15	3.03	2.79
NM9	4.18	4.12	4.28	3.99	3.15	3.04	2.82
NM10	4.24	4.13	4.29	4.02	3.16	3.03	2.81
Average	**4.16**	**4.12**	**4.27**	**4.03**	**3.18**	**3.05**	**2.84**

Table 3.31: Free-surface standard deviation σ_η (cm) at 7 wave gauge locations for N test series, SWL = 4 cm

Run	WG1	WG2	WG3	WG4	WG5	WG6	WG7
NH1	4.01	4.04	4.13	3.99	3.23	3.08	2.82
NH2	4.08	4.09	4.16	4.01	3.24	3.09	2.81
NH3	4.13	4.13	4.20	4.06	3.23	3.06	2.80
NH4	4.14	4.14	4.19	4.06	3.24	3.03	2.78
NH5	4.17	4.15	4.19	4.09	3.26	3.04	2.77
NH6	4.05	4.08	4.11	4.04	3.22	3.02	2.75
NH7	4.09	4.14	4.15	4.09	3.25	3.00	2.74
NH8	4.12	4.17	4.16	4.10	3.23	2.99	2.74
NH9	4.14	4.19	4.16	4.13	3.25	2.97	2.74
NH10	4.15	4.18	4.15	4.12	3.27	2.95	2.71
Average	**4.11**	**4.13**	**4.16**	**4.07**	**3.24**	**3.02**	**2.77**

Table 3.32: Free-surface standard deviation σ_η (cm) at 7 wave gauge locations for D test series, SWL = 0 cm

Run	WG1	WG2	WG3	WG4	WG5	WG6	WG7
DL1	4.09	4.08	4.19	3.91	2.90	2.60	2.35
DL2	4.15	4.14	4.26	3.92	2.94	2.63	2.36
DL3	4.17	4.16	4.26	3.98	2.95	2.62	2.37
DL4	4.19	4.18	4.28	3.99	2.96	2.63	2.39
DL5	4.19	4.18	4.28	3.95	2.94	2.64	2.40
DL6	4.10	4.14	4.21	3.95	2.92	2.62	2.41
DL7	4.14	4.16	4.23	3.98	2.90	2.62	2.42
DL8	4.15	4.19	4.25	3.99	2.90	2.61	2.43
DL9	4.16	4.20	4.25	3.98	2.91	2.61	2.45
DL10	4.16	4.20	4.24	3.98	2.91	2.62	2.47
Average	**4.15**	**4.16**	**4.25**	**3.96**	**2.92**	**2.62**	**2.41**

Table 3.33: Free-surface standard deviation σ_η (cm) at 7 wave gauge locations for D test series, SWL = 2 cm

Run	WG1	WG2	WG3	WG4	WG5	WG6	WG7
DM1	4.09	4.13	4.26	4.00	3.13	3.02	2.93
DM2	4.14	4.19	4.30	4.03	3.14	3.03	2.92
DM3	4.17	4.21	4.32	4.07	3.13	3.01	2.92
DM4	4.18	4.22	4.34	4.05	3.11	3.02	2.93
DM5	4.22	4.25	4.36	4.06	3.14	3.02	2.92
DM6	4.17	4.15	4.28	4.02	3.13	3.03	2.94
DM7	4.22	4.20	4.32	4.05	3.14	3.03	2.95
DM8	4.23	4.20	4.32	4.06	3.14	3.03	2.94
DM9	4.25	4.23	4.34	4.05	3.14	3.03	2.95
DM10	4.27	4.25	4.36	4.07	3.14	3.04	2.96
Average	**4.19**	**4.20**	**4.32**	**4.05**	**3.13**	**3.03**	**2.94**

Table 3.34: Free-surface standard deviation σ_η (cm) at 7 wave gauge locations for D test series, SWL = 4 cm

Run	WG1	WG2	WG3	WG4	WG5	WG6	WG7
DH1	4.13	4.13	4.18	4.08	3.26	3.14	3.09
DH2	4.15	4.18	4.23	4.10	3.23	3.14	3.03
DH3	4.14	4.15	4.23	4.10	3.19	3.11	2.95
DH4	4.13	4.14	4.26	4.08	3.20	3.11	2.91
DH5	4.13	4.14	4.25	4.08	3.22	3.10	2.89
DH6	4.11	4.12	4.27	4.08	3.26	3.15	2.93
DH7	4.15	4.15	4.29	4.12	3.29	3.14	2.93
DH8	4.16	4.16	4.30	4.14	3.29	3.15	2.92
DH9	4.21	4.18	4.32	4.16	3.28	3.14	2.92
DH10	4.22	4.18	4.31	4.17	3.30	3.13	2.93
Average	**4.15**	**4.15**	**4.26**	**4.11**	**3.25**	**3.13**	**2.95**

Table 3.35: Free-surface standard deviation σ_η (cm) at 7 wave gauge locations for R test series, SWL = 0 cm

Run	WG1	WG2	WG3	WG4	WG5	WG6	WG7
RL1	3.95	3.96	4.01	3.64	2.66	2.38	2.05
RL2	4.13	4.15	4.16	3.73	2.59	2.44	2.18
RL3	4.17	4.20	4.19	3.75	2.61	2.41	2.19
RL4	4.18	4.22	4.20	3.78	2.60	2.43	2.18
RL5	4.17	4.21	4.21	3.79	2.59	2.43	2.19
RL6	4.21	4.24	4.22	3.79	2.62	2.45	2.19
RL7	4.21	4.24	4.22	3.80	2.61	2.44	2.20
RL8	4.22	4.25	4.22	NR	2.61	2.45	2.20
RL9	4.21	4.24	4.21	3.81	2.61	2.46	2.20
RL10	4.19	4.21	4.18	3.79	2.61	2.46	2.20
Average	**4.16**	**4.20**	**4.18**	**3.76**	**2.61**	**2.44**	**2.18**

Table 3.36: Free-surface standard deviation σ_η (cm) at 7 wave gauge locations for R test series, SWL = 2 cm

Run	WG1	WG2	WG3	WG4	WG5	WG6	WG7
RM1	4.04	3.99	4.14	3.83	2.95	2.87	2.72
RM2	4.11	4.06	4.24	3.86	2.96	2.87	2.71
RM3	4.15	4.08	4.24	3.88	2.95	2.87	2.72
RM4	4.15	4.10	4.25	3.87	2.96	2.88	2.71
RM5	4.15	4.09	4.24	3.88	2.96	2.87	2.73
RM6	4.17	4.10	4.24	3.87	2.96	2.87	2.72
RM7	4.16	4.09	4.25	3.86	2.95	2.87	2.72
RM8	4.13	4.08	4.24	3.87	2.94	2.88	2.71
RM9	4.15	4.08	4.24	3.87	2.95	2.87	2.73
RM10	4.14	4.07	4.22	3.85	2.94	2.87	2.71
Average	**4.14**	**4.07**	**4.23**	**3.86**	**2.95**	**2.87**	**2.72**

Table 3.37: Free-surface standard deviation σ_η (cm) at 7 wave gauge locations for R test series, SWL = 4 cm

Run	WG1	WG2	WG3	WG4	WG5	WG6	WG7
RH1	4.09	4.13	4.15	3.98	3.19	3.09	2.90
RH2	4.12	4.16	4.20	4.02	3.18	3.08	2.84
RH3	4.15	4.19	4.22	4.04	3.20	3.08	2.86
RH4	4.16	4.21	4.23	4.06	3.19	3.08	2.87
RH5	4.16	4.21	4.25	4.05	3.19	3.09	2.84
RH6	4.17	4.21	4.23	4.06	3.20	3.10	2.85
RH7	4.15	4.20	4.22	4.06	3.19	3.10	2.84
RH8	4.16	4.19	4.22	4.05	3.18	3.09	2.85
RH9	4.15	4.19	4.21	4.06	3.19	3.09	2.86
RH10	4.17	4.20	4.23	4.06	3.19	3.10	2.85
Average	**4.15**	**4.19**	**4.22**	**4.04**	**3.19**	**3.09**	**2.86**

Table 3.38: Free-surface standard deviation σ_η (cm) at 7 wave gauge locations for R test series, SWL = 6 cm

Run	WG1	WG2	WG3	WG4	WG5	WG6	WG7
RE1	4.15	4.15	4.29	4.06	3.21	3.21	3.13
RE2	4.24	4.23	4.35	4.12	3.34	3.34	3.09
RE3	4.25	4.25	4.37	4.12	3.30	3.30	3.08
RE4	4.16	4.21	4.23	4.06	3.19	3.08	2.87
RE5	4.19	4.21	4.35	4.12	3.21	3.18	3.05
RE6	4.27	4.26	4.36	4.12	3.33	3.27	3.05
RE7	4.24	4.25	4.38	4.13	3.21	3.18	3.09
RE8	4.27	4.27	4.37	4.14	3.33	3.28	3.07
RE9	4.28	4.27	4.36	4.12	3.33	3.29	3.06
RE10	4.29	4.28	4.37	4.12	3.33	3.28	3.04
Average	**4.23**	**4.24**	**4.34**	**4.11**	**3.28**	**3.24**	**3.05**

Table 3.39: Free-surface standard deviation σ_η (cm) at 7 wave gauge locations for B test series, SWL = 0 cm

Run	WG1	WG2	WG3	WG4	WG5	WG6	WG7
BL1	3.84	3.80	3.96	3.64	2.62	2.36	1.86
BL2	4.01	3.98	4.14	3.73	2.67	2.39	1.89
BL3	3.95	3.92	4.07	3.71	2.65	2.36	1.89
BL4	4.00	3.97	4.13	3.74	2.68	2.38	1.87
BL5	3.96	3.94	4.09	3.72	2.67	2.36	1.88
BL6	3.95	3.93	4.07	3.70	2.66	2.37	1.89
BL7	3.98	3.96	4.11	3.74	2.67	2.37	1.89
BL8	3.98	3.97	4.11	3.71	2.67	2.36	1.88
BL9	3.96	3.95	4.08	3.72	2.67	2.37	1.88
BL10	3.97	3.96	4.10	3.72	2.68	2.36	1.88
Average	**3.96**	**3.94**	**4.09**	**3.71**	**2.66**	**2.37**	**1.88**

Table 3.40: Free-surface standard deviation σ_η (cm) at 7 wave gauge locations for B test series, SWL = 2 cm

Run	WG1	WG2	WG3	WG4	WG5	WG6	WG7
BM1	3.95	3.91	4.13	3.81	2.70	2.60	2.47
BM2	3.96	3.94	4.14	3.84	2.80	2.65	2.51
BM3	4.00	3.96	4.20	3.84	2.82	2.66	2.52
BM4	4.01	3.96	4.19	3.84	2.82	2.67	2.51
BM5	4.02	3.99	4.20	3.82	2.82	2.66	2.53
BM6	4.02	3.99	4.19	3.84	2.81	2.67	2.52
BM7	4.02	3.99	4.21	3.83	2.83	2.68	2.51
BM8	4.02	3.99	4.20	3.83	2.82	2.67	2.50
BM9	4.00	3.96	4.18	3.84	2.83	2.68	2.50
BM10	4.00	3.97	4.18	3.85	2.82	2.67	2.52
Average	**3.96**	**3.94**	**4.09**	**3.71**	**2.66**	**2.37**	**1.88**

Table 3.41: Free-surface standard deviation σ_η (cm) at 7 wave gauge locations for B test series, SWL = 4 cm

Run	WG1	WG2	WG3	WG4	WG5	WG6	WG7
BH1	3.83	3.83	4.05	3.89	2.96	2.83	2.96
BH2	3.86	3.85	4.07	3.82	2.95	2.85	2.96
BH3	3.90	3.90	4.12	3.83	2.97	2.83	2.62
BH4	3.93	3.93	4.15	3.84	2.96	2.83	2.62
BH5	3.94	3.93	4.16	3.85	2.95	2.82	2.61
BH6	3.94	3.94	4.15	3.85	2.95	2.82	2.60
BH7	3.93	3.93	4.16	3.85	2.96	2.82	2.76
BH8	3.93	3.93	4.16	3.85	2.94	2.82	2.92
BH9	3.93	3.94	4.16	3.86	2.93	2.80	2.90
BH10	3.94	3.94	4.17	3.85	2.95	2.80	2.90
Average	**3.91**	**3.91**	**4.14**	**3.85**	**2.95**	**2.82**	**2.79**

Table 3.42: Free-surface standard deviation σ_η (cm) at 7 wave gauge locations for B test series, SWL = 6 cm

Run	WG1	WG2	WG3	WG4	WG5	WG6	WG7
BE1	4.16	4.11	4.28	4.03	3.27	3.28	3.07
BE2	4.18	4.14	4.30	4.05	3.28	3.28	3.03
BE3	4.20	4.17	4.33	4.05	3.27	3.27	3.01
BE4	4.22	4.19	4.34	4.06	3.27	3.27	3.01
BE5	4.21	4.19	4.34	4.06	3.28	3.29	3.00
BE6	4.22	4.20	4.35	4.05	3.28	3.26	3.00
BE7	4.20	4.19	4.34	4.05	3.27	3.29	2.99
BE8	4.19	4.18	4.32	4.05	3.26	3.27	2.99
BE9	4.20	4.19	4.32	4.06	3.27	3.28	2.99
BE10	4.20	4.18	4.32	4.04	3.25	3.27	2.99
Average	**4.20**	**4.17**	**4.32**	**4.05**	**3.27**	**3.28**	**3.01**

Unlike the values for $\bar{\eta}$ at WG1-7, the values for $\bar{\eta}$ at WG8 located in x = 18.6 m in the swash zone were affected by the bottom elevation change at that location. The averaging for the WG8 buried partially in the sand above SWL was performed for the wet duration only. The wet probability P_w, which is defined as the ratio between the wet and total duration, was 1.0 at WG1-WG7; however, at the WG8 in the swash zone, P_w increased with the increase of SWL by 2 cm increment in each test series as listed in Tables 3.43-3.56 with time t in the middle of each run. These tables list the wet probability P_w, mean free-surface elevation $\bar{\eta}$ and free-surface standard deviation σ_η for WG8 in test series N, D, R, and B where the bottom elevation z_b and the mean depth $\bar{h}$ are related as $\bar{h} = (\bar{\eta} - z_b)$. The value of z_b was measured after 5 and 10 runs in N and D test series.

Table 3.43: Wet probability P_w, mean free-surface elevation $\bar{\eta}$ (cm), and free-surface standard deviation σ_η (cm) for WG8 in N test series, SWL = 0 cm

Run	***t (s)***	P_w	z_b *(cm)*	$\bar{h}$ *(cm)*	$\bar{\eta}$ *(cm)*	σ_η *(cm)*
	0		8.66343			
NL1	200	0.39	8.67	0.87	9.54	0.65
NL2	600	0.35	8.68	0.83	9.51	0.67
NL3	1000	0.32	8.69	0.86	9.55	0.73
NL4	1400	0.33	8.69	0.89	9.58	0.77
NL5	1800	0.31	8.70	0.90	9.60	0.77
	2000		8.71			
NL6	2200	0.32	8.73	0.97	9.70	0.76
NL7	2600	0.31	8.79	1.00	9.79	0.8
NL8	3000	0.30	8.84	0.91	9.75	0.8
NL9	3400	0.30	8.89	0.91	9.80	0.84
NL10	3800	0.33	8.94	0.97	9.91	0.8
	4000		8.96			
Average		**0.33**		**0.91**	**9.67**	**0.76**

Table 3.44: Wet probability P_w, mean free-surface elevation $\bar{\eta}$ (cm), and free-surface standard deviation σ_η (cm) for WG8 in N test series, SWL = 2 cm

Run	*t (s)*	P_w	z_b *(cm)*	$\bar{h}$ *(cm)*	$\bar{\eta}$ *(cm)*	σ_η *(cm)*
	0		6.96388			
NM1	200	0.54	6.81	1.49	8.30	0.95
NM2	600	0.53	6.50	1.56	8.06	0.99
NM3	1000	0.59	6.18	1.35	7.53	1.05
NM4	1400	0.57	5.87	1.59	7.46	1.05
NM5	1800	0.60	5.56	1.75	7.31	1.06
	2000		5.41			
NM6	2200	0.61	5.31	1.87	7.18	1.1
NM7	2600	0.61	5.11	1.78	6.89	1.1
NM8	3000	0.61	4.92	1.83	6.75	1.11
NM9	3400	0.63	4.72	1.86	6.58	1.15
NM10	3800	0.64	4.53	1.92	6.45	1.15
	4000		4.43			
Average		**0.60**		**1.70**	**7.25**	**1.07**

Table 3.45: Wet probability P_w, mean free-surface elevation $\bar{\eta}$ (cm), and free-surface standard deviation σ_η (cm) for WG8 in N test series, SWL = 4 cm

Run	***t (s)***	P_w	z_b *(cm)*	$\bar{h}$ *(cm)*	$\bar{\eta}$ *(cm)*	σ_η *(cm)*
	0		2.43275			
NH1	200	0.76	2.18	2.47	4.65	1.53
NH2	600	0.78	1.68	2.46	4.14	1.57
NH3	1000	0.80	1.18	2.68	3.86	1.63
NH4	1400	0.83	0.69	2.73	3.42	1.69
NH5	1800	0.86	0.19	2.56	2.75	1.72
	2000		-0.06			
NH6	2200	0.89	-0.23	2.27	2.04	1.76
NH7	2600	0.91	-0.55	2.03	1.48	1.8
NH8	3000	0.92	-0.87	1.87	1.00	1.81
NH9	3400	0.94	-1.20	1.71	0.51	1.83
NH10	3800	0.95	-1.52	1.59	0.07	1.88
	4000		-1.68			
Average		**0.86**		**2.24**	**2.39**	**1.72**

Table 3.46: Wet probability P_w, mean free-surface elevation $\bar{\eta}$ (cm), and free-surface standard deviation σ_η (cm) for WG8 in D test series, SWL = 0 cm

Run	***t (s)***	P_w	z_b *(cm)*	$\bar{h}$ *(cm)*	$\bar{\eta}$ *(cm)*	σ_η *(cm)*
	0		16.55			
DL1	200	0.07	16.27	0.40	16.67	0.57
DL2	600	0.03	15.71	1.04	16.75	1.1
DL3	1000	0.05	15.15	1.10	16.25	1.02
DL4	1400	0.06	14.58	1.02	15.60	0.9
DL5	1800	0.06	14.02	0.91	14.93	0.77
	2000		13.74			
DL6	2200	0.06	13.78	0.96	14.74	0.83
DL7	2600	0.06	13.85	0.78	14.63	0.79
DL8	3000	0.06	13.93	0.74	14.67	0.72
DL9	3400	0.07	14.00	0.74	14.74	0.73
DL10	3800	0.07	14.08	0.80	14.88	0.7
	4000		14.12			
Average		**0.06**		**0.85**	**15.39**	**0.81**

Table 3.47: Wet probability P_w, mean free-surface elevation $\bar{\eta}$ (cm), and free-surface standard deviation σ_η (cm) for WG8 in D test series, SWL = 2 cm

Run	*t (s)*	P_w	z_b *(cm)*	$\bar{h}$ *(cm)*	$\bar{\eta}$ *(cm)*	σ_η *(cm)*
	0		11.76			
DM1	200	0.24	11.69	1.05	12.74	0.81
DM2	600	0.24	11.55	1.19	12.74	0.84
DM3	1000	0.26	11.42	1.14	12.56	0.81
DM4	1400	0.26	11.28	1.17	12.45	0.79
DM5	1800	0.28	11.14	1.14	12.28	0.79
	2000		11.07			
DM6	2200	0.25	11.07	1.16	12.23	0.73
DM7	2600	0.28	11.08	1.13	12.21	0.74
DM8	3000	0.27	11.09	1.15	12.24	0.73
DM9	3400	0.26	11.10	1.20	12.30	0.72
DM10	3800	0.26	11.12	1.19	12.31	0.73
	4000		11.12			
Average		**0.26**		**1.15**	**12.41**	**0.77**

Table 3.48: Wet probability P_w, mean free-surface elevation $\bar{\eta}$ (cm), and free-surface standard deviation σ_η (cm) for WG8 in D test series, SWL = 4 cm

Run	*t (s)*	P_w	z_b *(cm)*	$\bar{h}$ *(cm)*	$\bar{\eta}$ *(cm)*	σ_η *(cm)*
	0		9.06			
DH1	200	0.38	8.55	1.59	10.14	1.01
DH2	600	0.42	7.52	1.75	9.27	1.12
DH3	1000	0.54	6.49	1.68	8.17	1.23
DH4	1400	0.56	5.46	1.84	7.30	1.25
DH5	1800	0.59	4.43	1.97	6.40	1.32
	2000		3.91			
DH6	2200	0.64	3.58	2.18	5.76	1.37
DH7	2600	0.67	2.91	2.48	5.39	1.42
DH8	3000	0.70	2.25	2.61	4.86	1.49
DH9	3400	0.73	1.58	2.72	4.30	1.6
DH10	3800	0.76	0.92	2.89	3.81	1.65
	4000		0.58			
Average		**0.60**		**2.17**	**6.54**	**1.35**

Table 3.49: Wet probability P_w, mean free-surface elevation $\bar{\eta}$ (cm), and free-surface standard deviation σ_η (cm) for WG8 in R test series, SWL = 0 cm

Run	***t (s)***	P_w	z_b ***(cm)***	$\bar{h}$ ***(cm)***	$\bar{\eta}$ ***(cm)***	σ_η ***(cm)***
	0		6.15			
RL1	200	NR	6.10	NR	NR	NR
RL2	600	0.50	6.01	1.74	7.75	0.78
RL3	1000	0.50	5.91	1.85	7.76	0.81
RL4	1400	0.47	5.81	1.66	7.47	0.78
RL5	1800	0.58	5.72	1.79	7.51	0.79
RL6	2200	0.52	5.62	1.77	7.39	0.80
RL7	2600	0.51	5.53	1.47	7.00	0.76
RL8	3000	0.46	5.43	1.79	7.22	0.76
RL9	3400	0.38	5.33	2.00	7.33	0.77
RL10	3800	0.38	5.24	1.86	7.10	0.74
	4000		5.19			
Average		**0.48**		**1.77**	**7.39**	**0.78**

NR implies "not reliable" data

Table 3.50: Wet probability P_w, mean free-surface elevation $\bar{\eta}$ (cm), and free-surface standard deviation σ_η (cm) for WG8 in R test series, SWL = 2 cm

Run	*t (s)*	P_w	z_b *(cm)*	$\bar{h}$ *(cm)*	$\bar{\eta}$ *(cm)*	σ_η *(cm)*
	0		5.19			
RM1	200	0.72	5.20	2.72	7.92	1.24
RM2	600	0.74	5.23	1.98	7.21	1.31
RM3	1000	0.72	5.25	2.18	7.43	1.32
RM4	1400	0.73	5.27	2.27	7.54	1.34
RM5	1800	0.75	5.30	2.42	7.72	1.34
RM6	2200	0.76	5.32	2.36	7.68	1.38
RM7	2600	0.79	5.35	2.55	7.90	1.40
RM8	3000	0.78	5.37	2.58	7.95	1.40
RM9	3400	0.77	5.39	2.36	7.70	1.40
RM10	3800	0.79	5.42	2.44	7.86	1.42
	4000		5.43			
Average		**0.76**		**2.39**	**7.70**	**1.36**

Table 3.51: Wet probability P_w, mean free-surface elevation $\bar{\eta}$ (cm), and free-surface standard deviation σ_η (cm) for WG8 in R test series, SWL = 4 cm

Run	*t (s)*	P_w	z_b *(cm)*	$\bar{h}$ *(cm)*	$\bar{\eta}$ *(cm)*	σ_η *(cm)*
	0		5.43			
RH1	200	0.86	5.34	3.45	8.79	1.84
RH2	600	0.92	5.15	3.96	9.11	1.92
RH3	1000	0.90	4.97	4.02	8.99	1.94
RH4	1400	0.91	4.79	4.14	8.93	2.01
RH5	1800	0.89	4.60	3.45	8.05	2.03
RH6	2200	0.90	4.42	3.48	7.90	2.03
RH7	2600	0.90	4.23	3.51	7.74	2.06
RH8	3000	0.91	4.05	3.41	7.46	2.06
RH9	3400	0.91	3.87	3.22	7.09	2.06
RH10	3800	0.91	3.68	3.39	7.07	2.06
	4000		3.59			
Average		**0.90**		**3.60**	**8.11**	**2.00**

Table 3.52: Wet probability P_w, mean free-surface elevation $\bar{\eta}$ (cm), and free-surface standard deviation σ_η (cm) for WG8 in R test series, SWL = 6 cm

Run	*t (s)*	P_w	z_b *(cm)*	$\bar{h}$ *(cm)*	$\bar{\eta}$ *(cm)*	σ_η *(cm)*
	0		3.59			
RE1	200	0.92	3.45	3.76	7.21	2.79
RE2	600	0.91	3.17	3.27	6.44	2.86
RE3	1000	0.93	2.89	3.09	5.98	2.83
RE4	1400	0.94	2.61	2.95	5.56	2.86
RE5	1800	0.95	2.33	2.93	5.26	2.81
RE6	2200	0.94	2.05	3.01	5.06	2.78
RE7	2600	0.95	1.77	2.98	4.75	2.81
RE8	3000	0.94	1.49	3.08	4.57	2.78
RE9	3400	0.94	1.21	3.01	4.22	2.81
RE10	3800	0.95	0.93	3.11	4.04	2.81
	4000		0.79			
Average		**0.94**		**3.12**	**5.31**	**2.81**

Table 3.53: Wet probability P_w, mean free-surface elevation $\bar{\eta}$ (cm), and free-surface standard deviation σ_η (cm) for WG8 in B test series, SWL = 0 cm

Run	*t (s)*	P_w	z_b *(cm)*	$\bar{h}$ *(cm)*	$\bar{\eta}$ *(cm)*	σ_η *(cm)*
	0		3.42			
BL1	200	0.26	3.47	3.66	7.13	1.35
BL2	600	0.24	3.57	-0.40	3.17	1.08
BL3	1000	0.35	3.66	1.02	4.68	0.98
BL4	1400	0.32	3.76	1.10	4.86	1.00
BL5	1800	0.26	3.86	0.84	4.70	0.97
BL6	2200	0.29	3.95	0.75	4.70	0.89
BL7	2600	0.24	4.05	0.85	4.90	0.90
BL8	3000	0.25	4.15	0.75	4.90	0.86
BL9	3400	0.29	4.24	0.68	4.92	0.80
BL10	3800	0.28	4.34	0.74	5.08	0.78
	4000		4.39			
Average		**0.28**		**1.00**	**4.90**	**0.96**

Table 3.54: Wet probability P_w, mean free-surface elevation $\bar{\eta}$ (cm), and free-surface standard deviation σ_η (cm) for WG8 in B test series, SWL = 2 cm

Run	*t (s)*	P_w	z_b *(cm)*	$\bar{h}$ *(cm)*	$\bar{\eta}$ *(cm)*	σ_η *(cm)*
	0		4.39			
BM1	200	NR	4.39	NR	NR	NR
BM2	600	0.53	4.38	1.22	5.60	0.95
BM3	1000	0.61	4.37	NR	NR	0.94
BM4	1400	0.67	4.36	1.37	5.73	0.97
BM5	1800	0.69	4.35	1.21	5.56	0.96
BM6	2200	0.68	4.34	1.30	5.64	0.96
BM7	2600	0.68	4.33	1.39	5.72	0.96
BM8	3000	0.72	4.32	1.45	5.77	0.96
BM9	3400	0.75	4.31	1.37	5.68	0.97
BM10	3800	0.73	4.30	1.41	5.71	0.97
	4000		4.30			
Average		**0.67**		**1.34**	**5.68**	**0.96**

NR implies "not reliable" data

Table 3.55: Wet probability P_w, mean free-surface elevation $\bar{\eta}$ (cm), and free-surface standard deviation σ_η (cm) for WG8 in B test series, SWL = 4 cm

Run	*t (s)*	P_w	z_b *(cm)*	$\bar{h}$ *(cm)*	$\bar{\eta}$ *(cm)*	σ_η *(cm)*
	0		4.30			
BH1	200	0.94	4.22	2.66	6.88	2.17
BH2	600	0.89	4.07	2.85	6.92	1.89
BH3	1000	0.93	3.92	3.79	7.71	1.90
BH4	1400	0.93	3.77	3.31	7.08	1.91
BH5	1800	0.92	3.62	3.60	7.22	1.98
BH6	2200	0.93	3.46	3.75	7.21	1.97
BH7	2600	0.94	3.31	2.66	5.97	2.17
BH8	3000	0.93	3.16	3.60	6.76	1.97
BH9	3400	0.93	3.01	3.39	6.40	2.02
BH10	3800	0.94	2.86	3.75	6.61	1.81
	4000		2.78			
Average		**0.93**		**3.34**	**6.88**	**1.98**

Table 3.56: Wet probability P_w, mean free-surface elevation $\bar{\eta}$ (cm), and free-surface standard deviation σ_η (cm) for WG8 in B test series, SWL = 6 cm

Run	*t (s)*	P_w	z_b *(cm)*	$\bar{h}$ *(cm)*	$\bar{\eta}$ *(cm)*	σ_η *(cm)*
	0		2.78			
BE1	200	0.94	2.71	2.66	5.37	2.17
BE2	600	0.95	2.57	4.58	7.15	2.88
BE3	1000	0.93	2.42	4.21	6.63	3.02
BE4	1400	0.90	2.28	4.00	6.28	3.15
BE5	1800	0.90	2.14	4.14	6.28	3.16
BE6	2200	0.90	1.99	4.14	6.13	3.16
BE7	2600	0.91	1.85	4.17	6.02	3.14
BE8	3000	0.92	1.71	4.52	6.23	2.90
BE9	3400	0.93	1.56	4.31	5.87	2.81
BE10	3800	0.90	1.42	4.51	5.93	2.75
	4000		1.35			
Average		**0.93**		**4.12**	**6.19**	**2.91**

The mean $\overline{U}$ and standard deviation (SD) σ_U of the measured cross shore velocity *U* (explained in each table) for all the runs in series N, D, R, and B are listed in Tables 3.57 – 3.70. The measured alongshore and vertical velocities were small in comparison with the cross-shore velocity in this experiment. The negative mean horizontal velocity $\overline{U}$ represents wave-induced offshore return current, and the positive value of σ_U is related to the wave-induced oscillatory velocity. The return current and oscillatory velocity decreased from the breaker zone to the inner surf zone. The values of $\overline{U}$ of the order of -4cm/s were harder to measure accurately than those of σ_U of the order of 20 cm/s. The cross-shore wave transformation in the shoaling and surf zones was similar for all the runs because the beach profile in these zones was approximately in equilibrium under the specified incident waves. Further comparison of the experimental and numerical results for 140 runs in series N, D, R and B are shown in Figures 5.1- 5.14 in Chapter 5 with detailed explanations.

Table 3.57: Mean cross-shore $\bar{U}$ and SD σ_U of the 2D ADV co-located with WG4 at x = 8.30 m, Red Vectrino co-located with WG5 at x = 12.90 m and Blue Vectrino co-located with WG6 at x = 15.52 m for test series N, SWL = 0 cm

Run	2D ADV at WG4		Red Vectrino at WG5		Blue Vectrino at WG6	
	$\bar{U}$ (*cm/s*)	σ_u (*cm/s*)	$\bar{U}$ (*cm/s*)	σ_u (*cm/s*)	$\bar{U}$ (*cm/s*)	σ_u (*cm/s*)
NL1	-5.66	19.35	-3.60	15.82	-4.05	17.53
NL2	-5.46	19.47	-3.55	15.86	-3.71	17.14
NL3	-5.44	20.07	-3.66	16.19	-3.90	17.39
NL4	-6.02	20.24	-3.36	16.24	-3.82	17.43
NL5	-6.03	20.29	-3.41	16.29	-3.88	17.55
NL6	-5.73	20.35	-3.54	16.16	-3.50	16.71
NL7	-5.72	20.50	-3.30	16.48	-3.80	16.83
NL8	-5.82	20.52	NR	NR	-3.64	17.05
NL9	-5.35	20.59	NR	NR	-3.98	16.97
NL10	-5.31	20.45	NR	NR	-3.25	17.01
Average	**-5.65**	**20.18**	**-3.49**	**16.15**	**-3.75**	**17.16**

NR implies "not reliable" data

Table 3.58: Mean cross-shore $\overline{U}$ and SD σ_U of the 2D ADV co-located with WG4 at x = 8.30 m, Red Vectrino co-located with WG5 at x = 12.90 m and Blue Vectrino co-located with WG6 at x = 15.52 m for test series N, SWL = 2 cm

Run	2D ADV at WG4		Red Vectrino at WG5		Blue Vectrino at WG6	
	$\overline{U}$ (cm/s)	σ_u (cm/s)	$\overline{U}$ (cm/s)	σ_u (cm/s)	$\overline{U}$ (cm/s)	σ_u (cm/s)
NM1	-4.26	19.90	-3.43	17.39	-2.75	17.67
NM2	-4.46	20.16	-3.71	17.48	-2.86	17.50
NM3	-5.40	19.99	-3.85	17.87	NR	NR
NM4	-4.72	20.12	-3.84	17.73	-3.14	17.25
NM5	-4.61	20.25	-3.76	17.62	-3.18	17.41
NM6	-4.59	20.20	NR	NR	-3.01	17.14
NM7	-4.93	20.41	-4.01	17.71	-3.22	16.73
NM8	-4.79	20.41	-3.73	17.66	-3.34	16.61
NM9	-5.16	20.48	-4.24	17.84	-3.13	16.79
NM10	-5.47	20.45	-3.92	17.70	-2.91	16.76
Average	**-4.84**	**20.24**	**-3.83**	**17.67**	**-3.06**	**17.10**

NR implies "not reliable" data

Table 3.59: Mean cross-shore $\overline{U}$ and SD σ_U of the 2D ADV co-located with WG4 at x = 8.30 m, Red Vectrino co-located with WG5 at x = 12.90 m and Blue Vectrino co-located with WG6 at x = 15.52 m for test series N, SWL = 4 cm

Run	2D ADV at WG4		Red Vectrino at WG5		Blue Vectrino at WG6	
	$\overline{U}$ (cm/s)	σ_u (cm/s)	$\overline{U}$ (cm/s)	σ_u (cm/s)	$\overline{U}$ (cm/s)	σ_u (cm/s)
NH1	-4.40	20.09	-4.08	17.41	-3.72	17.61
NH2	-4.50	20.32	-4.35	17.30	-3.75	17.57
NH3	-4.81	20.35	-4.10	17.22	-3.79	17.58
NH4	-4.53	20.16	-4.02	17.10	NR	NR
NH5	-4.54	20.17	-3.86	17.00	-3.38	17.65
NH6	-3.96	20.10	-4.02	16.50	-3.79	17.70
NH7	-4.30	19.98	-4.07	16.46	-3.40	17.86
NH8	-4.53	19.88	-4.04	16.36	-3.68	17.65
NH9	-4.10	20.08	-4.27	16.16	-3.28	17.69
NH10	-4.38	19.86	NR	NR	NR	NR
Average	**-4.41**	**20.10**	**-4.09**	**16.83**	**-3.60**	**17.66**

NR implies "not reliable" data

Table 3.60: Mean cross-shore $\overline{U}$ and SD σ_U of the 2D ADV co-located with WG4 at x = 8.30 m, Red Vectrino co-located with WG5 at x = 12.90 m and Blue Vectrino co-located with WG6 at x = 15.52 m for test series D, SWL = 0 cm

Run	2D ADV at WG4		Red Vectrino at WG5		Blue Vectrino at WG6	
	$\overline{U}$ (cm/s)	σ_u (cm/s)	$\overline{U}$ (cm/s)	σ_u (cm/s)	$\overline{U}$ (cm/s)	σ_u (cm/s)
DL1	NR	NR	-3.24	16.08	-3.01	18.47
DL2	-5.36	20.79	-3.73	16.18	-3.54	18.40
DL3	-5.47	20.76	-3.97	16.32	-2.97	18.32
DL4	-5.08	21.15	-3.79	16.22	-3.08	18.34
DL5	-5.14	21.00	-3.88	16.31	-3.09	18.65
DL6	-4.66	21.13	-3.63	16.26	-3.55	18.45
DL7	-5.15	21.24	NR	NR	NR	NR
DL8	-4.95	21.38	-4.05	16.32	-2.99	18.50
DL9	-5.06	21.45	-4.17	16.28	-2.96	18.49
DL10	-5.44	21.05	-3.74	16.18	-3.08	18.31
Average	**-5.15**	**21.11**	**-3.80**	**16.24**	**-3.14**	**18.44**

NR implies "not reliable" data

Table 3.61: Mean cross-shore $\overline{U}$ and SD σ_U of the 2D ADV co-located with WG4 at x = 8.30 m, Red Vectrino co-located with WG5 at x = 12.90 m and Blue Vectrino co-located with WG6 at x = 15.52 m for test series D, SWL = 2 cm

Run	2D ADV at WG4		Red Vectrino at WG5		Blue Vectrino at WG6	
	$\overline{U}$ (cm/s)	σ_u (cm/s)	$\overline{U}$ (cm/s)	σ_u (cm/s)	$\overline{U}$ (cm/s)	σ_u (cm/s)
DM1	-4.75	19.85	-4.19	17.18	-2.82	18.54
DM2	-5.45	20.88	-4.45	17.13	-3.07	18.29
DM3	-5.03	21.05	-4.40	17.21	-3.60	18.02
DM4	-4.72	20.84	-4.09	17.16	-3.19	18.01
DM5	-5.03	20.96	-4.55	17.00	NR	NR
DM6	-5.26	20.87	-4.44	16.99	-2.69	18.14
DM7	-4.54	21.05	-4.25	16.94	-3.29	18.02
DM8	-5.41	21.16	-4.14	16.99	-3.40	17.91
DM9	-4.78	21.14	NR	NR	-2.96	17.88
DM10	-5.48	20.94	-4.24	17.20	-2.59	17.94
Average	**-5.05**	**20.87**	**-4.31**	**17.09**	**-3.07**	**18.08**

NR implies "not reliable" data

Table 3.62: Mean cross-shore $\overline{U}$ and SD σ_U of the 2D ADV co-located with WG4 at x = 8.30 m, Red Vectrino co-located with WG5 at x = 12.90 m and Blue Vectrino co-located with WG6 at x = 15.52 m for test series D, SWL = 4 cm

Run	2D ADV at WG4		Red Vectrino at WG5		Blue Vectrino at WG6	
	$\overline{U}$ (cm/s)	σ_u (cm/s)	$\overline{U}$ (cm/s)	σ_u (cm/s)	$\overline{U}$ (cm/s)	σ_u (cm/s)
DH1	-4.26	20.79	-4.14	17.66	-3.00	18.05
DH2	-4.10	20.59	-4.47	17.58	-2.93	17.83
DH3	-4.34	20.74	-4.52	17.23	NR	NR
DH4	-4.36	20.80	-4.20	17.45	-3.07	17.54
DH5	-3.97	21.08	-4.68	17.31	-3.18	17.48
DH6	-3.72	20.65	-4.50	17.55	-3.87	17.33
DH7	-4.60	20.70	-4.92	17.38	-3.44	17.79
DH8	-4.46	20.65	-4.53	17.35	-3.37	17.94
DH9	-4.14	20.70	-4.09	17.12	-3.17	18.01
DH10	-3.99	20.77	-4.33	17.05	-3.49	18.11
Average	**-4.19**	**20.75**	**-4.44**	**17.37**	**-3.28**	**17.79**

NR implies "not reliable" data

Table 3.63: Mean cross-shore $\overline{U}$ and SD σ_U of the 2D ADV co-located with WG4 at x = 8.30 m, Red Vectrino co-located with WG5 at x = 12.90 m and Blue Vectrino co-located with WG6 at x = 15.52 m for test series R, SWL = 0 cm

Run	2D ADV at WG4		Red Vectrino at WG5		Blue Vectrino at WG6	
	$\overline{U}$ (cm/s)	σ_u (cm/s)	$\overline{U}$ (cm/s)	σ_u (cm/s)	$\overline{U}$ (cm/s)	σ_u (cm/s)
RL1	-5.50	20.84	-3.80	18.71	-2.86	17.47
RL2	-6.34	21.35	-3.64	15.64	-3.04	16.40
RL3	-5.72	21.44	-3.73	15.75	NR	NR
RL4	-6.03	21.17	-4.15	15.68	-3.30	16.29
RL5	-5.96	21.12	-4.31	15.76	-3.20	16.35
RL6	-5.40	21.51	-4.00	15.79	-3.02	16.34
RL7	-5.37	21.57	-4.22	15.80	-3.31	16.06
RL8	-5.71	21.21	-4.18	15.97	-2.92	16.18
RL9	-6.26	21.19	-4.19	16.09	-3.56	16.19
RL10	-5.70	21.19	-3.90	15.91	-2.77	16.01
Average	**-5.80**	**21.26**	**-3.99**	**16.11**	**-3.11**	**16.37**

NR implies "not reliable" data

Table 3.64: Mean cross-shore $\overline{U}$ and SD σ_U of the 2D ADV co-located with WG4 at x = 8.30 m, Red Vectrino co-located with WG5 at x = 12.90 m and Blue Vectrino co-located with WG6 at x = 15.52 m for test series R, SWL = 2 cm

Run	2D ADV at WG4		Red Vectrino at WG5		Blue Vectrino at WG6	
	$\overline{U}$ (cm/s)	σ_u (cm/s)	$\overline{U}$ (cm/s)	σ_u (cm/s)	$\overline{U}$ (cm/s)	σ_u (cm/s)
RM1	-4.94	20.99	NR	NR	NR	NR
RM2	-5.01	20.97	-4.83	16.52	-2.81	17.34
RM3	-5.36	20.88	-4.31	16.45	-3.34	17.22
RM4	-5.35	21.00	-4.49	16.52	-3.22	17.28
RM5	-5.36	21.08	-4.62	16.60	NR	NR
RM6	-5.28	21.07	NR	NR	-3.08	17.24
RM7	-5.08	20.96	-4.73	16.61	NR	NR
RM8	-4.48	20.92	-5.58	18.89	-2.86	17.09
RM9	-4.76	20.96	-4.20	16.71	-3.02	17.22
RM10	-4.92	20.77	-4.59	16.69	-2.85	17.08
Average	**-5.05**	**20.96**	**-4.74**	**16.90**	**-3.03**	**17.21**

NR implies "not reliable" data

Table 3.65: Mean cross-shore $\overline{U}$ and SD σ_U of the 2D ADV co-located with WG4 at x = 8.30 m, Red Vectrino co-located with WG5 at x = 12.90 m and Blue Vectrino co-located with WG6 at x = 15.52 m for test series R, SWL = 4 cm

Run	2D ADV at WG4		Red Vectrino at WG5		Blue Vectrino at WG6	
	$\overline{U}$ (cm/s)	σ_u (cm/s)	$\overline{U}$ (cm/s)	σ_u (cm/s)	$\overline{U}$ (cm/s)	σ_u (cm/s)
RH1	-4.87	20.38	-4.10	16.96	-3.33	17.34
RH2	-4.52	20.30	-4.28	16.77	-3.50	17.24
RH3	-4.68	20.53	-4.67	16.78	-3.16	17.27
RH4	-4.28	20.61	-4.56	16.80	-3.29	17.37
RH5	-4.12	20.59	-4.66	16.80	-3.31	17.41
RH6	-4.97	20.61	-4.46	16.77	-3.20	17.38
RH7	-4.17	20.61	-4.25	16.67	-3.46	17.35
RH8	-4.47	20.61	-4.41	16.55	-3.10	17.31
RH9	-4.12	20.49	-4.27	16.55	-2.94	17.34
RH10	-4.31	20.72	-4.26	16.71	-2.88	17.18
Average	**-4.45**	**20.55**	**-4.41**	**16.76**	**-3.22**	**17.31**

NR implies "not reliable" data

Table 3.66: Mean cross-shore $\overline{U}$ and SD σ_U of the 2D ADV co-located with WG4 at x = 8.30 m, Red Vectrino co-located with WG5 at x = 12.90 m and Blue Vectrino co-located with WG6 at x = 15.52 m for test series R, SWL = 6 cm

Run	2D ADV at WG4		Red Vectrino at WG5		Blue Vectrino at WG6	
	$\overline{U}$ (cm/s)	σ_u (cm/s)	$\overline{U}$ (cm/s)	σ_u (cm/s)	$\overline{U}$ (cm/s)	σ_u (cm/s)
RE1	-3.91	20.44	-4.20	17.51	-2.75	17.28
RE2	-3.80	20.65	NR	NR	NR	NR
RE3	-4.12	20.66	-4.45	17.33	-2.75	17.61
RE4	-4.10	20.36	-4.09	19.85	-2.84	17.10
RE5	-3.66	20.34	-4.56	17.28	-2.84	17.04
RE6	-4.24	20.65	-4.44	17.38	NR	NR
RE7	-3.82	20.42	-4.73	17.35	NR	NR
RE8	-4.18	20.66	-4.53	17.19	NR	NR
RE9	-3.80	21.11	-4.40	17.17	-3.14	17.20
RE10	-4.04	21.11	-4.55	17.13	-2.91	17.34
Average	**-3.97**	**20.64**	**-4.44**	**17.63**	**-2.87**	**17.31**

NR implies "not reliable" data

Table 3.67: Mean cross-shore $\overline{U}$ and SD σ_U of the 2D ADV co-located with WG4 at x = 8.30 m, Red Vectrino co-located with WG5 at x = 12.90 m and Blue Vectrino co-located with WG6 at x = 15.52 m for test series B, SWL = 0 cm

Run	2D ADV at WG4		Red Vectrino at WG5		Blue Vectrino at WG6	
	$\overline{U}$ (cm/s)	σ_u (cm/s)	$\overline{U}$ (cm/s)	σ_u (cm/s)	$\overline{U}$ (cm/s)	σ_u (cm/s)
BL1	NR	NR	NR	NR	NR	NR
BL2	-4.50	21.46	-3.64	15.71	-3.18	16.83
BL3	-4.94	20.93	-3.78	15.62	NR	NR
BL4	-4.80	21.11	-3.79	15.82	NR	NR
BL5	-4.43	21.03	-3.69	15.85	-3.24	16.85
BL6	-4.28	20.57	-3.78	15.83	-3.50	16.83
BL7	-4.63	20.89	-3.77	15.76	-3.26	17.04
BL8	-4.46	20.77	-3.76	15.76	-3.23	17.02
BL9	-5.04	20.71	-3.72	15.73	-3.48	17.06
BL10	-4.72	20.73	-3.87	15.68	-3.01	16.92
Average	**-4.64**	**20.91**	**-3.76**	**15.75**	**-3.27**	**16.95**

NR implies "not reliable" data

Table 3.68: Mean cross-shore $\overline{U}$ and SD σ_U of the 2D ADV co-located with WG4 at x = 8.30 m, Red Vectrino co-located with WG5 at x = 12.90 m and Blue Vectrino co-located with WG6 at x = 15.52 m for test series B, SWL = 2 cm

Run	2D ADV at WG4		Red Vectrino at WG5		Blue Vectrino at WG6	
	$\overline{U}$ (cm/s)	σ_u (cm/s)	$\overline{U}$ (cm/s)	σ_u (cm/s)	$\overline{U}$ (cm/s)	σ_u (cm/s)
BM1	-5.08	21.03	-4.37	16.11	-2.99	16.08
BM2	-4.82	21.15	-3.48	18.15	-3.23	16.58
BM3	-5.00	21.16	-3.37	18.37	-2.96	16.67
BM4	-4.98	21.41	-3.39	18.44	-3.32	16.68
BM5	-4.88	21.44	-4.24	16.33	-2.79	16.67
BM6	-4.95	21.48	-4.27	16.32	-2.66	16.60
BM7	-5.12	21.21	-4.79	16.21	NR	NR
BM8	-5.04	21.21	-4.48	16.34	NR	NR
BM9	-4.71	21.33	NR	NR	NR	NR
BM10	-4.99	21.33	-4.27	16.30	-2.71	16.62
Average	**-4.96**	**21.28**	**-4.07**	**16.95**	**-2.95**	**16.54**

NR implies "not reliable" data

Table 3.69: Mean cross-shore $\overline{U}$ and SD σ_U of the 2D ADV co-located with WG4 at x = 8.30 m, Red Vectrino co-located with WG5 at x = 12.90 m and Blue Vectrino co-located with WG6 at x = 15.52 m for test series B, SWL = 4 cm

Run	2D ADV at WG4		Red Vectrino at WG5		Blue Vectrino at WG6	
	$\overline{U}$ (cm/s)	σ_u (cm/s)	$\overline{U}$ (cm/s)	σ_u (cm/s)	$\overline{U}$ (cm/s)	σ_u (cm/s)
BH1	-4.49	20.75	-3.94	16.16	-2.81	16.44
BH2	-4.25	20.86	-4.39	16.70	-3.34	16.72
BH3	-3.94	20.98	-4.19	16.22	-3.04	16.03
BH4	-3.73	20.87	-4.29	16.15	-3.00	16.02
BH5	-3.96	20.90	-4.07	16.06	NR	NR
BH6	-3.62	20.56	-4.39	16.52	-3.24	16.45
BH7	-3.23	20.66	-4.90	16.53	-3.17	16.51
BH8	-3.39	20.41	-4.58	16.51	-3.35	16.40
BH9	-4.11	20.51	-4.82	16.58	-3.32	16.33
BH10	-3.65	20.70	-4.54	16.52	-3.08	16.31
Average	**-3.84**	**20.72**	**-4.37**	**16.37**	**-3.15**	**16.36**

NR implies "not reliable" data

Table 3.70: Mean cross-shore $\overline{U}$ and SD σ_U of the 2D ADV co-located with WG4 at x = 8.30 m, Red Vectrino co-located with WG5 at x = 12.90 m and Blue Vectrino co-located with WG6 at x = 15.52 m for test series B, SWL = 6 cm

Run	2D ADV at WG4		Red Vectrino at WG5		Blue Vectrino at WG6	
	$\overline{U}$ (cm/s)	σ_u (cm/s)	$\overline{U}$ (cm/s)	σ_u (cm/s)	$\overline{U}$ (cm/s)	σ_u (cm/s)
BE1	-3.27	20.89	-4.23	17.21	-2.90	16.53
BE2	-3.32	20.95	-5.26	20.03	-3.44	16.60
BE3	-3.36	21.15	-4.46	16.93	-2.93	16.65
BE4	-3.26	20.99	-5.31	19.70	-3.32	16.64
BE5	-2.95	20.74	-4.13	17.14	-2.88	16.69
BE6	-2.97	20.76	-4.46	16.94	-3.23	16.67
BE7	-2.57	20.76	-4.60	16.85	-3.24	16.62
BE8	-2.63	20.84	-4.49	16.90	-2.86	16.79
BE9	-3.17	20.92	-3.95	16.96	-3.36	16.71
BE10	-2.13	21.17	-4.16	16.96	-3.06	16.72
Average	**-2.96**	**20.92**	**-4.51**	**17.56**	**-3.12**	**16.66**

NR implies "not reliable" data

3.2 Wave Overtopping and Overwash Rates

The volume of water and sand transported over the impermeable vertical wall were used to obtain the water overtopping rate q_o and sand overwash rate q_{bs} per unit width averaged over each 400 s run as listed in Tables 3.71 - 3.79 where tests with $q_o = 0$ and $q_{bs} = 0$ are omitted. Figure 3.1 shows the temporal variations of q_o and q_{bs} for all the runs in each of the four test series.

Table 3.71: Measured sediment overwash rate (q_{bs}), and water overtopping rate (q_o) for test series N, SWL = 0 cm

Run	q_{bs} (cm^2/s)	q_o (cm^2/s)
NL1	0.0011	0.199
NL2	0.0009	0.161
NL3	0.0024	0.242
NL4	0.0027	0.222
NL5	0.0026	0.243
NL6	0.0026	0.211
NL7	0.0022	0.214
NL8	0.0030	0.224
NL9	0.0029	0.214
NL10	0.0022	0.197

Table 3.72: Measured sediment overwash rate (q_{bs}), and water overtopping rate (q_o) for test series N, SWL = 2 cm

Run	q_{bs} (cm^2/s)	q_o (cm^2/s)
NM1	0.0223	1.447
NM2	0.0217	1.085
NM3	0.0228	1.046
NM4	0.0183	0.771
NM5	0.0200	0.833
NM6	0.0189	0.679
NM7	0.0180	0.620
NM8	0.0181	0.541
NM9	0.0183	0.560
NM10	0.0185	0.526

Table 3.73: Measured sediment overwash rate (q_{bs}), and water overtopping rate (q_o) for test series N, SWL = 4 cm

Run	q_{bs} (cm^2/s)	q_o (cm^2/s)
NH1	0.1175	2.362
NH2	0.1044	2.424
NH3	0.1102	2.900
NH4	0.1019	3.023
NH5	0.0972	3.061
NH6	0.0983	3.164
NH7	0.0956	3.256
NH8	0.0799	3.137
NH9	0.0863	3.182
NH10	0.0870	3.301

Table 3.74: Measured sediment overwash rate (q_{bs}), and water overtopping rate (q_o) for test series D, SWL = 2 cm

Run	q_{bs} (cm^2/s)	q_o (cm^2/s)
DM1	0.0001	0.005
DM2	0.0001	0.003
DM3	0.0000	0.000
DM4	0.0000	0.000
DM5	0.0003	0.009
DM6	0.0004	0.012
DM7	0.0007	0.016
DM8	0.0020	0.056
DM9	0.0046	0.143
DM10	0.0078	0.312

Table 3.75: Measured sediment overwash rate (q_{bs}), and water overtopping rate (q_o) for test series D, SWL = 4 cm

Run	q_{bs} (cm^2/s)	q_o (cm^2/s)
DH1	0.0629	2.426
DH2	0.0896	2.995
DH3	0.0863	2.645
DH4	0.0867	2.486
DH5	0.0837	2.447
DH6	0.0810	2.272
DH7	0.0845	2.328
DH8	0.0806	2.363
DH9	0.0801	2.408
DH10	0.0738	2.321

Table 3.76: Measured sediment overwash rate (q_{bs}), and water overtopping rate (q_o) for test series R, SWL = 4 cm

Run	q_{bs} (cm^2/s)	q_o (cm^2/s)
RH1	0.000014	0.0164
RH2	0.000007	0.0049
RH3	0.000006	0.0031
RH4	0.000008	0.0077
RH5	0.000033	0.0191
RH6	0.000033	0.0132
RH7	0.000043	0.0176
RH8	0.000041	0.0178
RH9	0.000054	0.0168
RH10	0.000022	0.0123

Table 3.77: Measured sediment overwash rate (q_{bs}), and water overtopping rate (q_o) for test series R, SWL = 6 cm

Run	q_{bs} (cm^2/s)	q_o (cm^2/s)
RE1	0.0124	0.745
RE2	0.0211	0.599
RE3	0.0184	0.484
RE4	0.0085	0.363
RE5	0.0097	0.331
RE6	0.0205	0.456
RE7	0.0125	0.397
RE8	0.0189	0.432
RE9	0.0199	0.479
RE10	0.0190	0.479

Table 3.78: Measured sediment overwash rate (q_{bs}), and water overtopping rate (q_o) for test series B, SWL = 4 cm

Run	q_{bs} (cm^2/s)	q_o (cm^2/s)
BH1	0.000134	0.0131
BH2	0.000174	0.0249
BH3	0.000297	0.0362
BH4	0.000097	0.0276
BH5	0.000064	0.0226
BH6	0.000051	0.0236
BH7	0.000048	0.0313
BH8	0.000046	0.0237
BH9	0.000033	0.0217
BH10	0.000016	0.0186

Table 3.79: Measured sediment overwash rate (q_{bs}), and water overtopping rate (q_o) for test series B, SWL = 6 cm

Run	q_{bs} (cm^2/s)	q_o (cm^2/s)
BE1	0.0239	0.975
BE2	0.0236	0.679
BE3	0.0212	0.645
BE4	0.0186	0.534
BE5	0.0178	0.450
BE6	0.0183	0.525
BE7	0.0173	0.437
BE8	0.0140	0.418
BE9	0.0145	0.420
BE10	0.0161	0.442

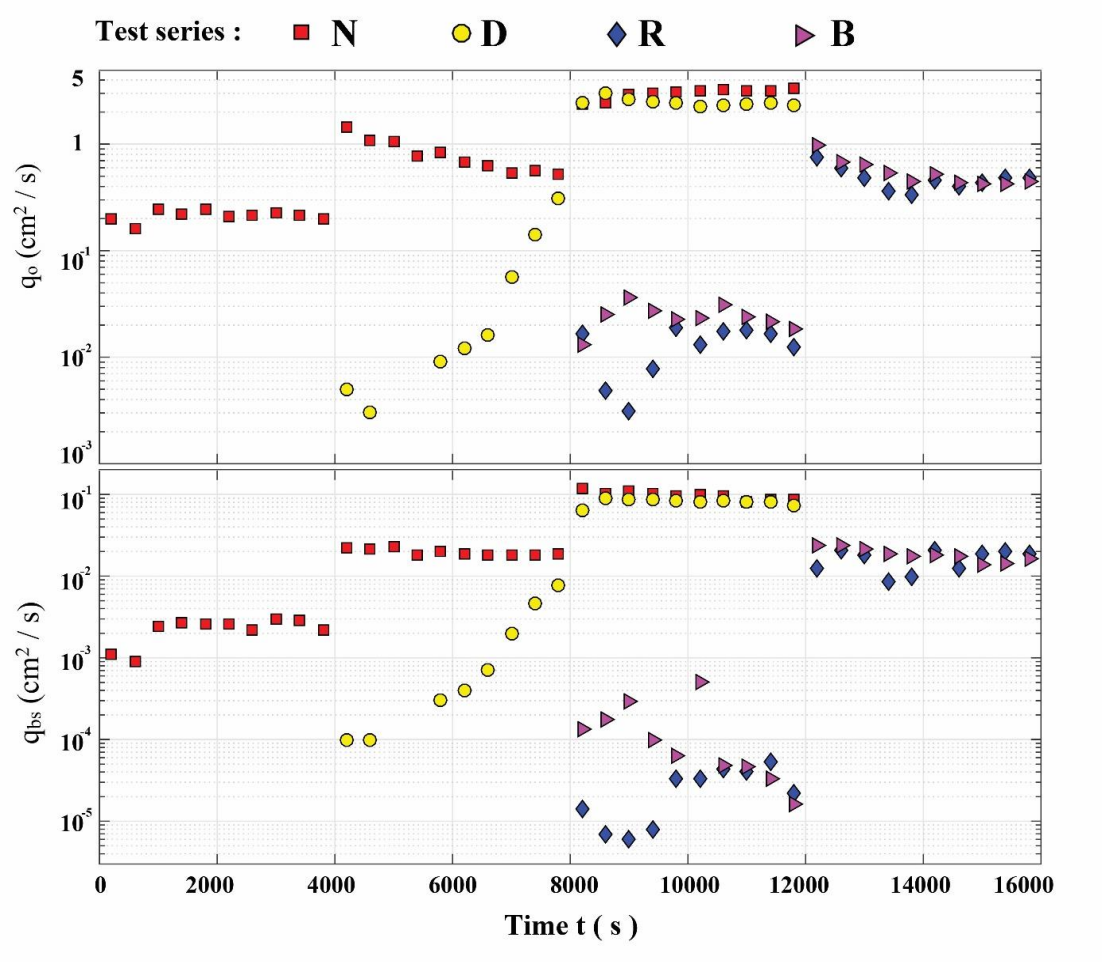

Figure 3.1: The temporal variations of q_o and q_{bs} for all the runs in each of the four test series: N, D, R, and B

Logarithmic plotting shown in Figure 3.1 does not contain the data points with q_o and q_{bs} = 0. The average rates are plotted at time t correspond to the middle of each run where t = 0 at the start of each test series. The SWL was increased by 2 cm increment at t = 4,000, 8,000, and 12,000 s for N and D test series, and up to 16,000 s for both R and B test series. As shown in Figure 3.1 and Tables 3.71 - 3.79, measured values of q_o and q_{bs} for given SWL were different among the N, D, R, and B test series.

Both q_o and q_{bs} did not change much during 10 runs with constant SWL but increased significantly with the increase of SWL.

For no protection (N) test series, both wave overtopping and sand overwash started to occur from the beginning of the test with SWL = 0 cm; however, for dune only (D) test series, dune prevented wave overtopping and overwash for SWL = 0 cm (t = 0 – 4,000 s) but the values soon approached to those for the N test series when SWL increased to 2 cm and became almost the same during t = 8,000 – 12,000 s with the dune's destruction. For rock seawall (R) test series and buried rock seawall (B) test series, no overtopping and overwash occurred for SWL = 0-2 cm and during t = 0 – 8,000 s. The values of q_o and q_{bs} were reduced significantly during t = 8,000 – 12,000 s in comparison to the N and D test series. Even with extreme water depth (SWL = 6 cm), the values of q_o and q_{bs} during t = 12,000 – 16,000 s were still smaller than those for N and D test series. R and B test series were similar in terms of q_o and q_{bs}; however, B test series produced slightly larger values during t = 8,000 – 12,000 s with SWL = 4 cm because of reduced roughness with sand in the stone voids. The dune in series B was destroyed during t = 8,000 – 12,000 s with q_o and q_{bs} of the order of 0.02 and 10^{-4} cm^2/s, respectively. The increase of q_o and q_{bs} to the order of 0.5 and 0.02 cm^2/s during t = 12,000 – 16,000 s for the R and B test series reduced the difference between these two test series because of sand removal from the buried stone seawall during t = 12,000 – 16,000 s.

3.3 Beach Profile Evolution

Figures 3.2- 3.5 are measured profiles of N, D, R, and B test series at t = 0, 4,000, 8,000, and 12,000 s for both N and D test series, and t = 0, 4,000, 8,000, 12,000, and 16,000 s for both R and B test series with the elevation = 0 corresponding to the SWL = 0 cm at t = 0. For brevity, t = 0, t_1 = 4,000 s, t_2 = 8,000 s, t_3 = 12,000 s and t_4 = 16,000 s in these figures. The profiles were measured along x = 0 – 20 m but the zone of x = 16 – 19.9 m of noticeable profile changes are presented for clarity. For N test series as shown in Figure 3.2, foreshore slope was eroded and become slightly steeper at t = 4,000 s. The eroded sand was deposited on the berm and transported over the vertical wall located at x = 19.9 m. A sediment budget analysis for the zone of x = 16 – 19.9 m indicated that some of the eroded sand was also dispersed offshore from x = 16 m. However, the deposited sand was not detectable from the profile measurement of 1 mm uncertainty. Increasing SWL by 2 cm caused the trend of foreshore erosion as well as berm accretion during t = 4,000 – 8,000 s with SWL = 2 cm. Additional increase of 2 cm of SWL caused upward increase of foreshore erosion with no berm accretion during t = 8,000 – 12,000 s.

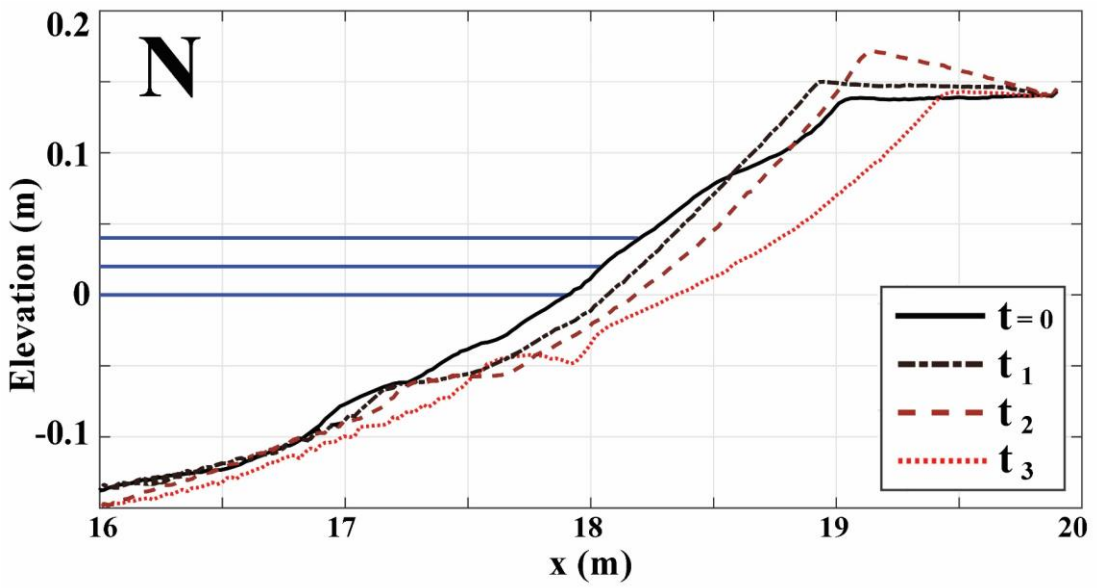

Figure 3.2: Series N profile evolution with 2 cm SWL increases: SWL = 0 cm, 2 cm, and 4 cm

Figure 3.3 is the profile evolution of the series D, dune only test series. There was no wave overtopping nor sand overwash during t = 0 – 4,000 s; however, seaward dune slope was eroded. When SWL was increased by 2 cm during t = 4,000- 8,000 s, wave overtopping and sand overwash were initiated and decreased the dune crest. Some of the overwashed sand was deposited on the berm after the 2 cm increase of SWL. Further SWL increase of 2 cm caused the destruction of the dune and foreshore was eroded at t = 12,000 s. The narrow dune is vulnerable and its effectiveness in comparison to series N with no dune is essentially limited to the condition of no wave overtopping.

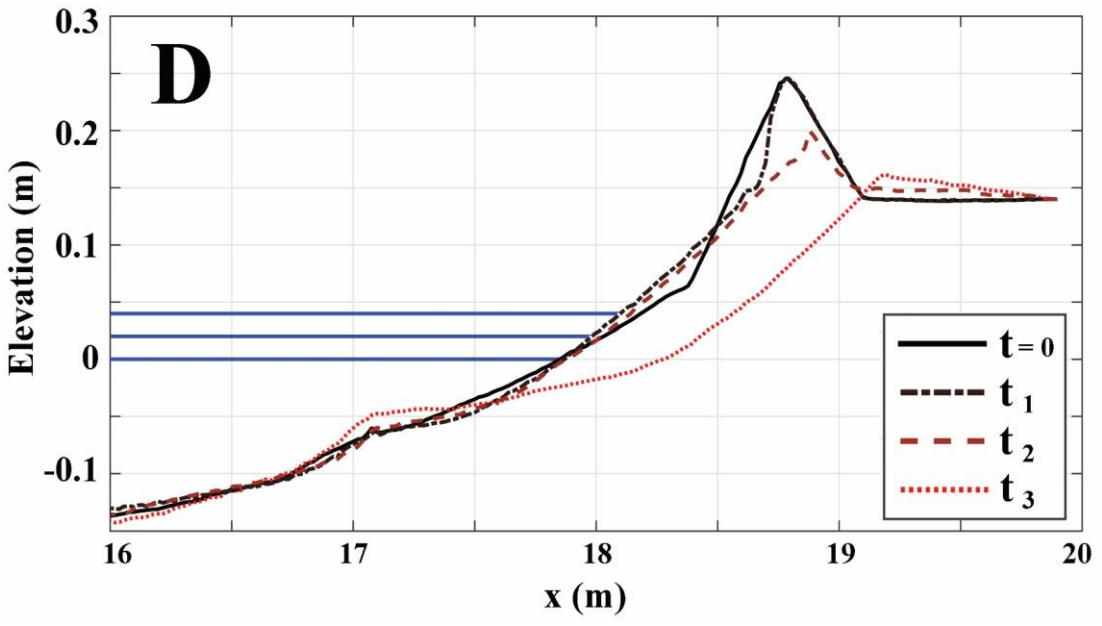

Figure 3.3: Series D profile evolution with 2 cm SWL increases: SWL = 0 cm, 2 cm, and 4 cm

The rock seawall test series R, Figure 3.4 shows the profile evolution of measured profiles at t = 0, 4,000, 8,000, 12,000 and 16,000 s. During t = 0 – 4,000 s with SWL = 0 cm and t = 4,000 – 8,000 s with SWL = 2 cm, respectively, no wave overtopping nor sand overwash occurred and the profile change was relatively small compare to test series N and D. Slight foreshore erosion occurred at t = 4,000 s. Wave uprush penetrated through the porous seawall and deposited sand on the berm at t = 8,000 s. During t = 8,000 – 12,000 s, with SWL = 4 cm, minor wave overtopping occurred and sand beach was eroded on foreshore and accreted on the berm. When the SWL was increased to 6 cm, wave overtopping and overwash increased significantly but relatively smaller than that of N and D test series. Scour trench was created landward of the seawall and the seaward slope and crest of the seawall was eroded.

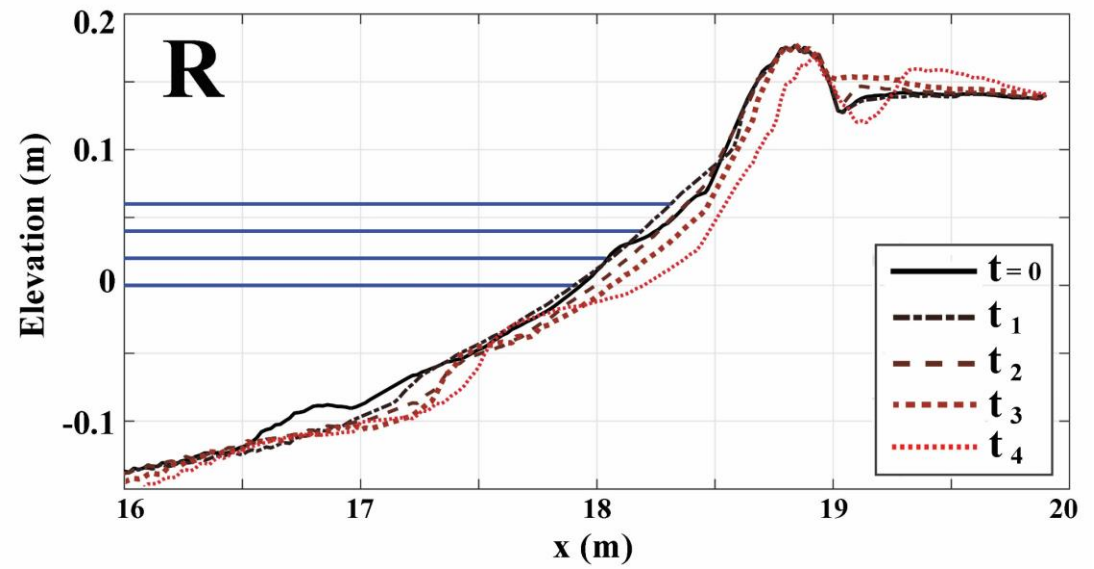

Figure 3.4: Series R profile evolution with 2 cm SWL increases: SWL = 0 cm, 2 cm, 4 cm, and 6 cm

The profile evolution of buried seawall test series, series B, is shown in Figure 3.5. During t = 0 – 4,000 s, similar to the dune test series D, the seaward dune slope was eroded but no wave overtoping occurred. Figure 3.6 compares the experimental photo taken at t = 4,000 s for series B with SWL = 0 cm and the uncovered relic seawall photo at Bay Head after Hurricane Sandy presented by Irish et al. (2013). The similarity of the photos suggests that wave overtopping at Bay Head during Hurricane Sandy might not have occurred. During t = 4,000 – 8,000 s, dune slope erosion continued with little dune crest lowering and still no wave overtopping. The dune was destroyed during t = 8,000 – 12,000 s. Overtopping and overwash rates became larger during t = 12,000 – 16,000 s (Figure 3.1) and no sand remained on the seawall by the end of this test series. The observed seawall exposure progression is presented by photos taken after every run (400 s) in Figures 3.7 – 3.10. After sand was removed, the

profile change became similar to that of series R and the profile changes during t = 4,000 – 16,000 s might suggest the performance of the relic seawall at the Bay Head for storms with higher storm surge than that of Hurricane Sandy.

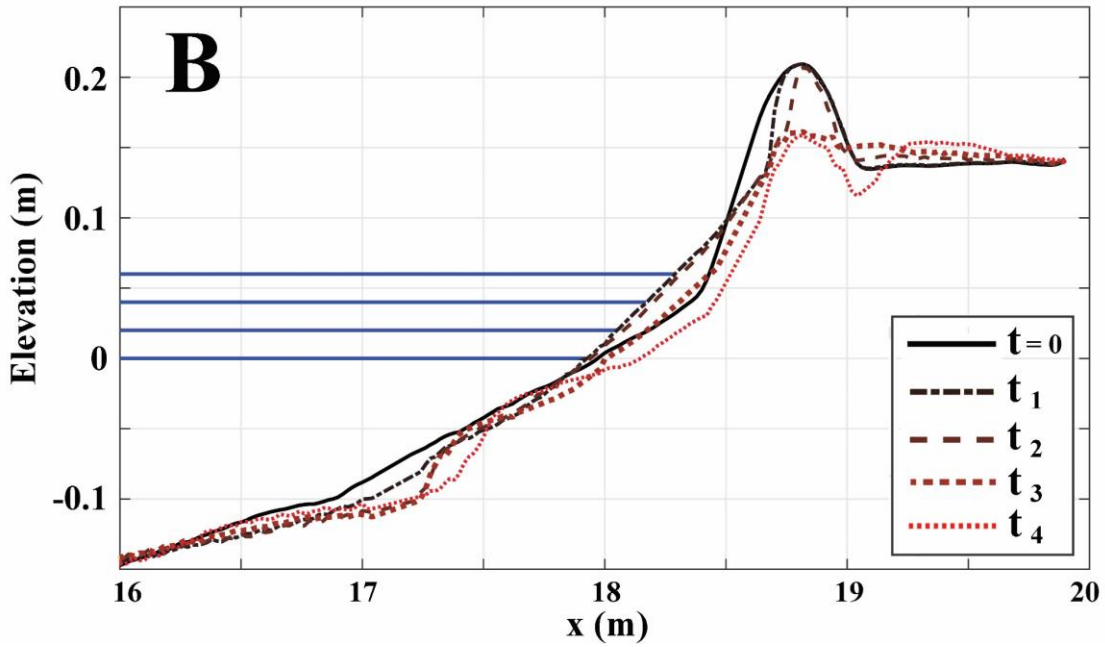

Figure 3.5: Series B profile evolution with 2 cm SWL increases: SWL = 0 cm, 2 cm, 4 cm, and 6 cm

Figure 3.6: Partially exposed stone due to dune erosion after 10 runs (4,000 s) in series B and after Hurricane Sandy at Bay Head (Irish et al 2013)

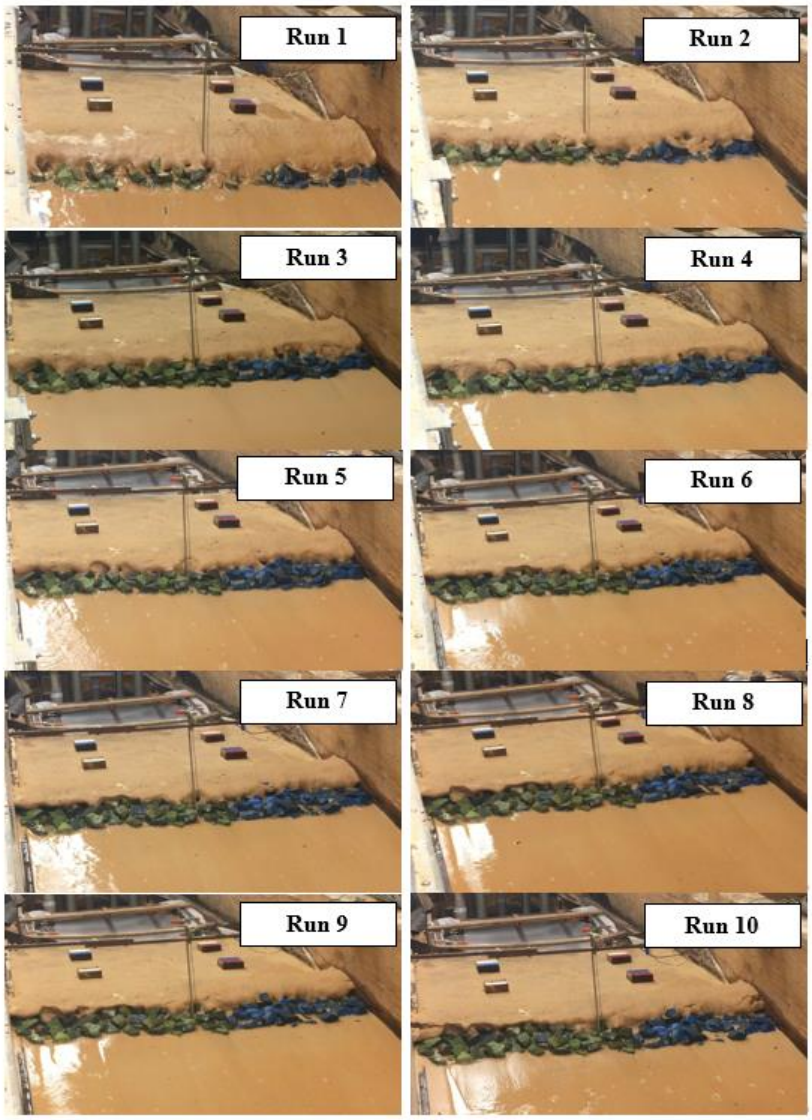

Figure 3.7: Seawall exposure progression for series B during t = 0-4,000 s

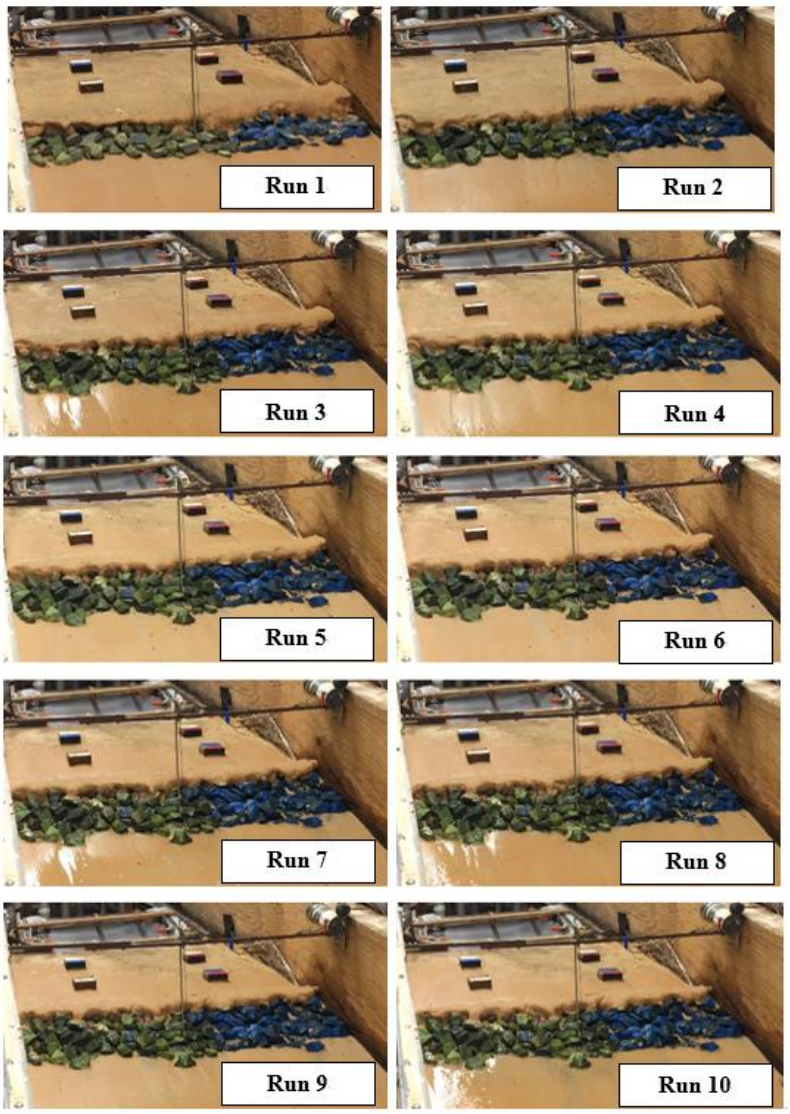

Figure 3.8: Seawall exposure progression for series B during t = 4,000-8,000 s

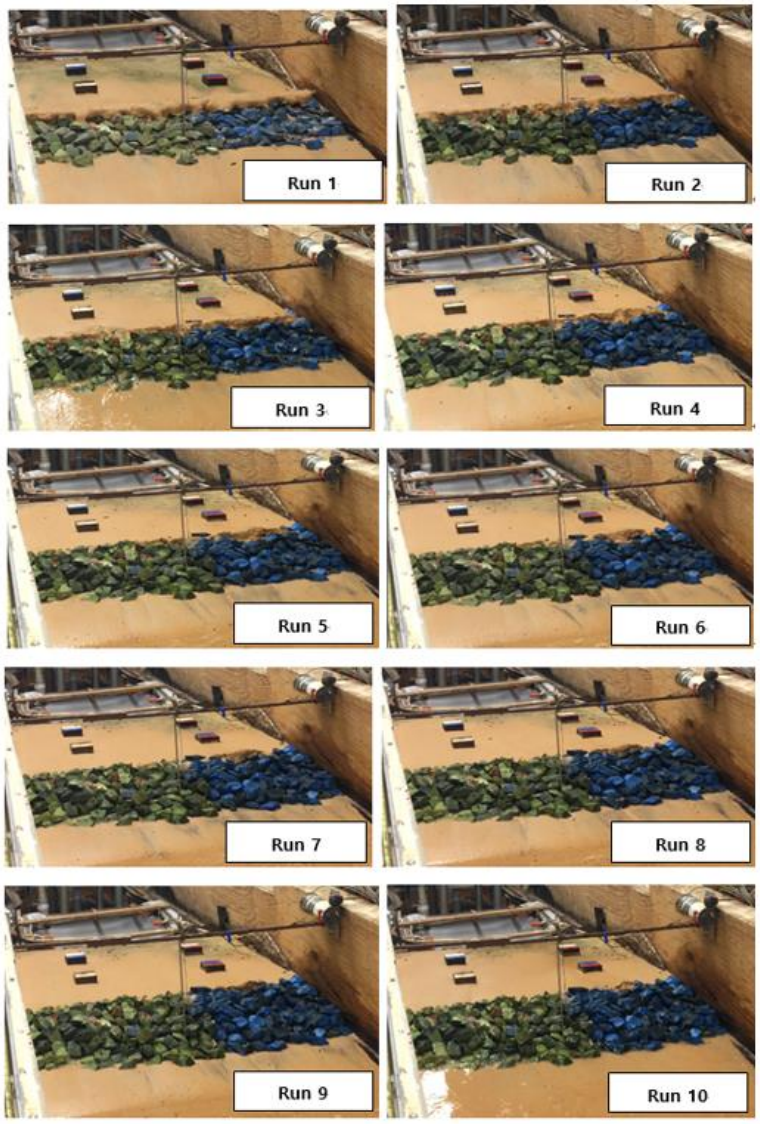

Figure 3.9: Seawall exposure progression for series B during t = 8,000-12,000 s

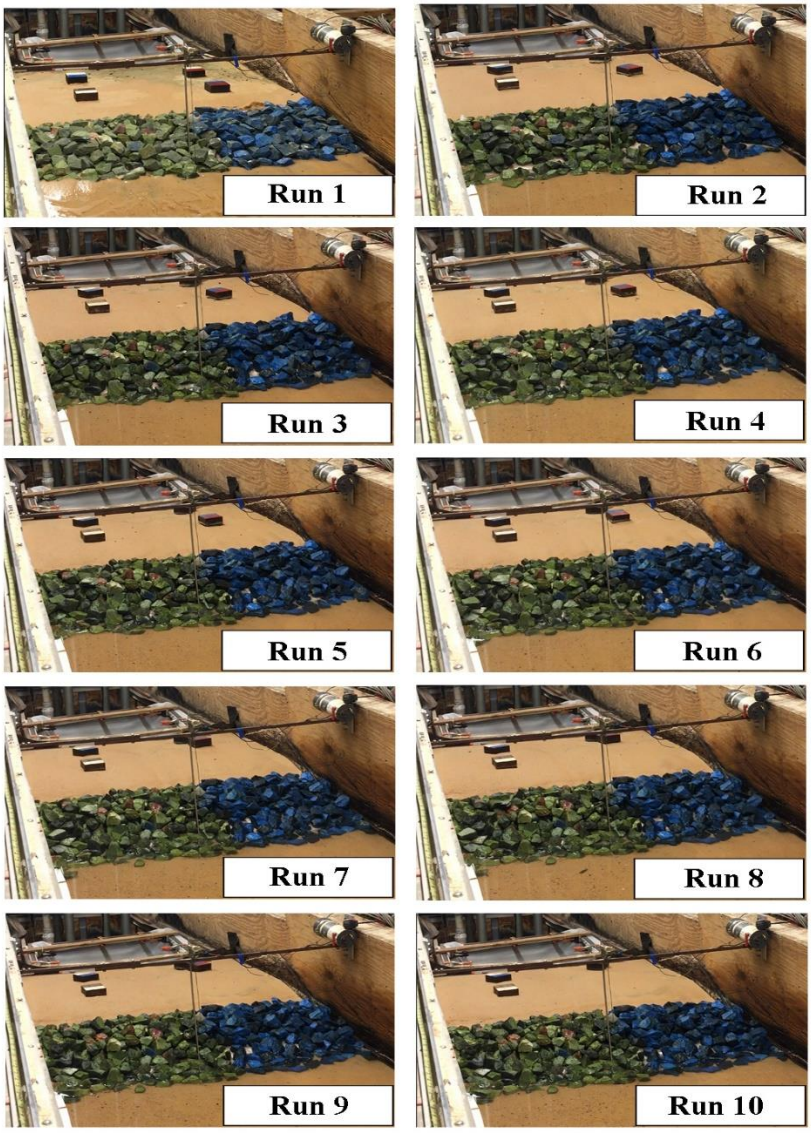

Figure 3.10: Seawall exposure progression for series B during t = 12,000-16,000 s

3.4 Deposited Sand Height inside Porous Seawall

After test series R and B, stones were removed carefully to measure sand deposited and remaining on the fabric mesh. This procedure was adopted in the previous experiment with a submerged breakwater in the surf zone on a beach using the same sand and stones by Garcia and Kobayashi (2015). Deposited sand height on the mesh was measured with the three dimensional laser scanner as shown in Figure 3.11. The deposited sand mass was also measured to estimate the porosity of the sand, which was about 0.58, and the loose sand height was converted to the beach sand height with porosity of 0.4. The measured and adjusted profiles are shown in the top panels in Figure 3.11. The deposited and adjusted sand heights are presented in the bottom panels. The sand poured into the stone voids the B test series initially were removed by wave action in the swash zone. The average sand height on the fabric mesh was 0.6 and 1.0 mm after series R and B, respectively.

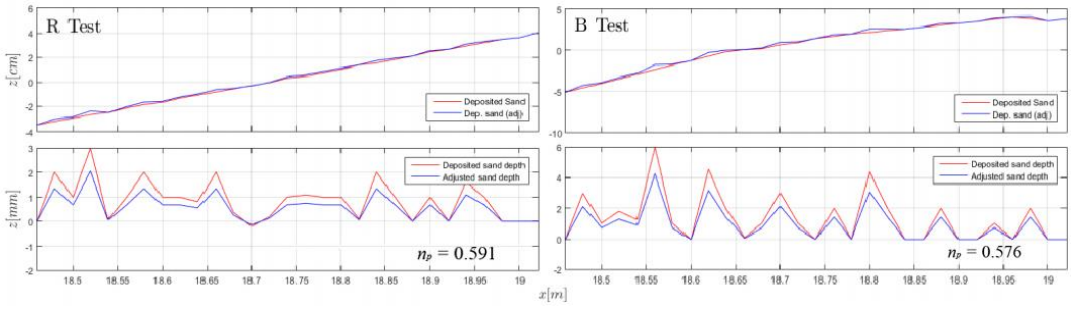

Figure 3.11: R and B series deposited and adjusted sand heights on the fabric mesh

3.5 Stone Damage and Settlement

Figures 3.12 - 3.19 show the laser line scanner images at the beginning and end of tests with SWL = 0, 2, 4, and 6 cm for R and B test series. Stone damage was minimal until t = 8,000 s. Damage is discernible in the images from t = 8,000 – 16,000 s for both test series. Since the stone structure of B series was covered with sand, damage was less as will be shown later. Moreover, sand cover in test series B protected the back of the structure from damage until the sand was completely removed at the end of the t = 16,000 s.

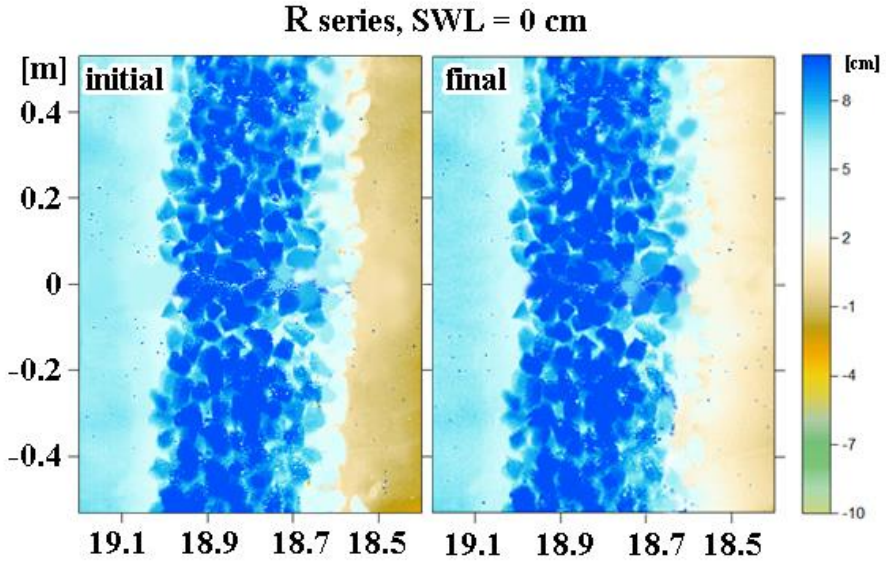

Figure 3.12: R test series initial (t =0 s) and final (t = 4,000 s) with SWL = 0 cm

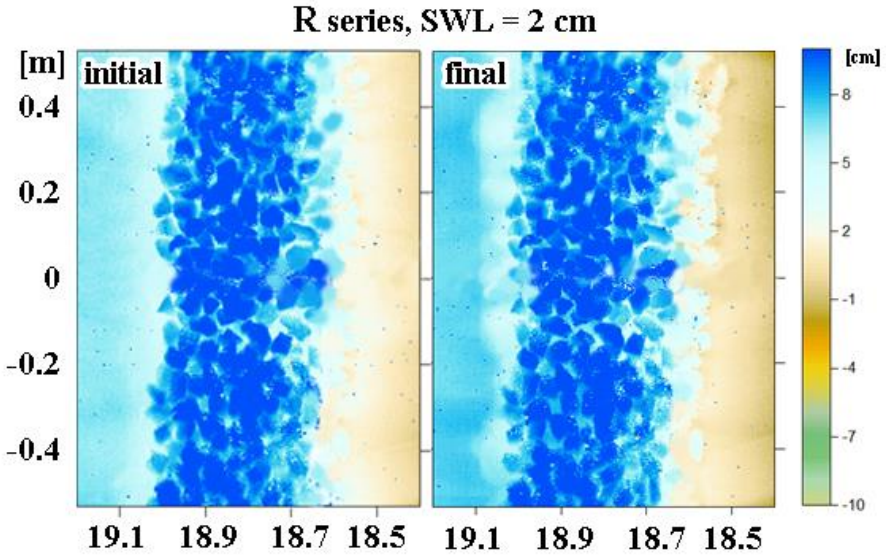

Figure 3.13: R test series initial (t =4,000 s) and final (t = 8,000 s) with SWL = 2 cm

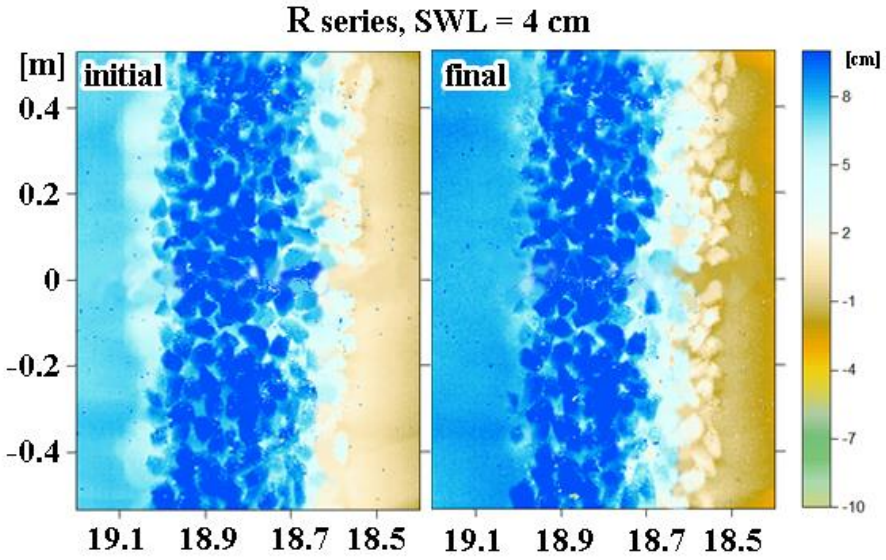

Figure 3.14: R test series initial (t =8,000 s) and final (t = 12,000 s) with SWL = 4 cm

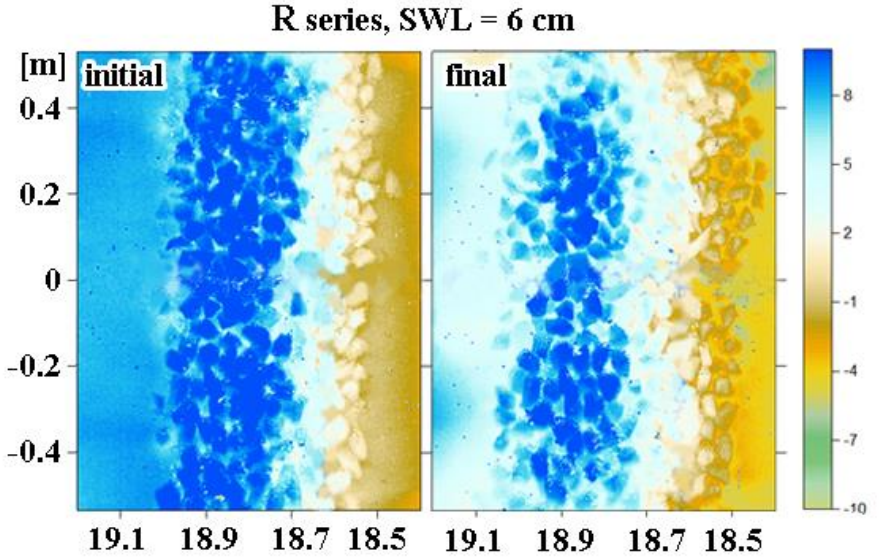

Figure 3.15: R test series initial (t =12,000 s) and final (t = 16,000 s) with SWL = 6 cm

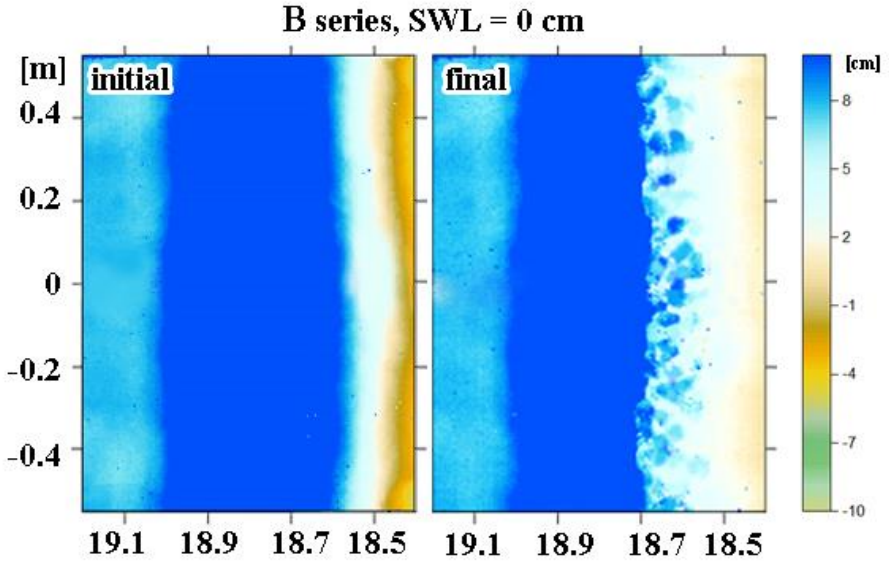

Figure 3.16: B test series initial (t =0 s) and final (t = 4,000 s) with SWL = 0 cm

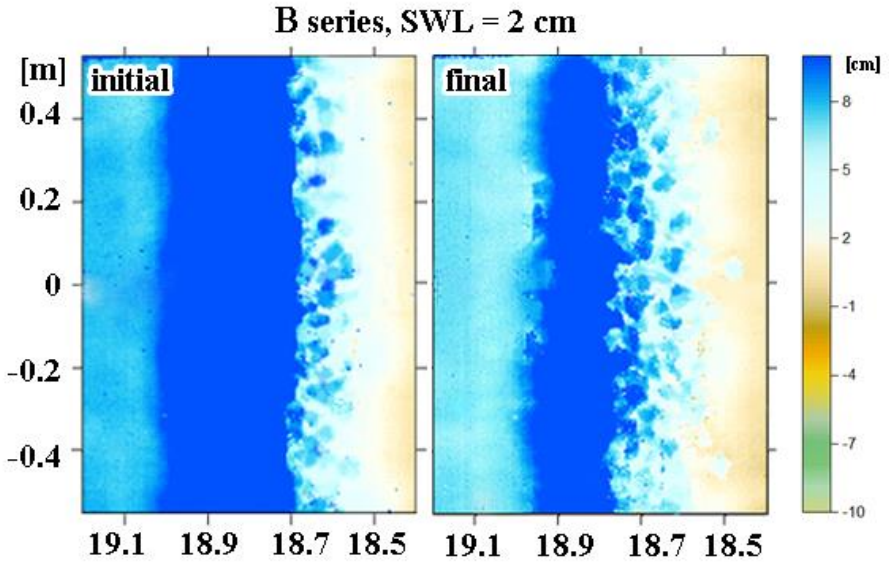

Figure 3.17: B test series initial (t =4,000 s) and final (t = 8,000 s) with SWL = 2 cm

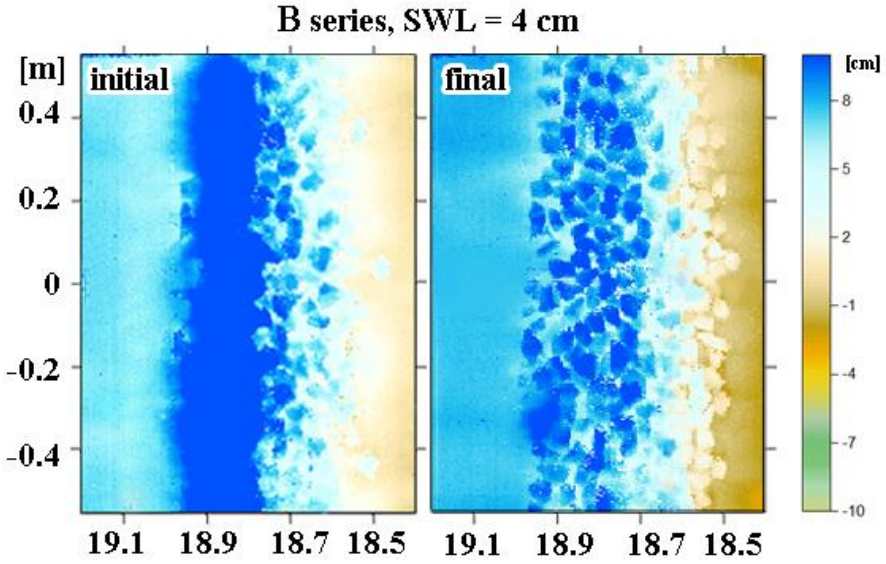

Figure 3.18: B test series initial (t =8,000 s) and final (t = 12,000 s) with SWL = 4 cm

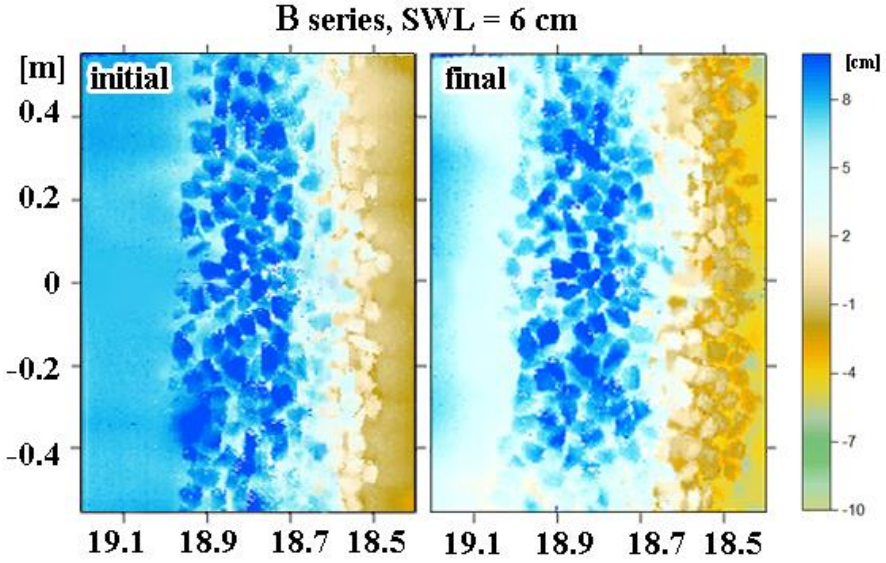

Figure 3.19: B test series initial (t =12,000 s) and final (t = 16,000 s) with SWL = 6 cm

The eroded area A_e of stone cross section for both R and B test series in the stone zone of x = 18.46 – 19.02 m is calculated at t = 4,000, 8,000, 12,000, and 16,000 s by comparing the measured profile with the initial profile at t = 0. The eroded area A_e is calculated for green stone and blue stone separately using alongshore averaged profiles for each segment shown in Figures 3.20-3.23 for R test series and in Figures 3.24-3.27 for B test series. For example, R test series with SWL = 0 cm (Figure 3.20) produced green stone eroded area A_e of about 10.4 cm^2 in comparison to blue stone eroded area of about 8.3 cm^2. This small difference is due to the size of the stone used for green and blue stones where the nominal diameter D_{n50} = 3.52 cm for the green stone and D_{n50} = 3.81 cm (8% larger) for the blue stones. The eroded area was similar or slightly smaller for the larger blue stone. The eroded area was smaller for B test series with the sand cover protection.

The damage progression of the stone seawall in both series R and B is analyzed using a standard method for a stone structure (e.g., Melby and Kobayashi 2011) using damage *S* defines as

$$S = A_e / (D_{n50})^2 \tag{3.1}$$

where *S* = 0 at t = 0. The temporal variation of *S* is shown in Figure 3.28. The incident significant wave height H_{mo} at x = 0 was approximately 17 cm for all the test series. The stability number $N_s = H_{mo} / [(\rho_s/\rho - 1) D_{n50}]$ with ρ = water density (1g/cm^3) and ρ_s = stone density (Table 2.2) is 2.5 and 2.2 for the green and blue stones if H_{mo} = 17cm at x = 0 is used in N_s. However, the offshore wave height is inadequate in predicting the stone damage in the swash zone. The intensity of wave uprush and downrush on the rock seawall increased with the 2 cm SWL increase at t= 4,000, 8,000, and 12,000 s. The damage at the end of series R and B was much larger than

expected. Stone movement was observed to be small and the cause of the large damage was examined in the following.

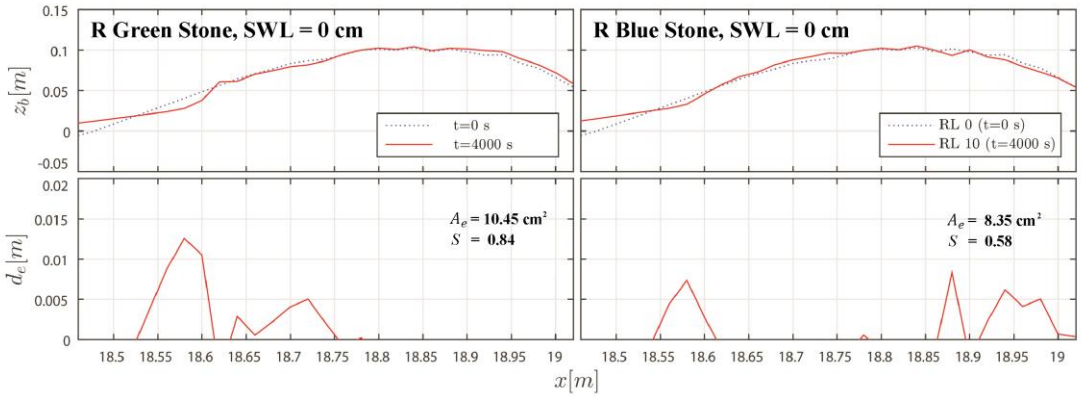

Figure 3.20: R test series green and blue stone eroded area and damage from t = 0 to t = 4,000 s

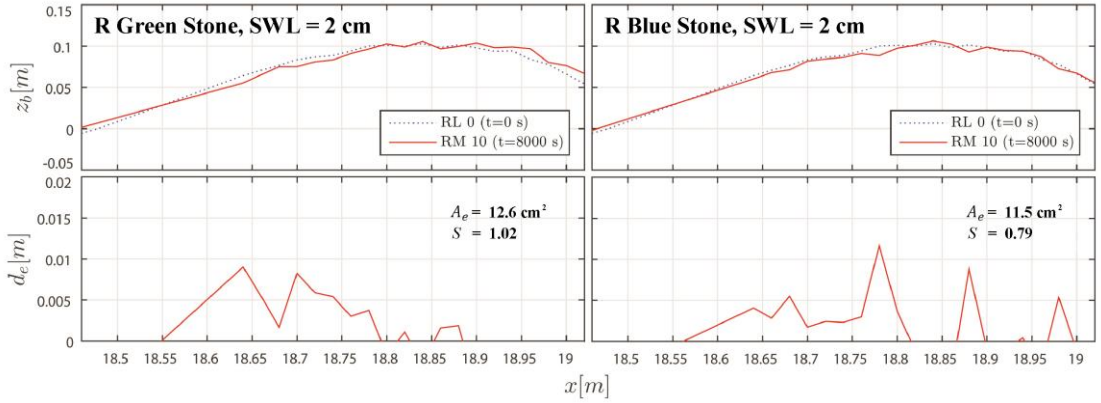

Figure 3.21: R test series green and blue stone eroded area and damage from t = 0 to t = 8,000 s

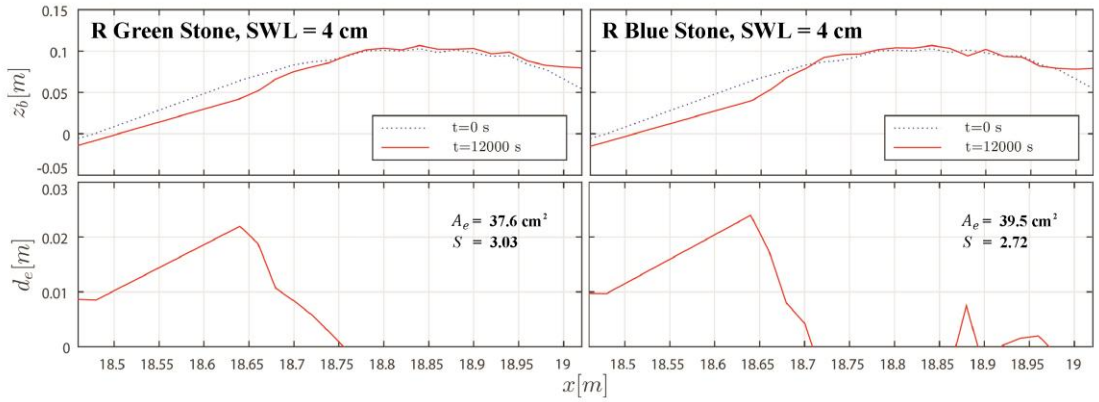

Figure 3.22: R test series green and blue stone eroded area and damage from t = 0 to t = 12,000 s

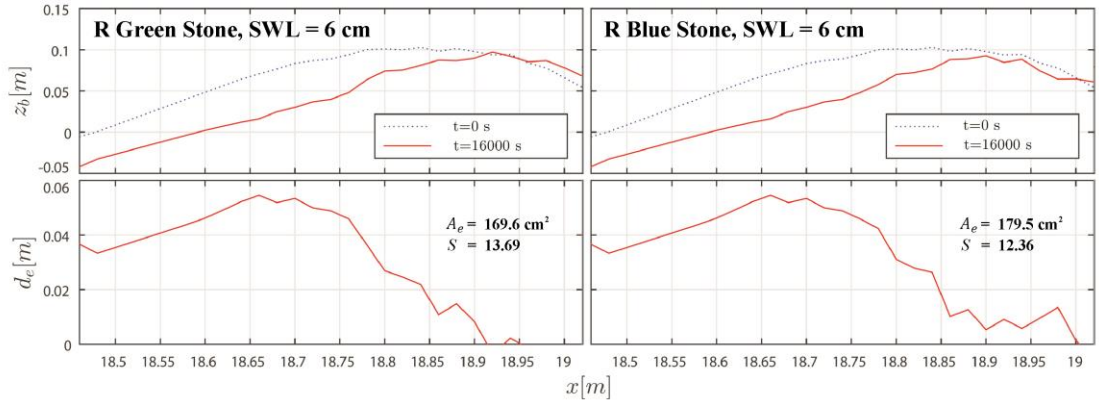

Figure 3.23: R test series green and blue stone eroded area and damage from t = 0 to t = 16,000 s

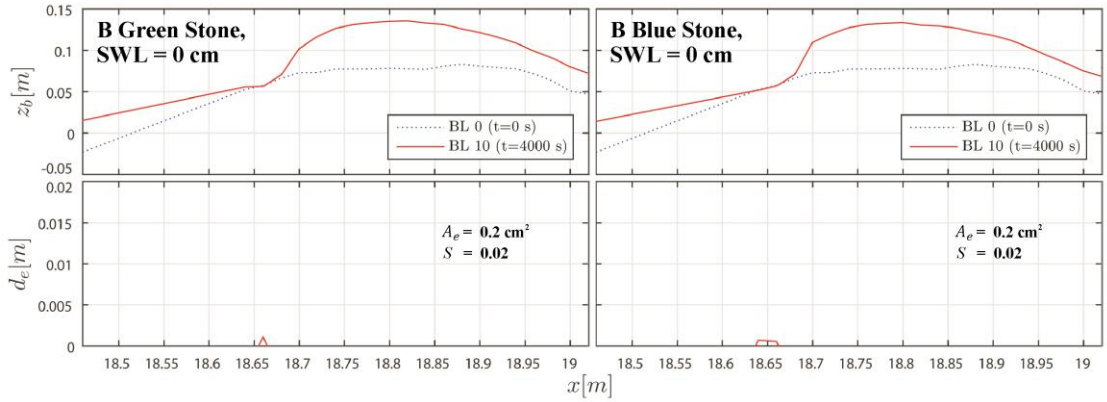

Figure 3.24: B test series green and blue stone eroded area and damage from t = 0 to t = 4,000 s

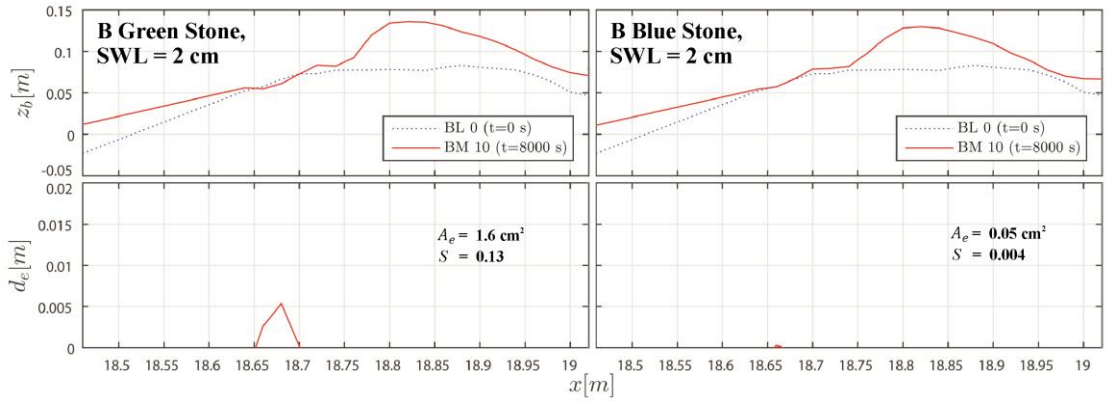

Figure 3.25: B test series green and blue stone eroded area and damage from t = 0 to t = 8,000 s

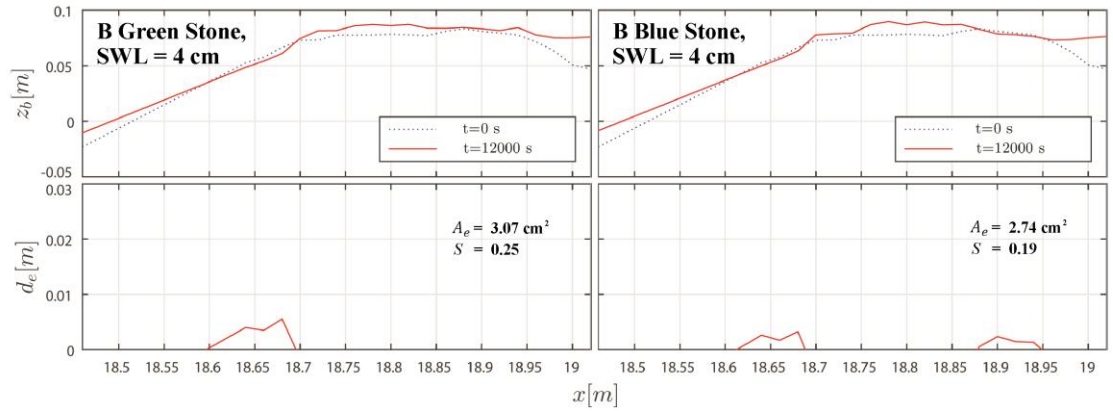

Figure 3.26: B test series green and blue stone eroded area and damage from t = 0 to t = 12,000 s

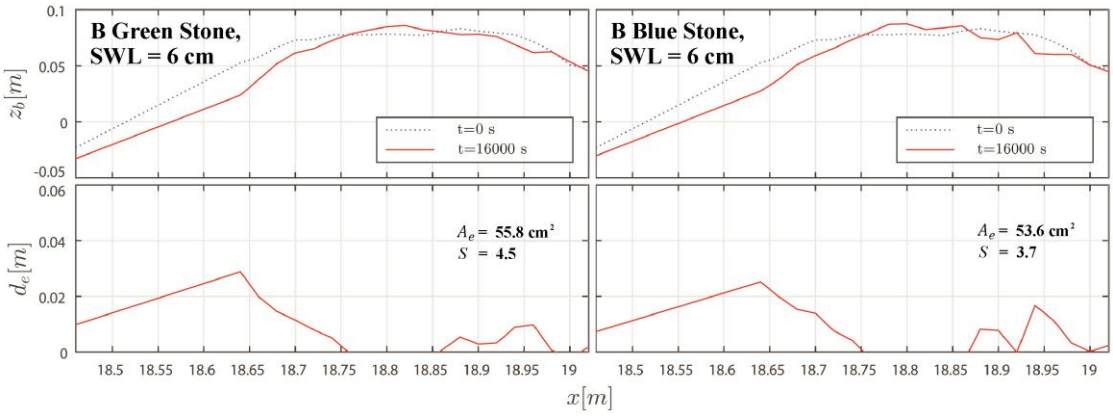

Figure 3.27: B test series green and blue stone eroded area and damage from t = 0 to t = 16,000 s

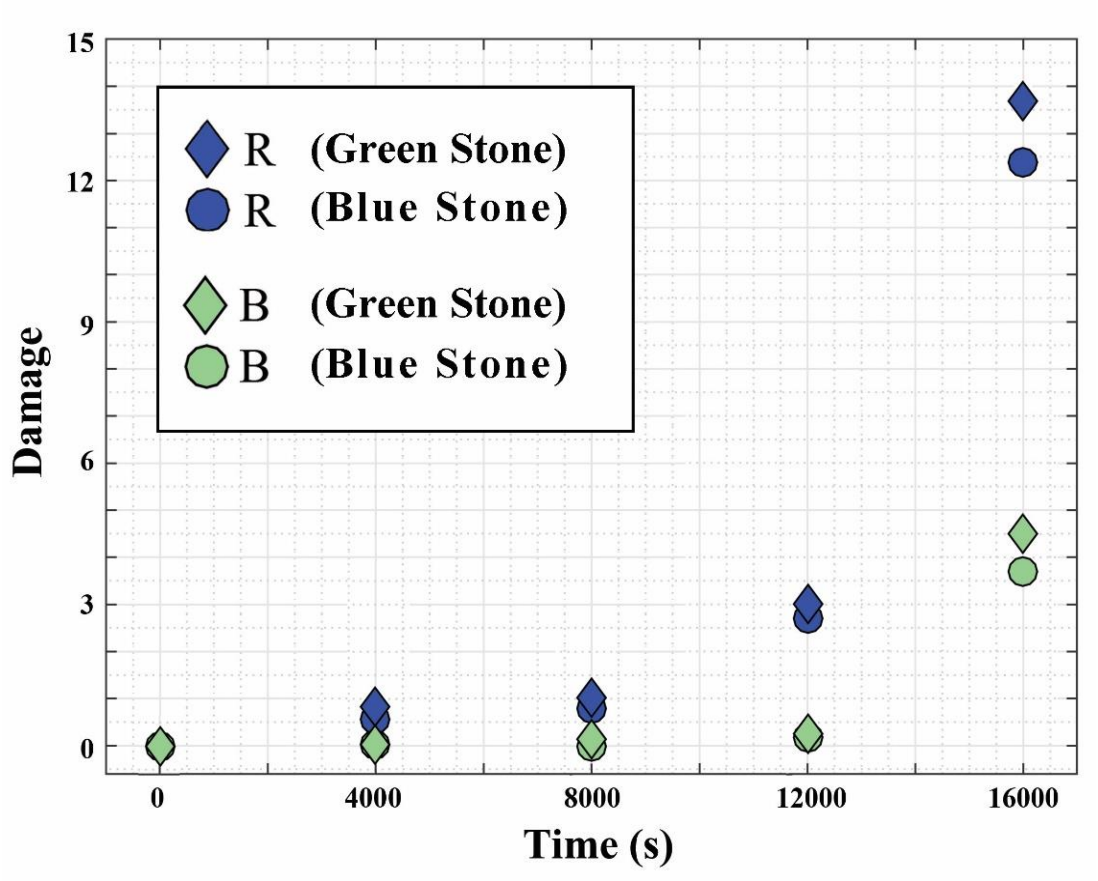

Figure 3.28: Damage progression of green and blue stones on R and B test series

Stone damage in series R and B may have been caused by stone settlement rather than stone displacement by wave action because the eroded area A_e is defined as the area of the lowered stone surface below the initial stone surface. Figure 3.29 shows the initial (t = 0) and final (t = 16,000 s) stone surface and fabric mesh (filter) elevations in the zone of x = 18.46 – 19.02 m for series R and B. The eroded (lowered) areas of the stone surface and filter were 170 cm^2 and 160 cm^2, respectively, for series R and 57 cm^2 and 37 cm^2, respectively, for series B. The cross-shore variations of the stone surface and filter settlement are similar below the seaward slope of the seawall

which was exposed to intense wave uprush and downrush after the foreshore was eroded (Figure 3.4 and 3.5). No measurement was made of sand transport and undermining below the filter in the swash zone in this experiment because the filter was presumed to prevent stone settlement. The reduced damage for series B in Figure 3.28 may be reinterpreted as the reduced sand undermining below the filter because of the additional sand placed on and inside the porous seawall.

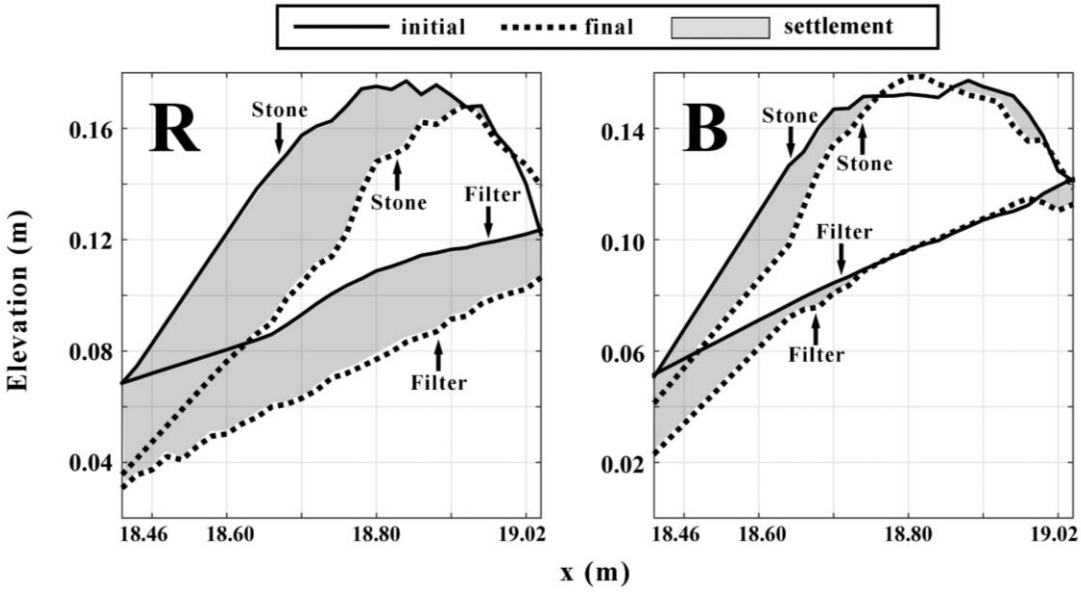

Figure 3.29: Stone and filter settlement for series R and B

3.6 Block Movement

Figures 3.30 – 3.37 show photos of four blocks on the berm before and after each run of series R and B. The blocks were dry when no wave overtopping occurred and became wet when wave overtopping initiated. Block movement started at t = 12,000 s when the SWL was increased to 6 cm. For series R during t = 12,000 – 16,000 s, the blocks moved during the first and second runs but stopped moving afterwards as listed in Table 3.80. For series B during t = 12,000 – 16,000 s, the four blocks moved during the second run. Block no. 3 continued sliding afterwards and slid over the vertical wall after 9 runs as shown in Table 3.81 and Figure 3.37. The blocks moved slightly more in series B than series R due to the sand cover on the seawall which increased wave overtopping somewhat (Figure 3.1).

Table 3.80: Block movement for series R during t = 12,000 – 16,000 s

Run	Block Number			
	1	2	3	4
RE1	slid	slid	slid	slid
RE2	wet	slid	wet	slid
RE3	wet	wet	wet	wet
RE4	wet	wet	wet	wet
RE5	wet	wet	wet	wet
RE6	wet	wet	wet	wet
RE7	wet	wet	wet	wet
RE8	wet	wet	wet	wet
RE9	wet	wet	wet	wet
RE10	wet	wet	wet	wet

Table 3.81: Block movement for series B during t = 12,000 – 16,000 s

Run	Block Number			
	1	2	3	4
BE1	wet	wet	wet	wet
BE2	slid	slid	slid	slid
BE3	wet	wet	slid	wet
BE4	wet	wet	slid	wet
BE5	wet	wet	slid	wet
BE6	wet	wet	slid	wet
BE7	wet	wet	slid	wet
BE8	wet	wet	slid	wet
BE9	wet	wet	off	wet
BE10	wet	wet	off	wet

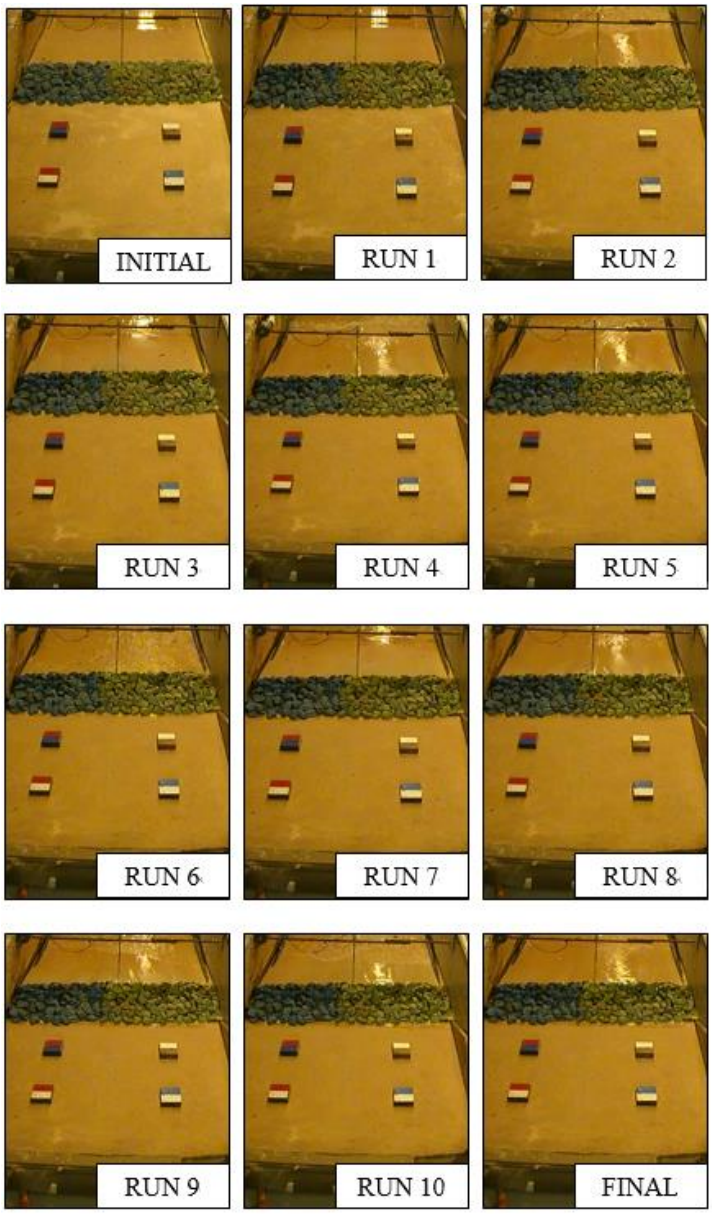

Figure 3.30: Four blocks on berm for series R during t = 0-4,000 s

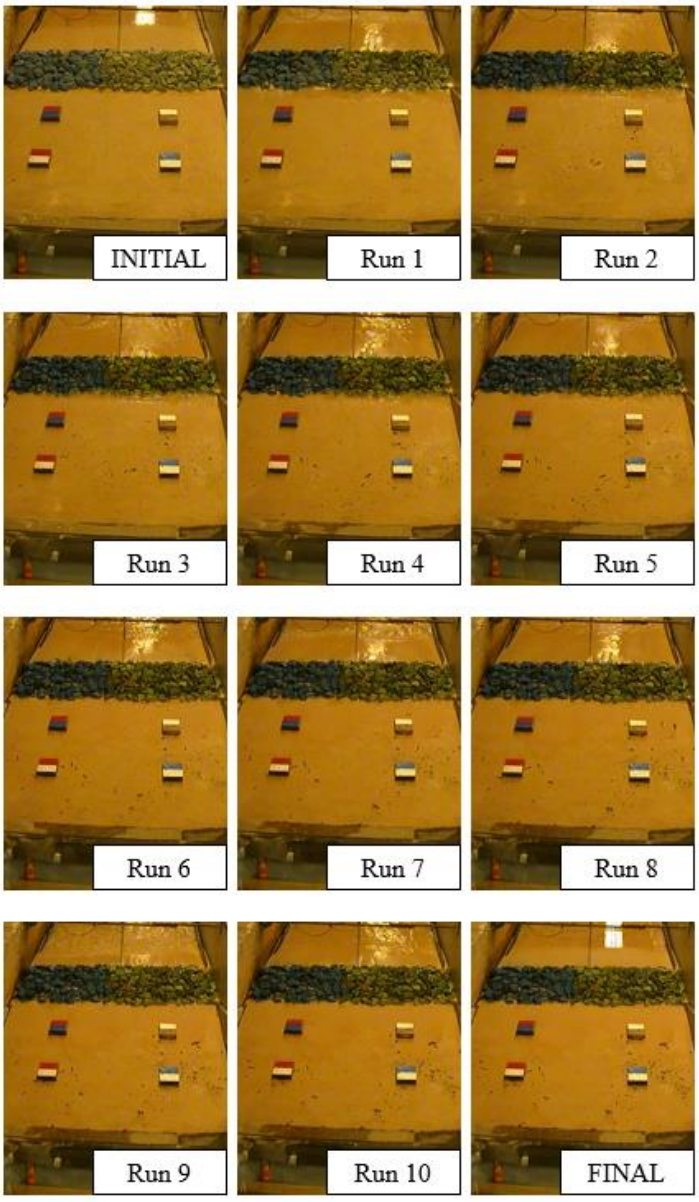

Figure 3.31: Four blocks on berm for series R during t = 4,000-8,000 s

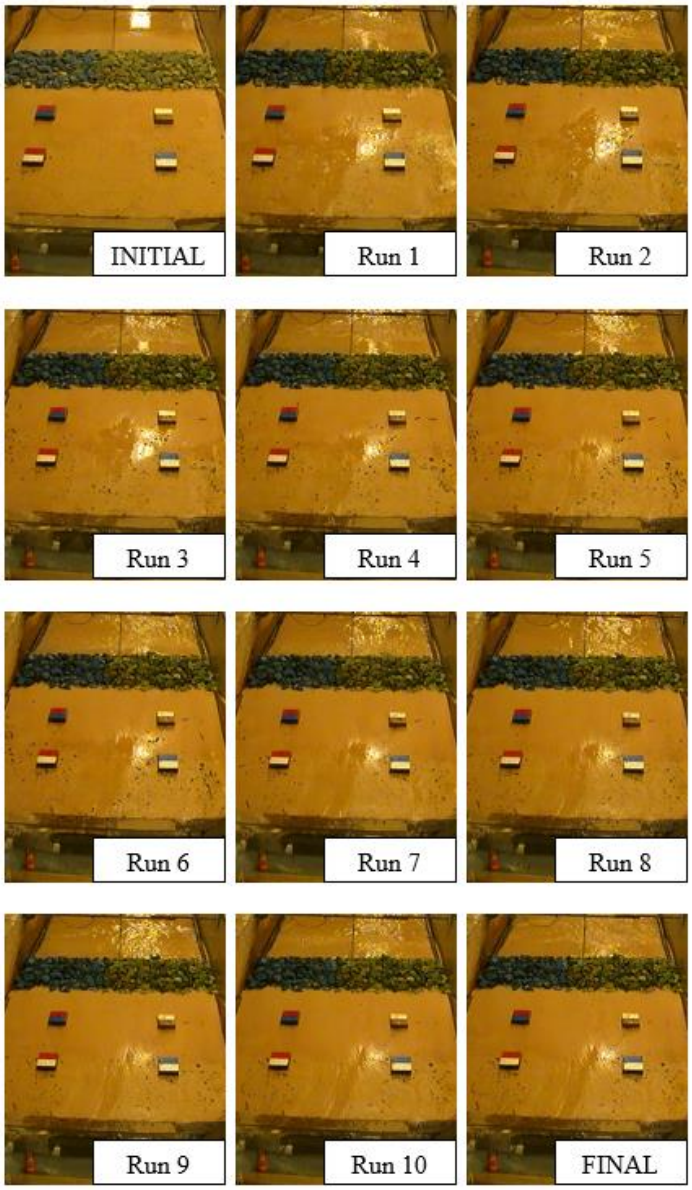

Figure 3.32: Four blocks on berm for series R during t = 8,000-12,000 s

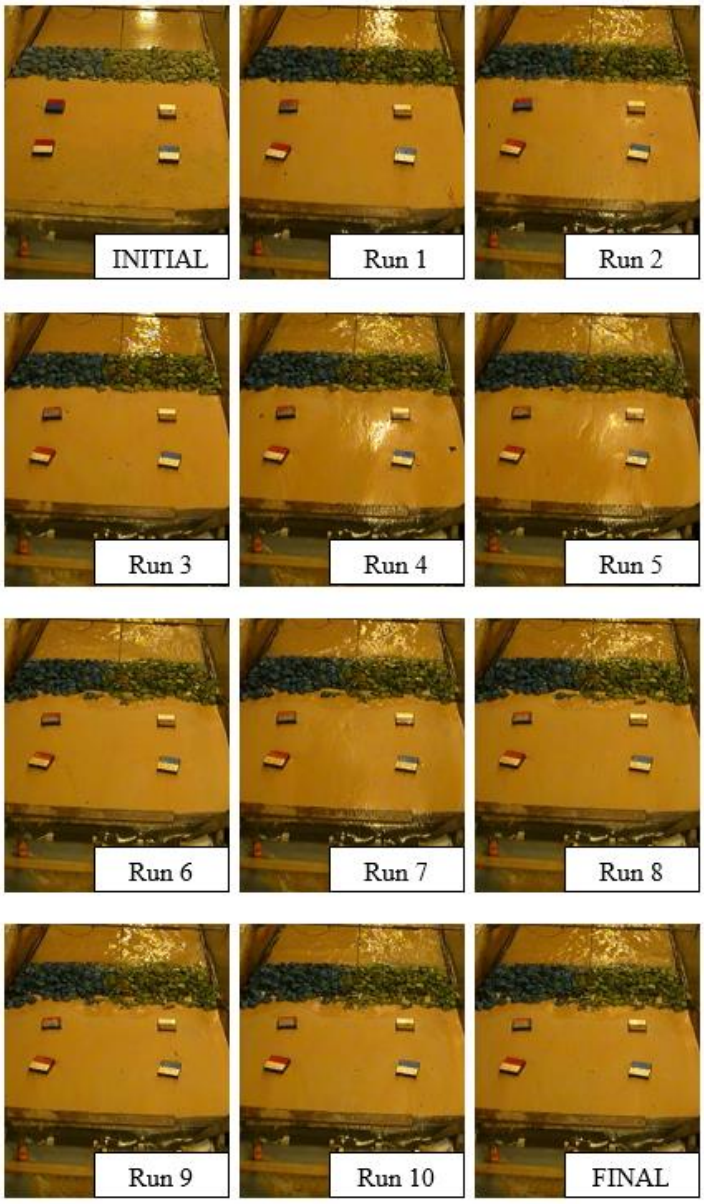

Figure 3.33: Four blocks on berm for series R during t = 12,000-16,000 s

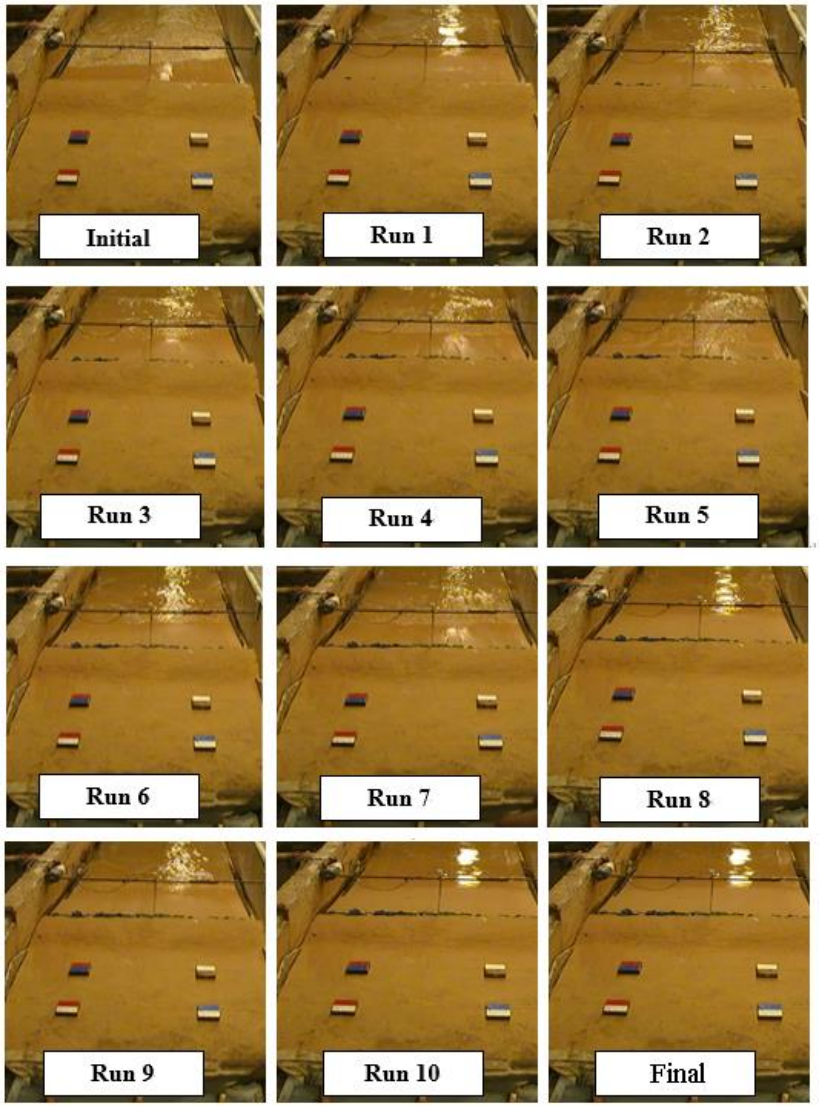

Figure 3.34: Four blocks on berm for series B during t = 0-4,000 s

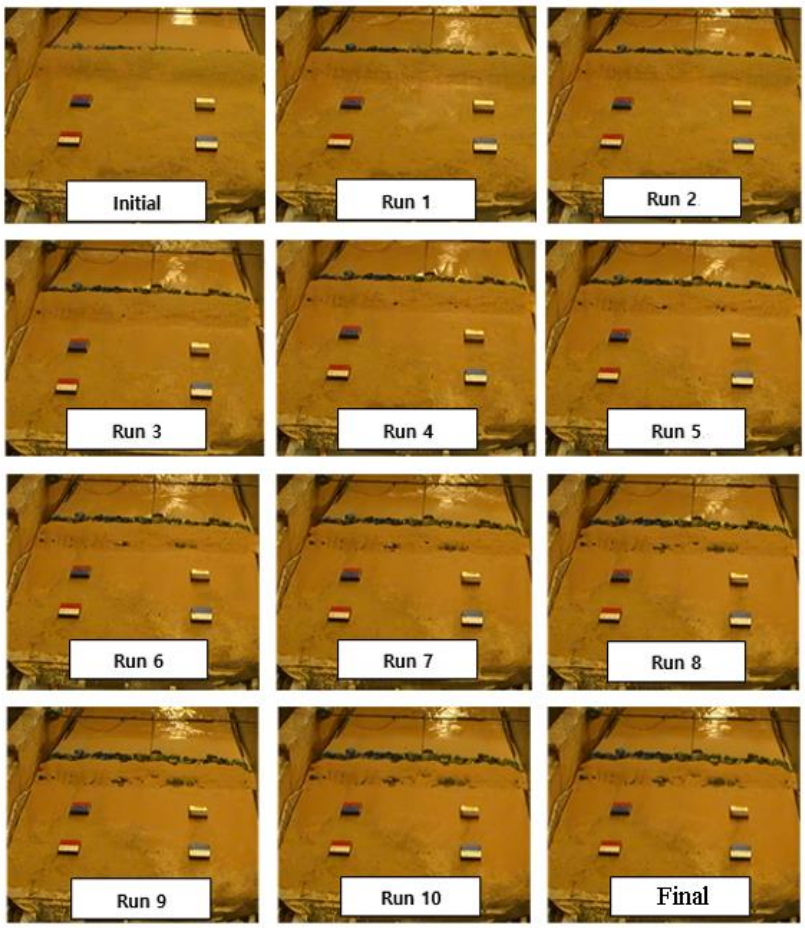

Figure 3.35: Four blocks on berm for series B during t = 4,000-8,000 s

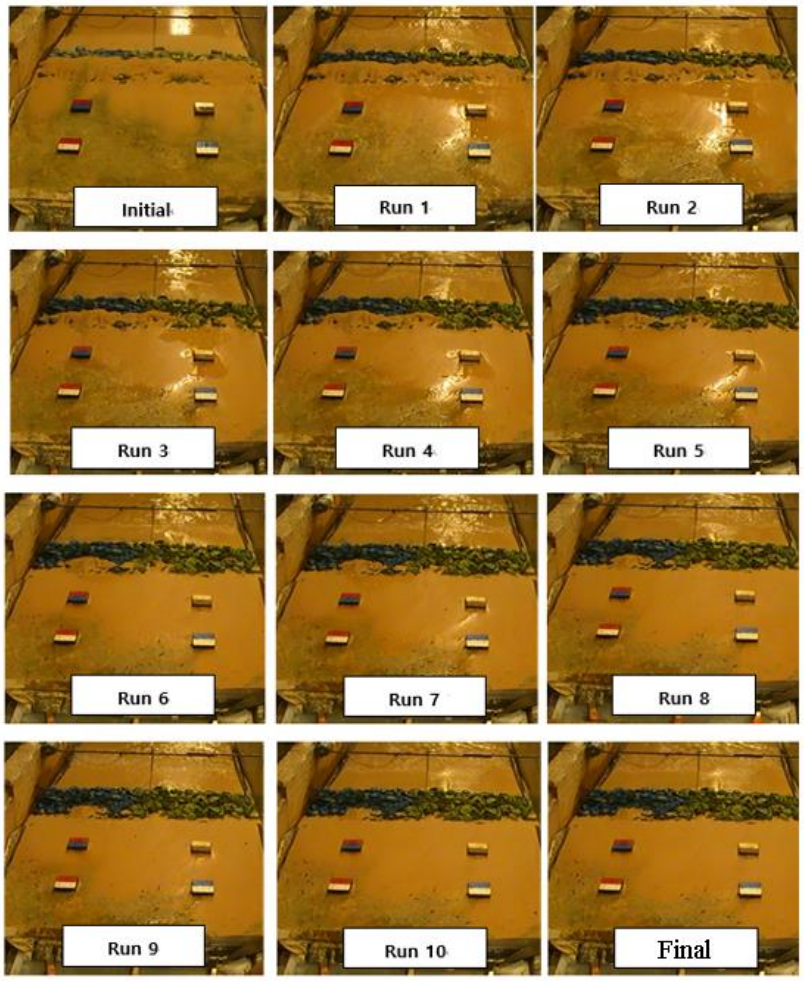

Figure 3.36: Four blocks on berm for series B during t = 8,000-12,000 s

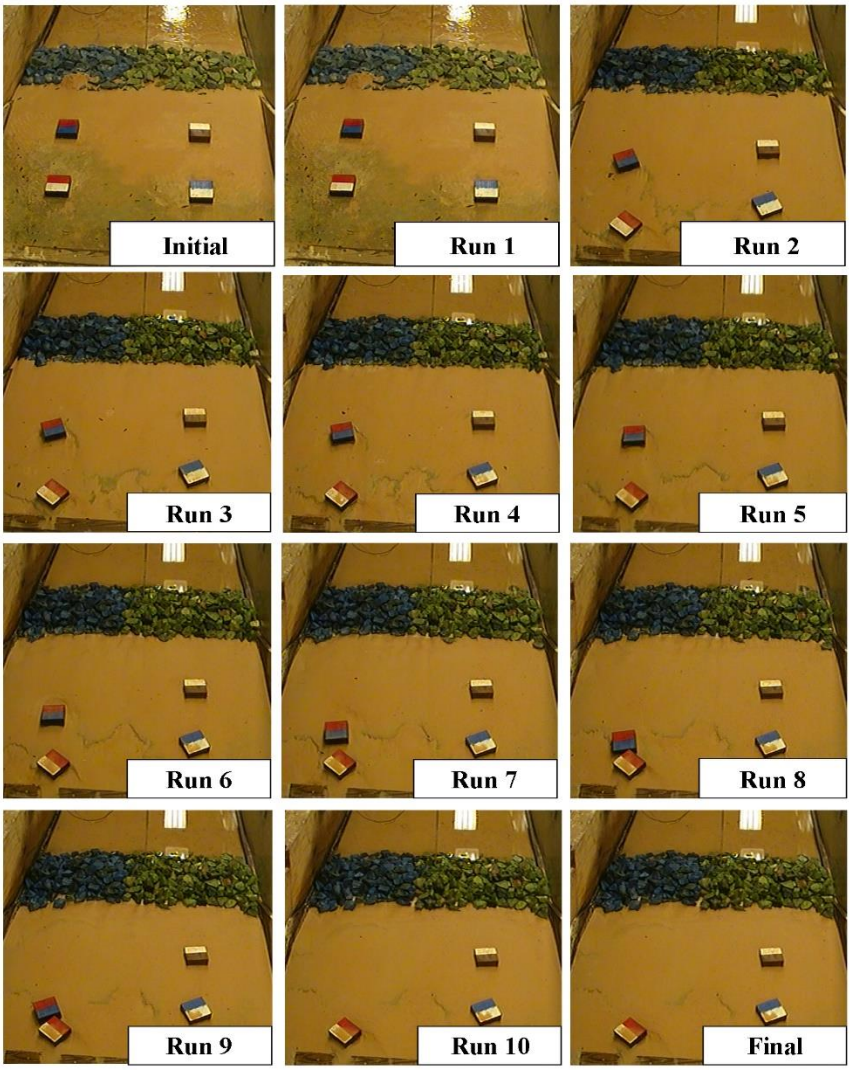

Figure 3.37: Four blocks on berm for series B during t = 12,000-16,000 s

Chapter 4

NUMERICAL MODEL

This chapter explains the cross-shore numerical model CSHORE extended to compute stone damage, sand transport on and inside seawall, and bottom elevation change. The original numerical model of CSHORE is described in detail in Kobayashi (2016).

4.1 Cross-Shore Model (CSHORE)

The components of CSHORE for normally incident waves used in this study include: a combined wave and current model based on time- averaged continuity, momentum, wave action, and roller energy equations; a sediment transport model for bed load and suspended load coupled with the continuity equation of bottom sediment; a permeable layer model for porous flow; and a probabilistic swash model on impermeable and permeable bottoms. In this extended CSHORE, the fine sand and stones used in the experiment are assumed to be impermeable and permeable, respectively. Input to the numerical model for each series includes the measured bottom elevation z_b of sand or stone surface at t = 0, measured values of $\bar{\eta}$, H_{mo}, and T_p at x = 0 for all the runs in the test series. The input parameters for CSHORE are taken as standard values in order to assess the degree of agreement in light of previous comparisons discussed in Kobayashi (2016).

4.2 Computed Stone Damage

The model CSHORE is extended to predict effect of the rock seawall on cross-shore sand transport in series R and B. The present CSHORE cannot predict the movement of both sand and stone simultaneously. Damage on the rock seawall in series R is computed assuming no sand movement on the initial sand bottom. Because of the two different stone sizes (green and blue stones used in series R and B), two computations are made for the seawall consisting of the green stone and the blue stone separately. The computed damage at the end (t = 16,000 s) of series R is 0.007 for the green stones and 0.004 for the blue stones, respectively. These computed damage results are much less than the measured damage of the order of 10 in Figure 3.28 in Chapter 3. This discrepancy prompted us to examine the filter settlement shown in Figure 3.29 in Chapter 3. In the following, the stones are assumed to be immobile. Use is made of the average diameter D_{n50} = 3.65 cm of the green and blue stones, accounting for the stone width difference (Table 2.2). The stone porosity is n_s = 0.44. The stone diameter and porosity are used to estimate the laminar and turbulent flow resistance inside the seawall (Kobayashi et al. 2010). The filter is assumed to be fixed because sand transport processes under the filter in the swash zone are unknown. The assumption of no filter settlement may be acceptable when damage was less than about 1 in Figure 3.28

4.3 Sand Transport on and inside Seawall

Figure 4.1 illustrates a simple model for sand transport on and inside the fixed seawall. The seawall is located in the zone of the fixed filter and stone. The three dimensional laser line scanner measured the bottom elevation z_b on the surface of sand or stone in series R and B. The lower limit of z_b in the stone zone is the stone surface elevation z_{bs} measured at t = 0. The sand surface elevation z_p is introduced to keep track of the sand surface in the stone zone where $z_p = z_b$ outside the stone zone and above the stone surface covered with sand. The lower limit of z_p in the stone zone is the filter elevation z_{ps} measured at t = 0. The measured cross-shore variations of z_{bs} and z_{ps} in the zone of x = 18.46 – 19.02 m are input to the extended CSHORE. For series R, there was no sand above the filter initially that $z_p = z_{ps}$ at t = 0. Different from series R, stone surface of series B was covered with sand initially that $z_p = z_b$ at t = 0. The thickness h_p of the porous layer with no sand is given by $h_p = (z_b – z_p)$ where the sand surface is assumed impermeable. The porosity of the porous layer is assumed to be the same as the stone porosity n_s. Some sand may have been deposited or remained in the porous layer but the volume of sand attached to individual stones was negligible when the stones were removed and the sand volume on the filter was measured after series R and B.

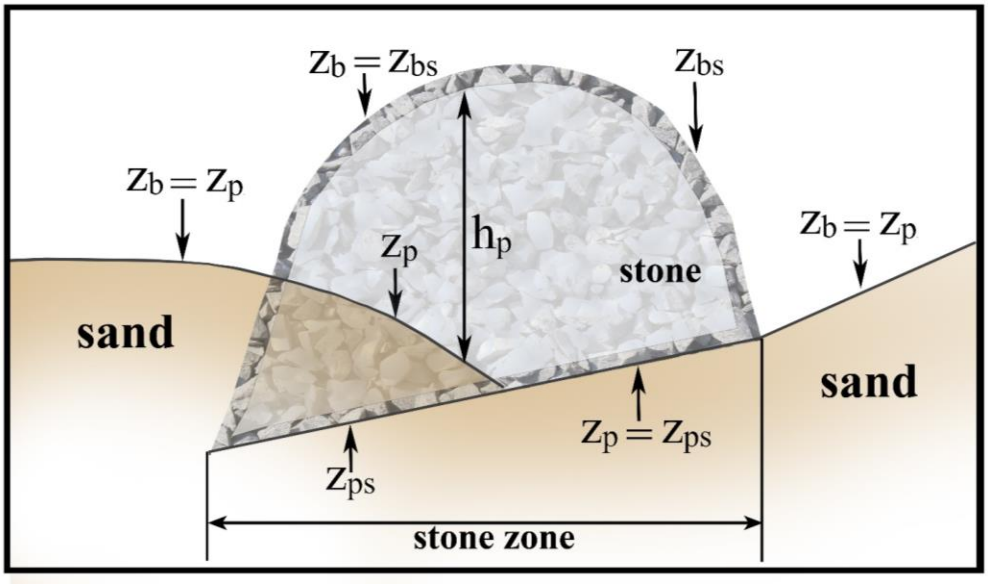

Figure 4.1: Simple model for sand transport on and inside the fixed seawall

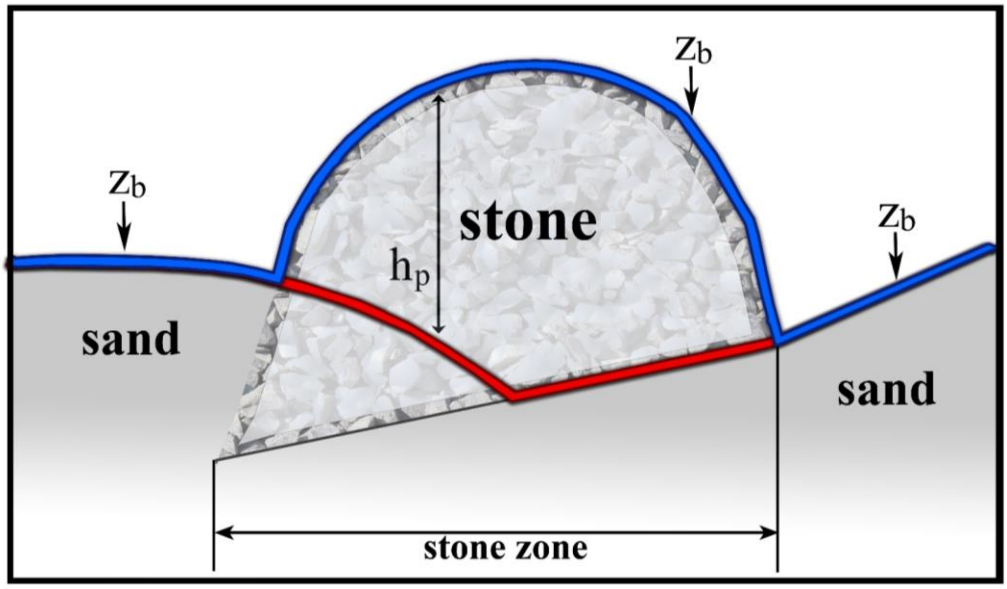

Figure 4.2: Hydrodynamic computation on bottom elevation z_b

The cross-shore model CSHORE computes the mean and standard deviation (SD) of the free surface elevation η above SWL and the depth-averaged cross-shore velocity U above the bottom elevation z_b (Figure 4.2). The water volume and momentum fluxes between the flow above z_b and the porous flow between z_b and z_p affect wave motion and overtopping in the swash zone (Kobayashi et al. 2010). The porous layer effect is limited to the zone of $h_p > 0$ which changes with time t. The cross-shore bed load and suspended load transport rates q_b and q_s are estimated using the empirical formulas in CSHORE developed for the case of $h_p = 0$ in the zones of no porous layer (Figure 4.3). To account for the porous layer effect crudely, the estimated q_b and q_s are multiplied by the reduction factor R_p expressed as

$$R_p = \exp(-C_p h_p / d_{50}) \quad \text{for} \quad h_p \geq 0 \tag{4.1}$$

where C_p = empirical constant; h_p = porous layer thickness; d_{50} = median sand diameter. Eq. (4.1) yields $R_p = 1$ for $h_p = 0$ and the exponential decrease of R_p with the increase of h_p. The value of C_p influences sand mobility inside the seawall. The calibrated value for series R and B with $d_{50} = 0.18$ mm is $C_p = 0.01$, which should be regarded as an order-of-magnitude estimate in light of the crude nature of Eq. (4.1).

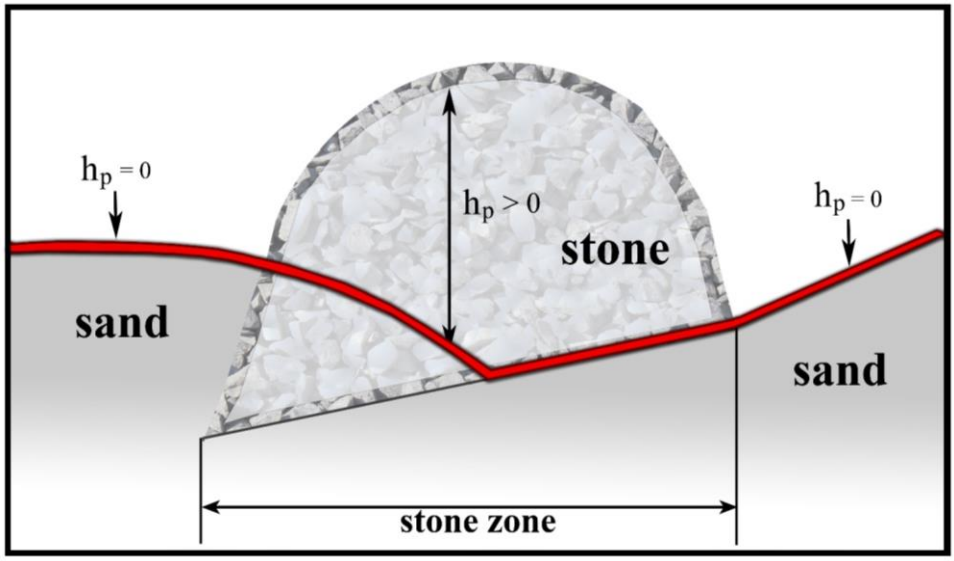

Figure 4.3: Sand transport on and inside seawall

4.4 Bottom Elevation Change

The temporal change of the bottom elevation z_b is computed using the continuity equation of bottom sand together with the estimated and reduced q_b and q_s. The computed increment Δz_b from z_b at time level t is added to obtain $z_b^* = (z_b + \Delta z_b)$ and $z_p^* = z_b^*$ at the next time level outside the stone zone. In the stone zone, erosion ($\Delta z_b < 0$) is limited by available sand. The deposited (including the sand porosity of 0.4) sand volume V_d above the filter per unit horizontal area is given by (see Figure 4.4)

$$V_d = n_s \left(z_p - z_{ps} \right) \qquad \text{for} \quad h_p > 0 \tag{4.2}$$

$$V_d = z_b - z_{bs} + n_s \left(z_{bs} - z_{ps} \right) \qquad \text{for} \quad h_p = 0 \tag{4.3}$$

where $h_p = (z_b - z_p)$ is positive or zero because $z_b \geq z_p \geq z_{ps}$. The stone porosity n_s indicates the void among stone units. The deposited sand height V_d at time level t is zero or positive. If the computed $\Delta z_b < (-V_d)$, $\Delta z_b = (-V_d)$ is used to estimate z_b^* and z_p^* at the next time level in the stone zone as presented below.

For sand deposition ($\Delta z_b > 0$) in the stone zone,

$$z_b^* = z_b + \Delta z_b - n_s h_p \;\; ; \;\; z_p^* = z_b^* \qquad \text{for} \quad \Delta z_b \geq \left(n_s h_p \right) \tag{4.4}$$

$$z_b^* = z_{bs} \;\; ; \;\; z_p^* = z_p + \left(\Delta z_b / n_s \right) \qquad \text{for} \quad \Delta z_b < \left(n_s h_p \right) \tag{4.5}$$

where the stone surface z_{bs} is covered with sand in Eq. (4.4) and exposed to water in Eq. (4.5).

For sand erosion ($\Delta z_b < 0$) in the stone zone,

$$z_b^* = z_{bs} \;\; ; \;\; z_p^* = z_p + \left(\Delta z_b / n_s \right) \qquad \text{for} \quad h_p > 0 \tag{4.6}$$

For $h_p = 0$ ($z_b = z_p$), sand on the stone surface is eroded as follows:

$$z_b^* = z_b + \Delta z_b \quad ; \quad z_p^* = z_b^* \quad \text{for} \quad D = (z_b - z_{bs} + \Delta z_b) \geq 0 \tag{4.7}$$

$$z_b^* = z_{bs} \quad ; \quad z_p^* = z_{bs} + \left(D/n_s\right) \quad \text{for} \quad D < 0 \tag{4.8}$$

where sand cover on the stone surface remains at the next time level in Eq. (4.7) but is eroded to the stone surface in Eq. (4.8). The above time-marching computation is repeated from the initial profile at t = 0 to the end of each series.

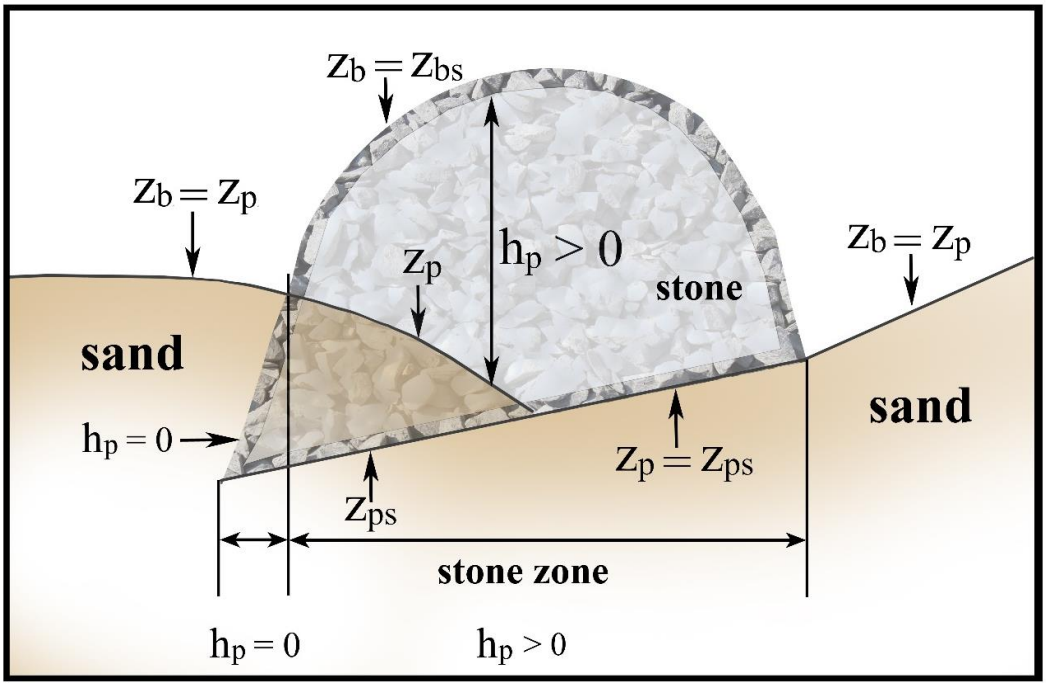

Figure 4.4: Sand volume V_d above filter in zones of $h_p = 0$ and $h_p > 0$

Chapter 5

COMPARISON WITH DATA

The extended CSHORE is compared with the analyzed data of the cross-shore wave transformation, wave overtopping and sand overwash rates, and beach profile evolutions for series N, D, R, and B.

5.1 Cross-Shore Wave Transformation

The measured cross-shore variations of $\bar{\eta}$, σ_η, P_w, $\overline{U}$, and σ_U are plotted for 10 runs with constant SWL in each series together with the computed cross-shore variations in Figures 5.1-5.14. These hydrodynamic variables are predicted within errors of about 20% except for WG8 at x = 18.6 m in the swash zone. The agreement at WG8, located in 14 cm landward of the toe of the seawall in series R and B, depends on the accuracy of the predicted bottom elevation change. The assumption of the fixed seawall implies no lowering of the bottom elevation at WG8. This may partly explain the underprediction of σ_η at WG8 in Figure 5.9 during t = 8,000 – 12,000 s in series R where damage was about 3 at t = 12,000 s in Figure 3.28 from Chapter 3. For series N and D with no seawall, σ_η at WG8 in Figure 5.3 and 5.6 is predicted better during t = 8,000 – 12,000 s as was the case with previous comparisons for cases without any stone structure in the swash zone (Kobayashi 2016).

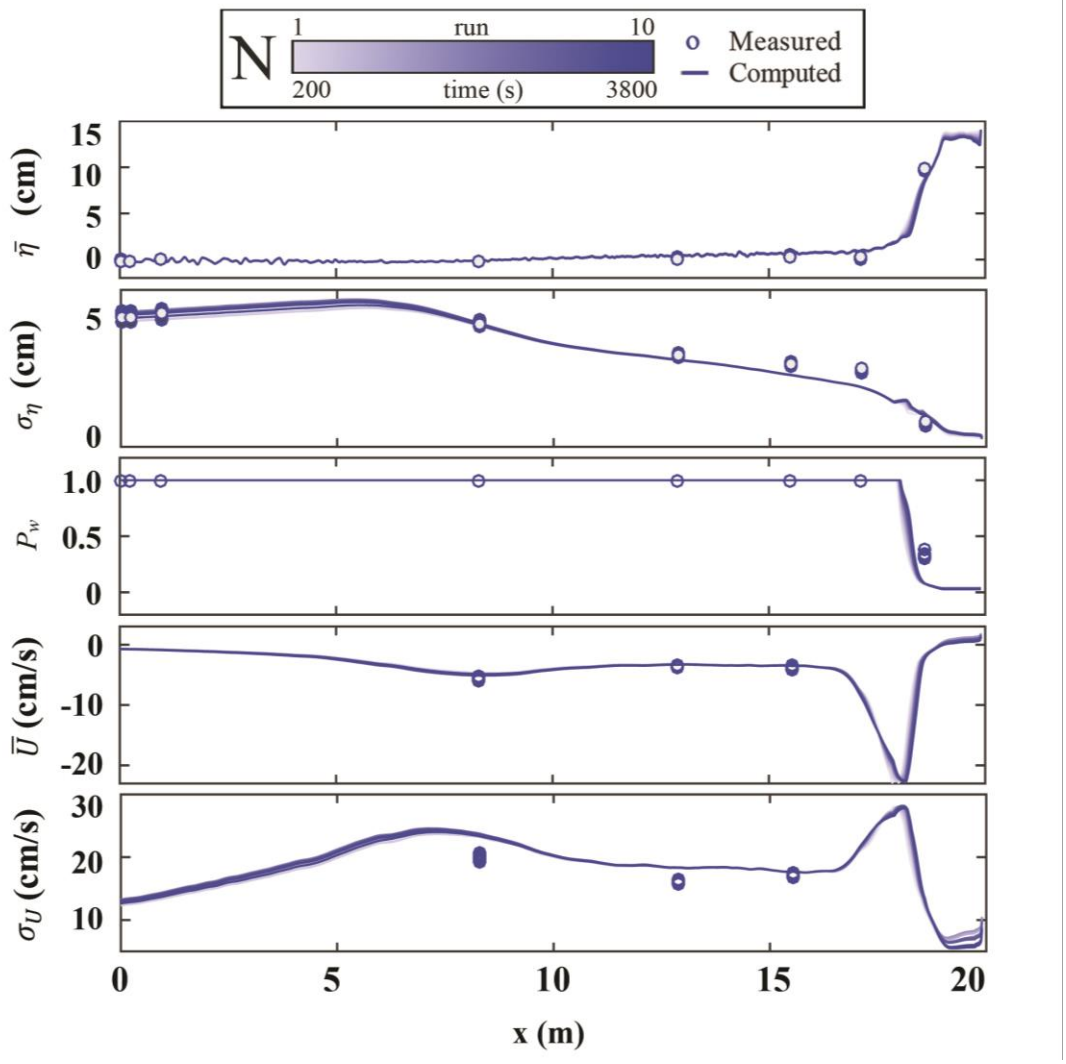

Figure 5.1: Mean and SD of free surface elevation η and horizontal velocity U together with wet probability P_w for 10 runs during time t = 0 – 4000 s in series N

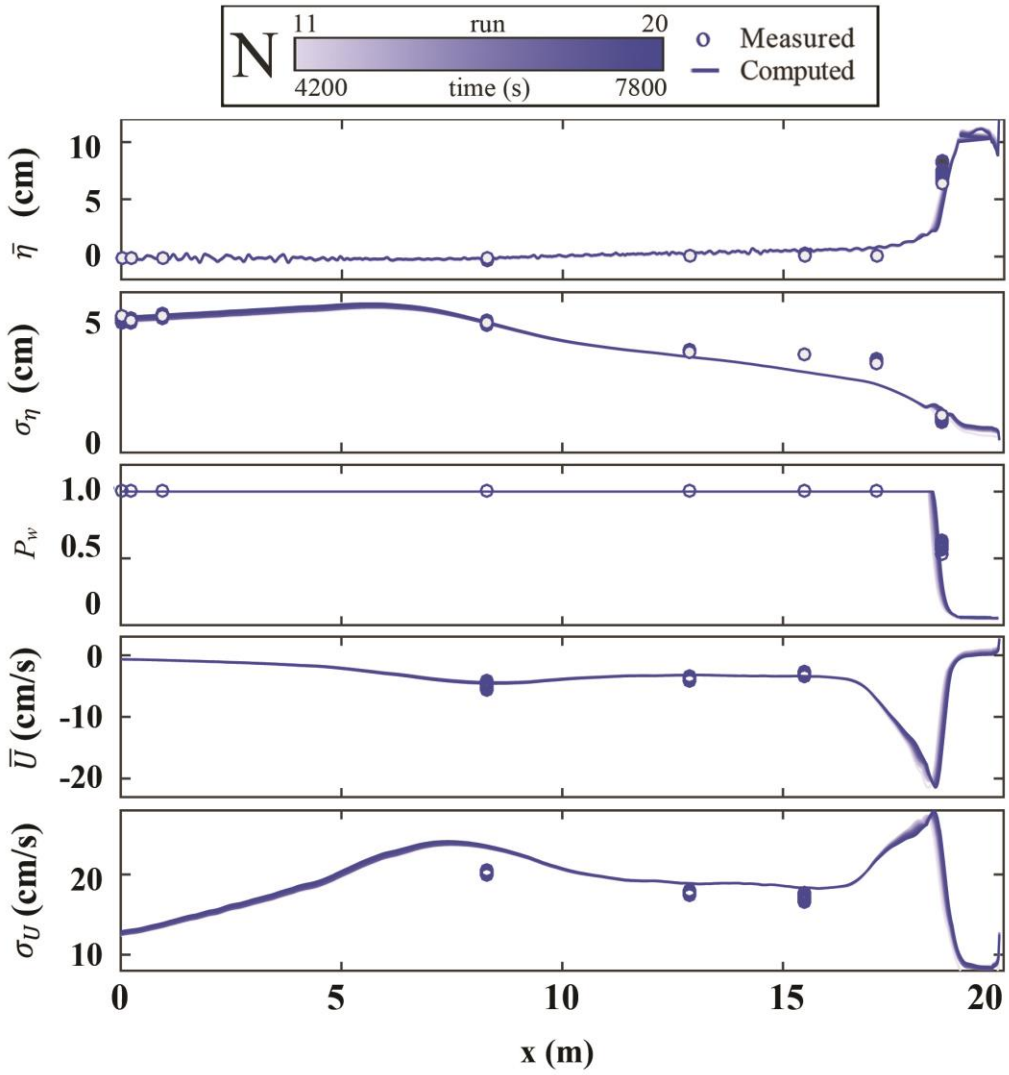

Figure 5.2: Mean and SD of free surface elevation η and horizontal velocity U together with wet probability P_w for 10 runs during time t = 4,000 – 8,000 s in series N

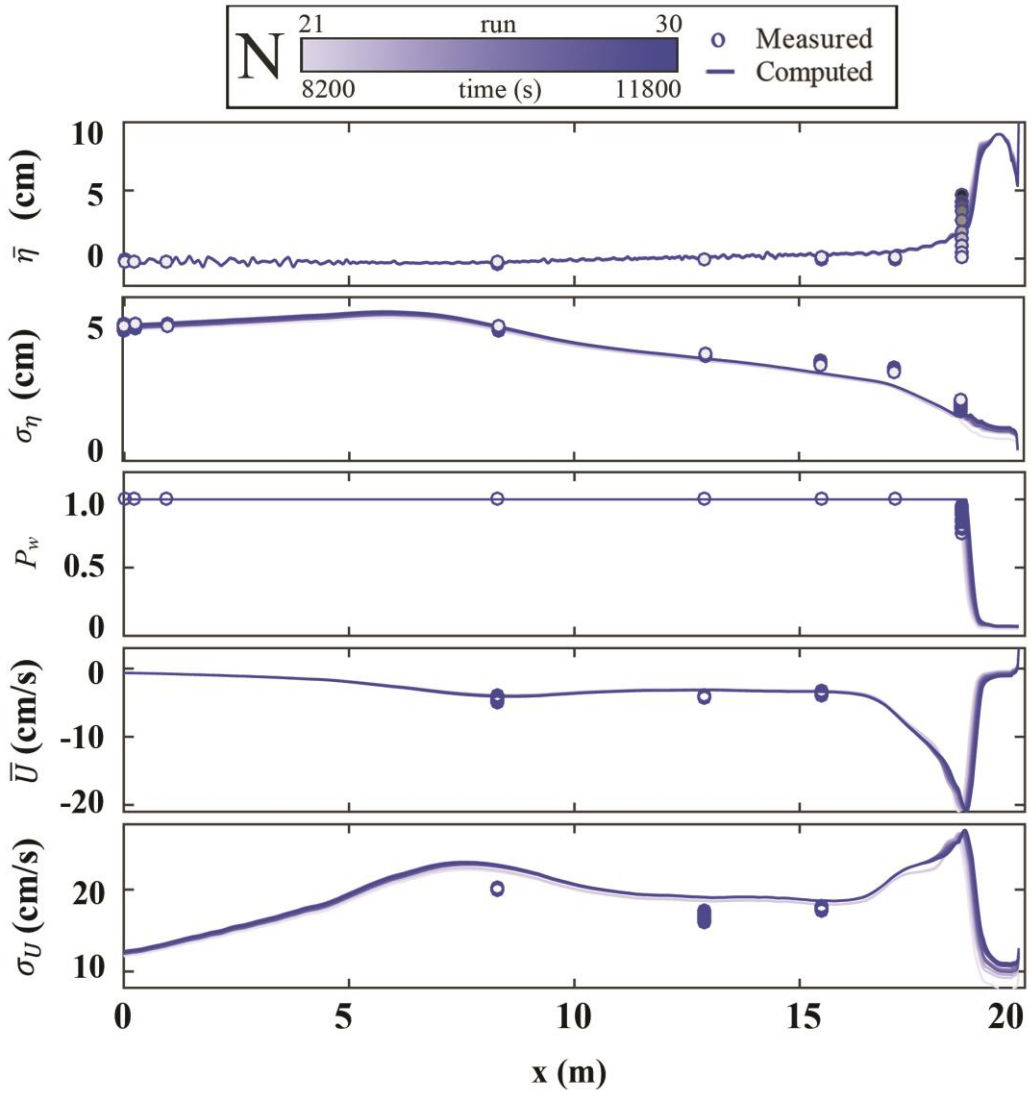

Figure 5.3: Mean and SD of free surface elevation η and horizontal velocity U together with wet probability P_w for 10 runs during time t = 8,000 – 12,000 s in series N

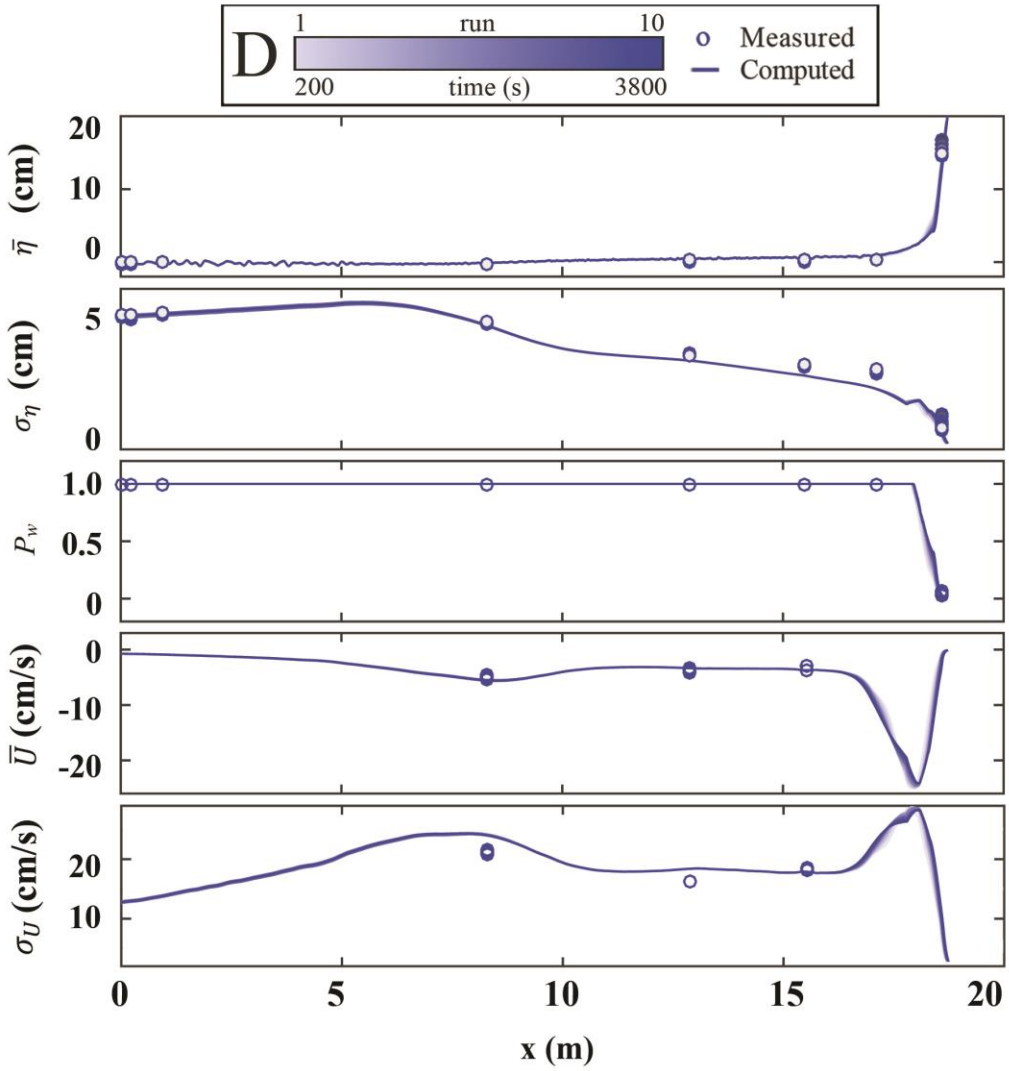

Figure 5.4: Mean and SD of free surface elevation η and horizontal velocity U together with wet probability P_w for 10 runs during time t = 0 – 4,000 s in series D

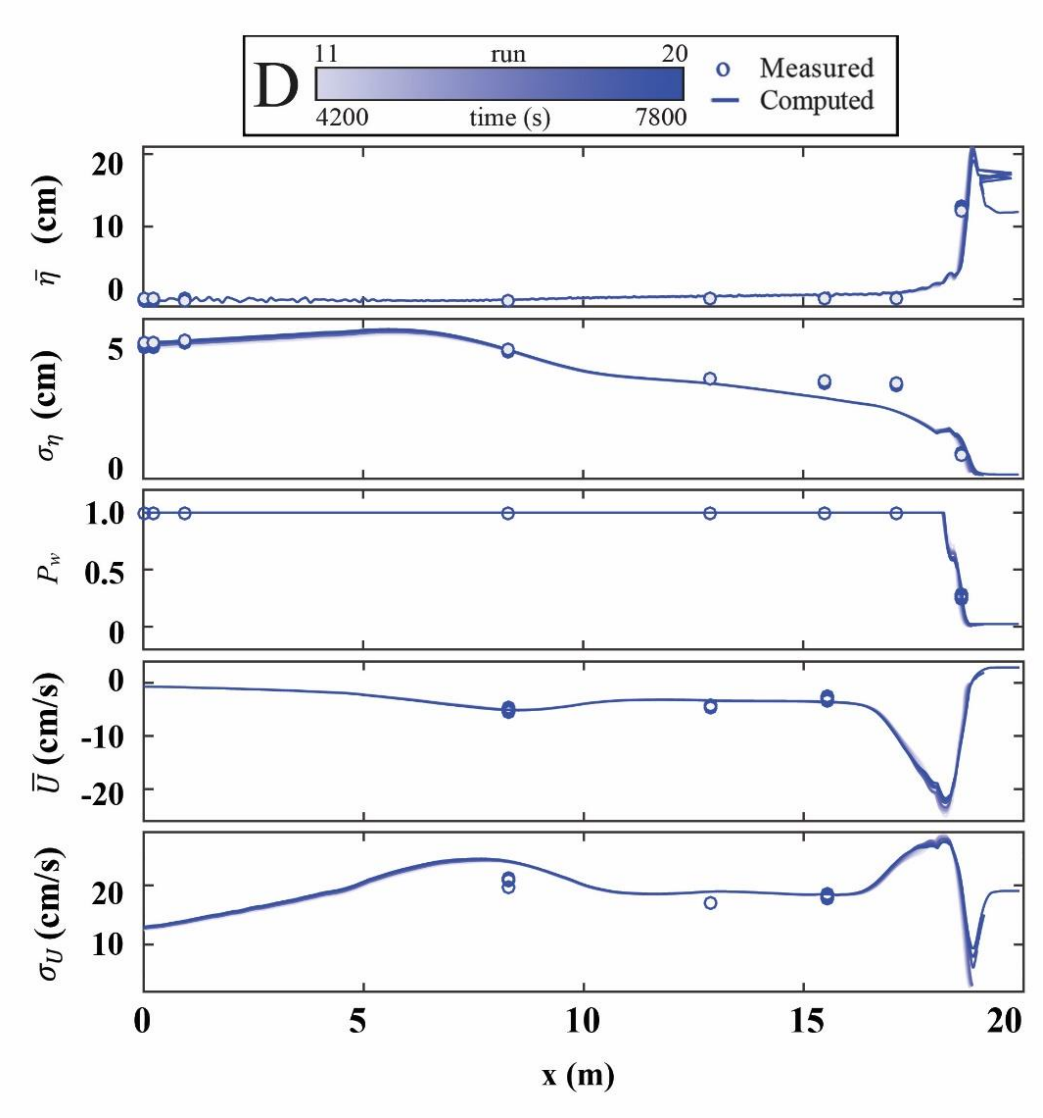

Figure 5.5: Mean and SD of free surface elevation η and horizontal velocity U together with wet probability P_w for 10 runs during time t = 4,000 – 8,000 s in series D

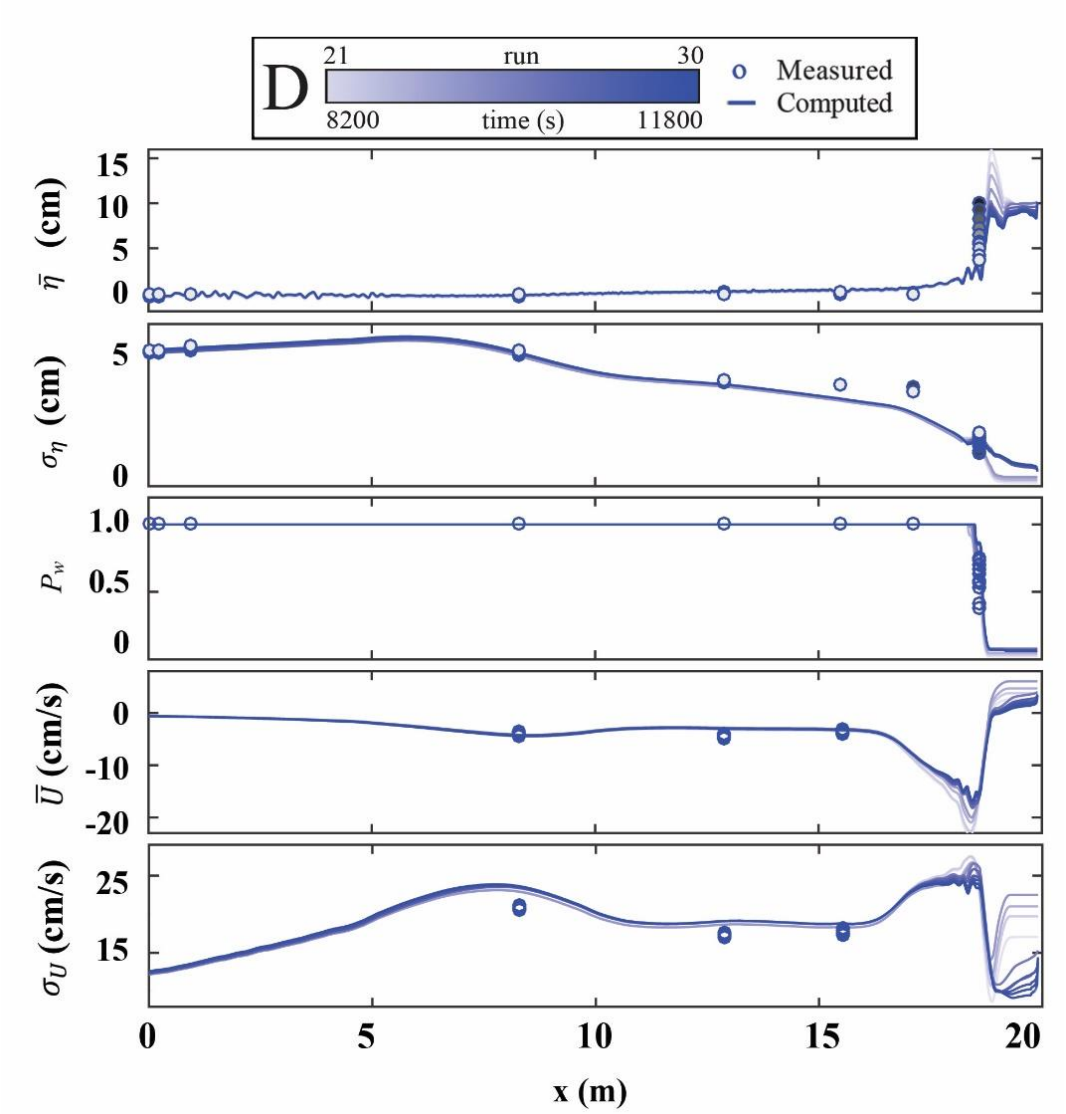

Figure 5.6: Mean and SD of free surface elevation η and horizontal velocity U together with wet probability P_w for 10 runs during time t = 8,000 – 12,000 s in series D

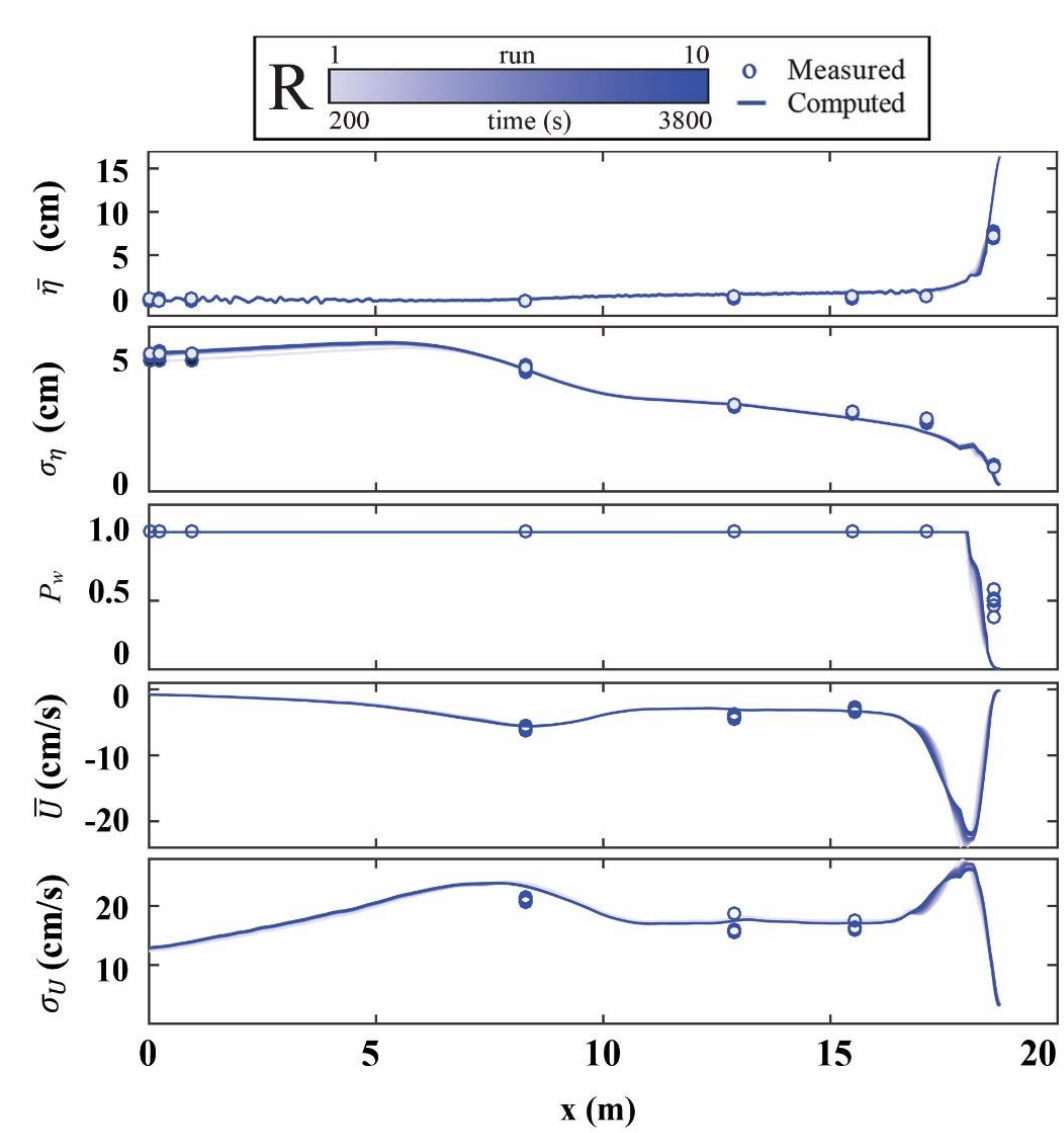

Figure 5.7: Mean and SD of free surface elevation η and horizontal velocity U together with wet probability P_w for 10 runs during time t = 0 – 4,000 s in series R

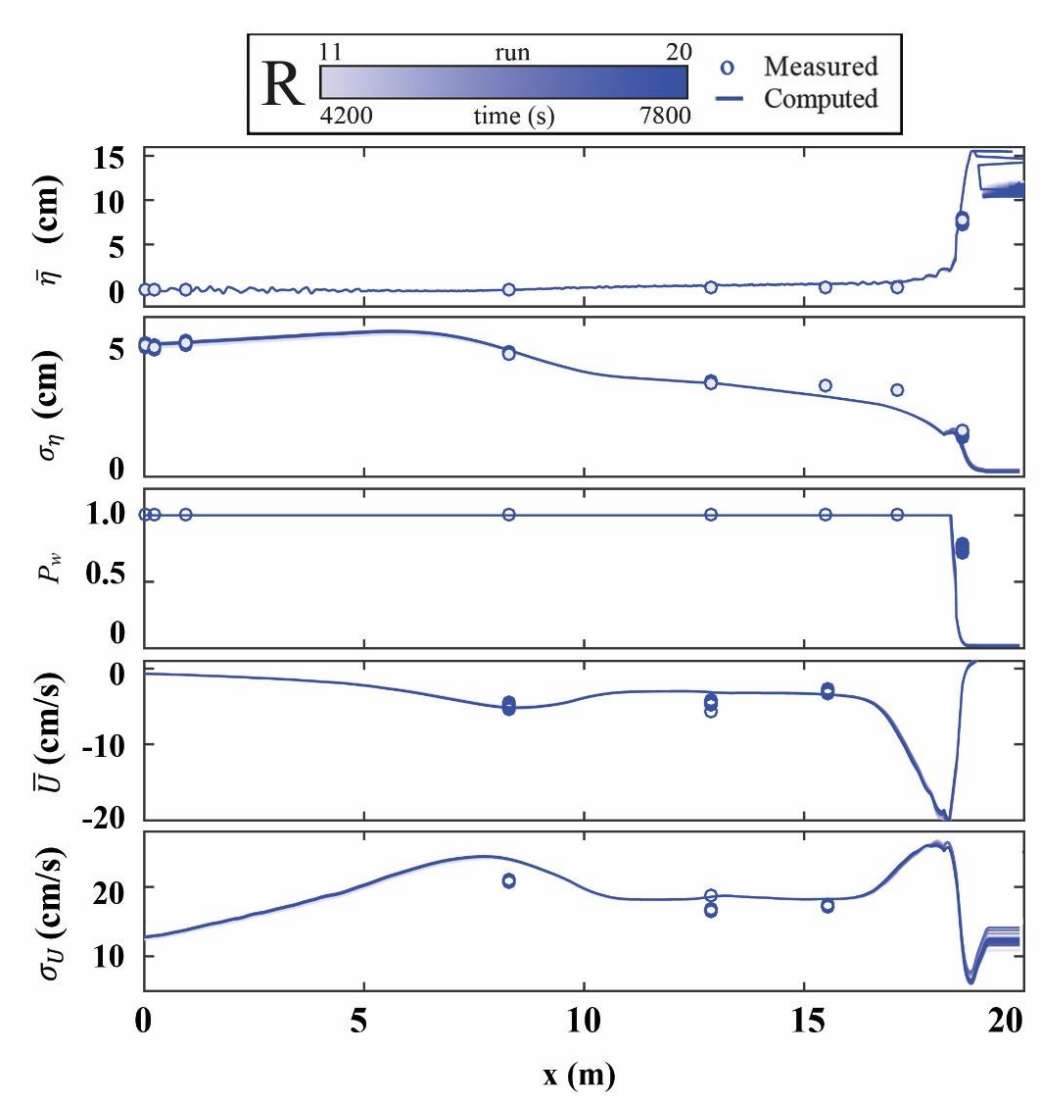

Figure 5.8: Mean and SD of free surface elevation η and horizontal velocity U together with wet probability P_w for 10 runs during time t = 4,000 – 8,000 s in series R

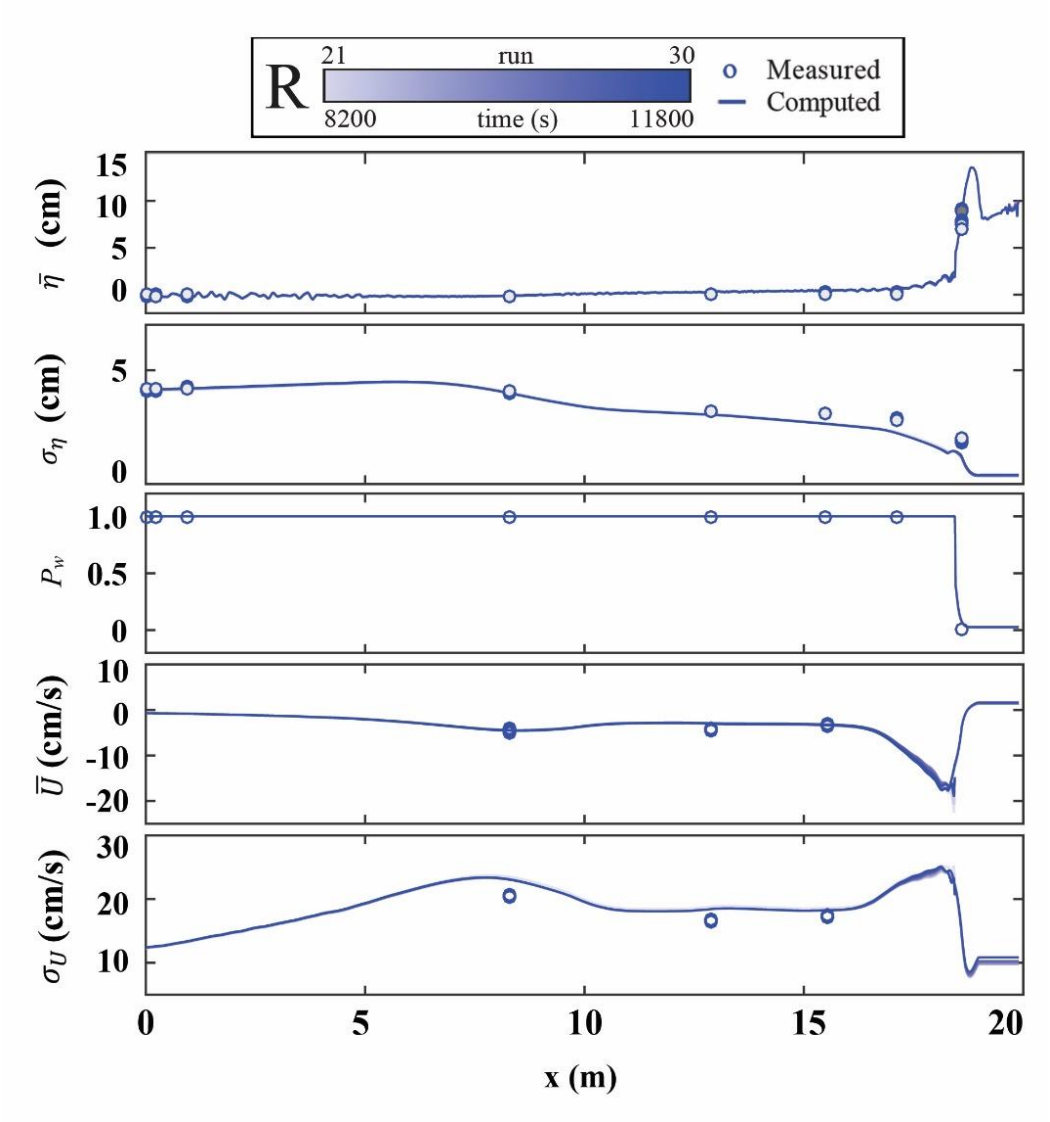

Figure 5.9: Mean and SD of free surface elevation η and horizontal velocity U together with wet probability P_w for 10 runs during time t = 8,000 – 12,000 s in series R

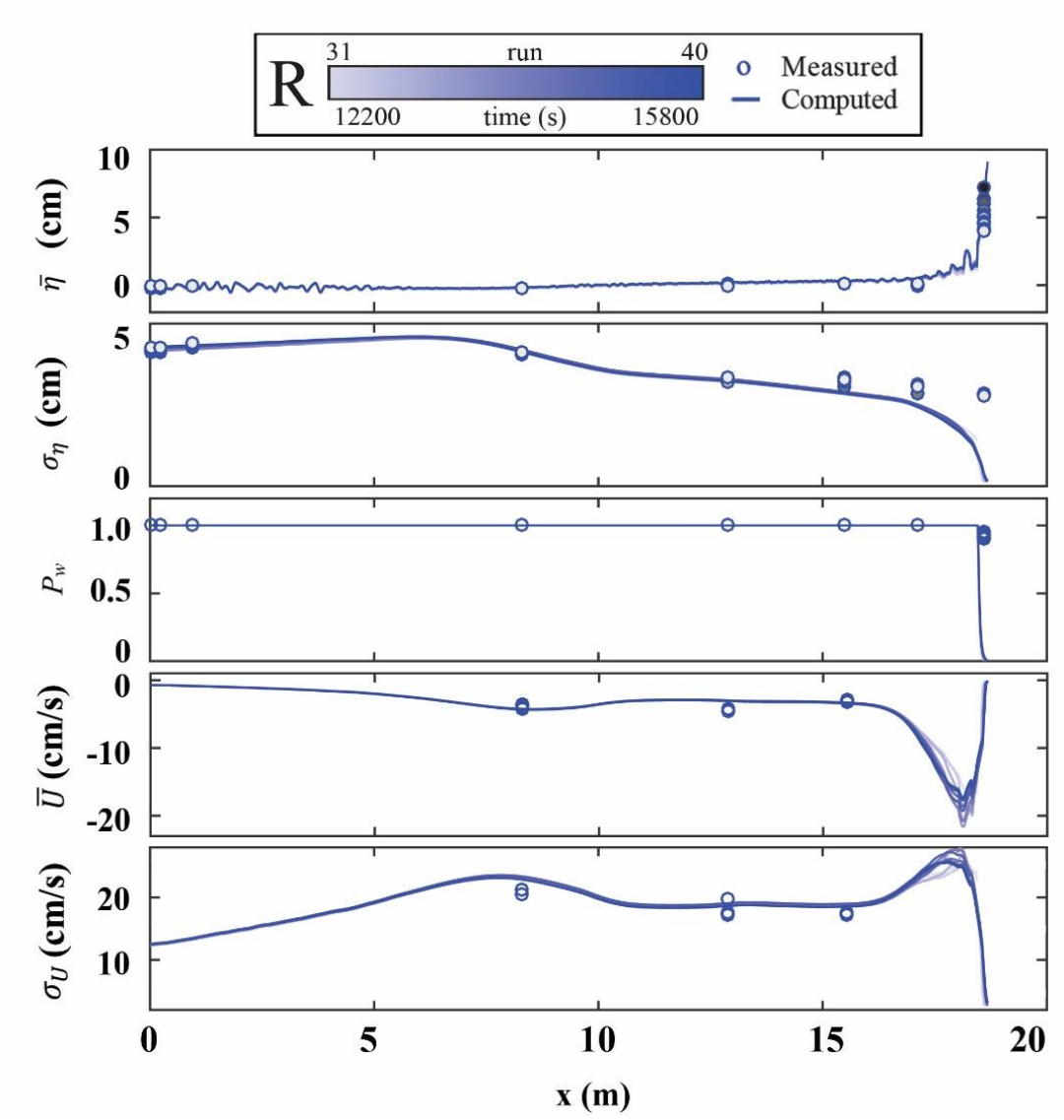

Figure 5.10: Mean and SD of free surface elevation η and horizontal velocity U together with wet probability P_w for 10 runs during time t = 12,000 – 16,000 s in series R

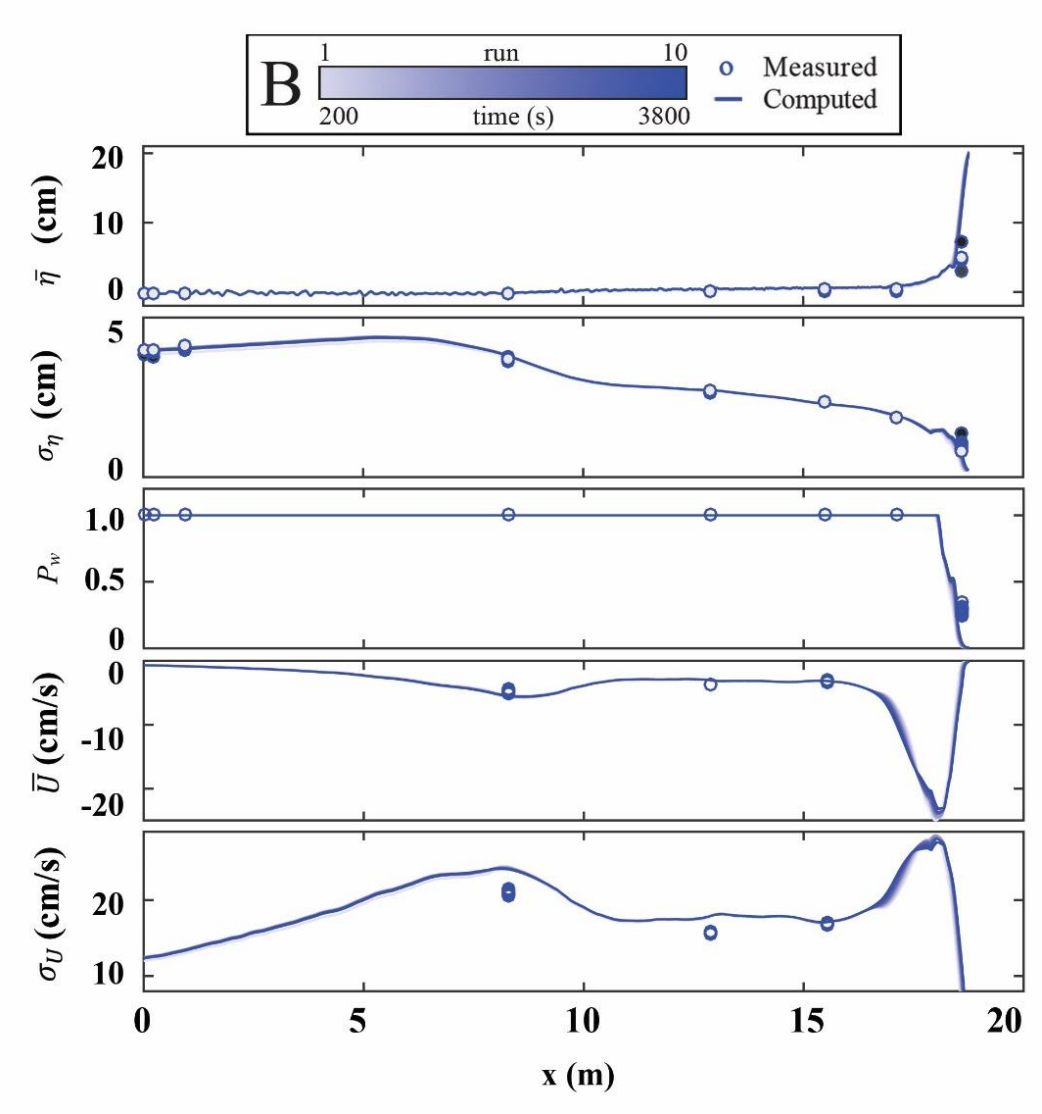

Figure 5.11: Mean and SD of free surface elevation η and horizontal velocity U together with wet probability P_w for 10 runs during time t = 0 – 4,000 s in series B

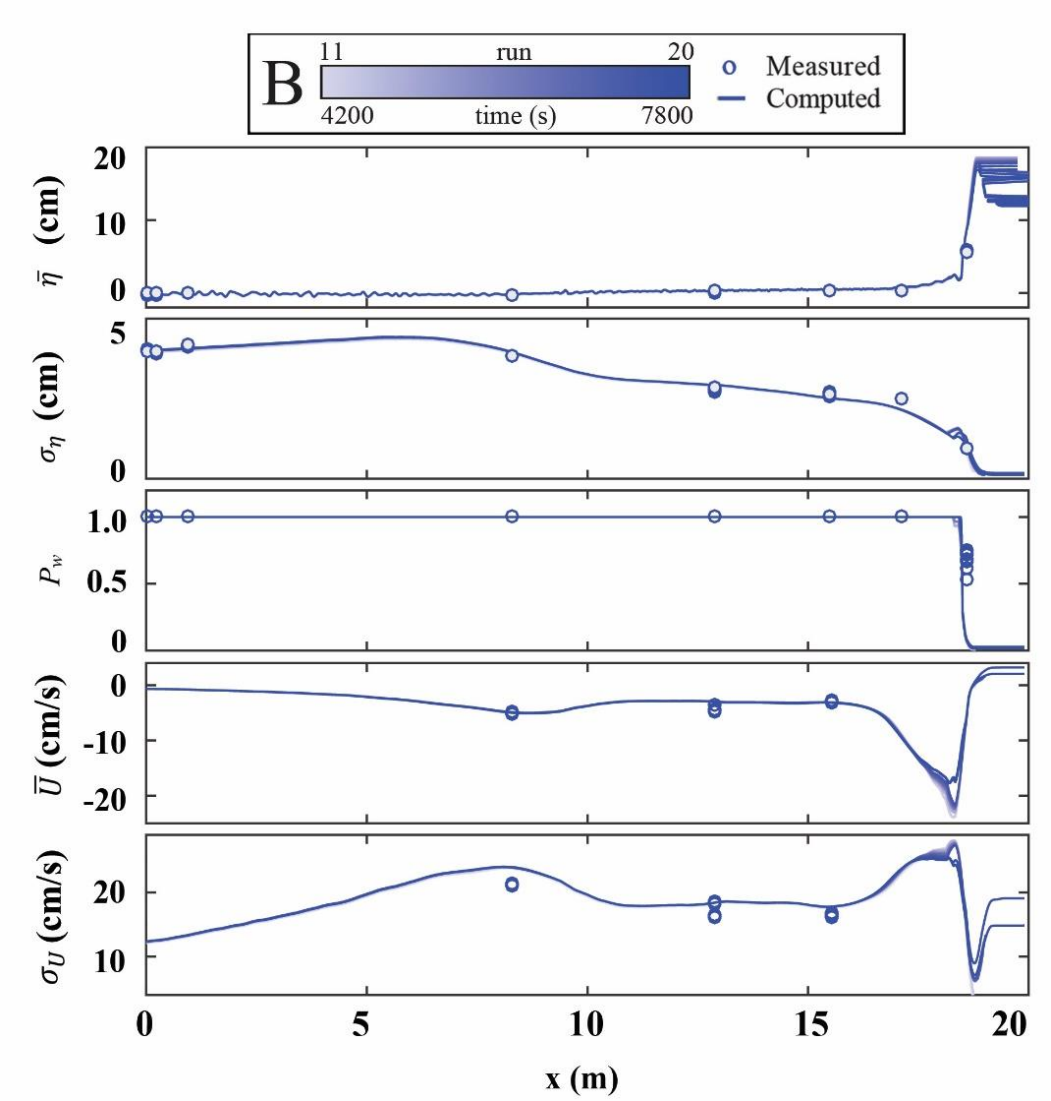

Figure 5.12: Mean and SD of free surface elevation η and horizontal velocity U together with wet probability P_w for 10 runs during time t = 4,000 – 8,000 s in series B

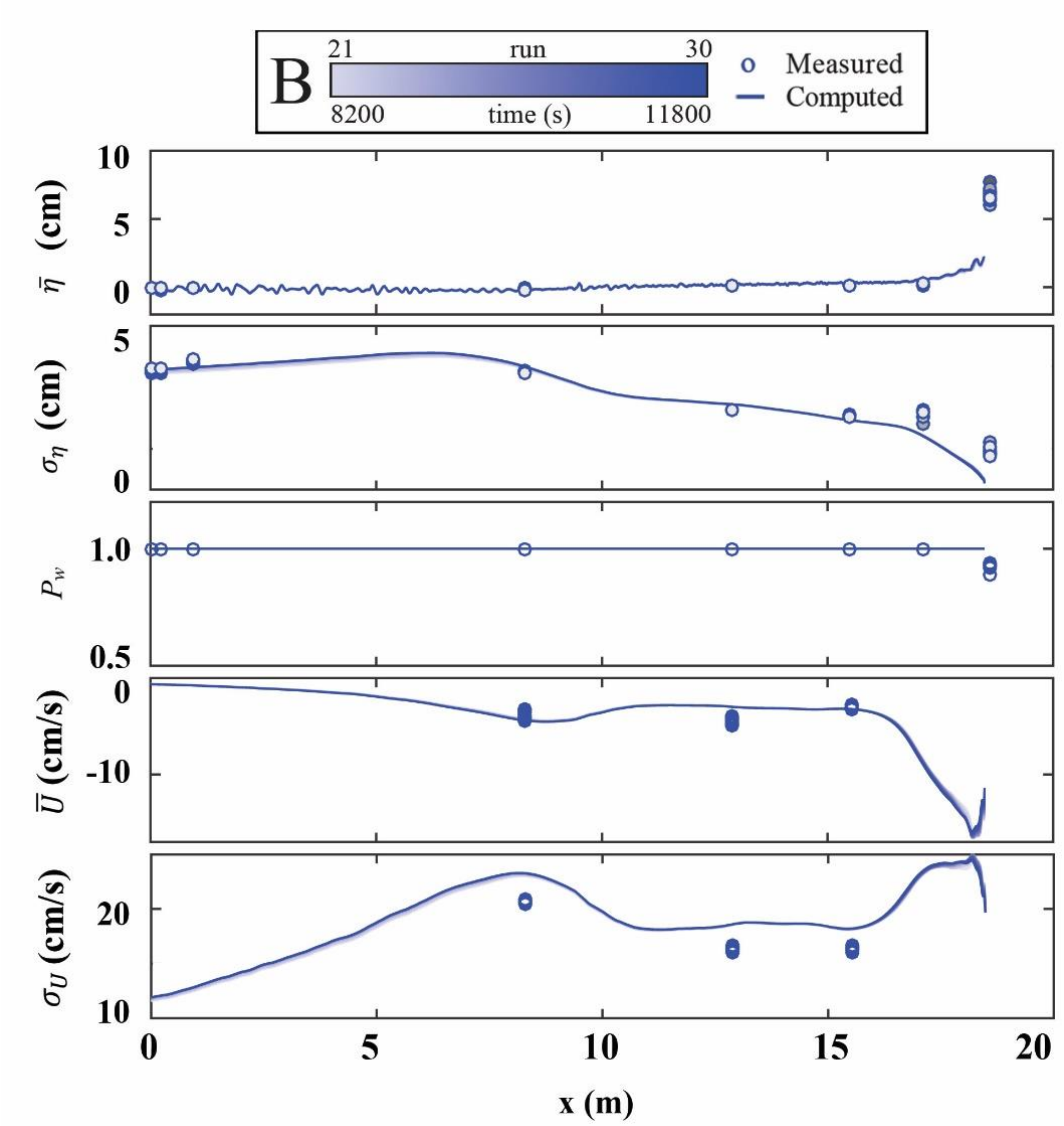

Figure 5.13: Mean and SD of free surface elevation η and horizontal velocity U together with wet probability P_w for 10 runs during time t = 8,000 – 12,000 s in series B

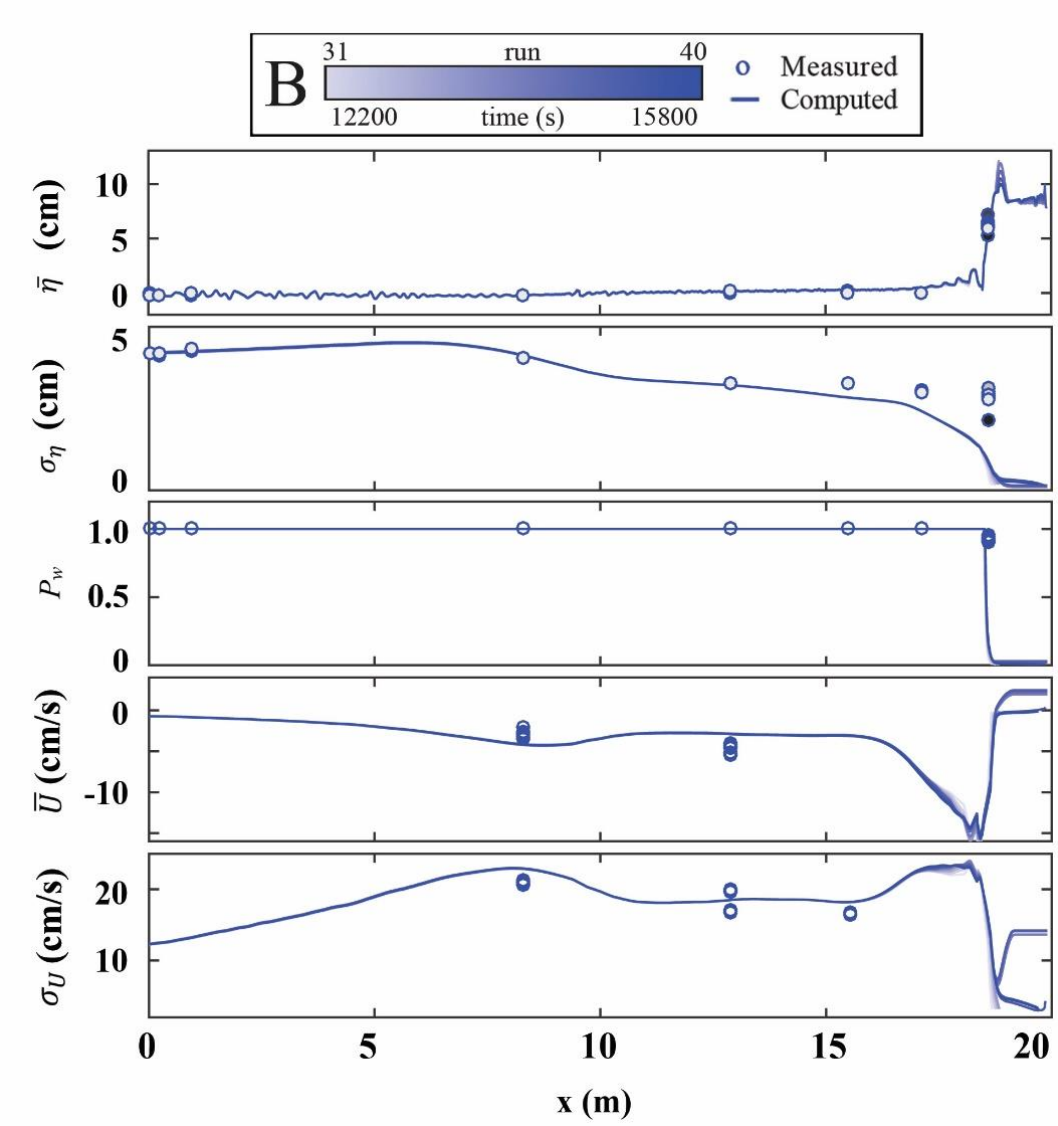

Figure 5.14: Mean and SD of free surface elevation η and horizontal velocity U together with wet probability P_w for 10 runs during time t = 12,000 – 16,000 s in series B

5.2 Wave Overtopping and Overwash Rates

The average wave overtopping rate q_o and sand overwash rate q_{bs} during each run are compared for series N and D in Figure 5.15 where the measured and computed points with $q_o = 0$ and $q_{bs} = 0$ are not shown in the logarithmic plot. CSHORE predicts no wave overtopping and overwash during t = 0 – 4,000 s in series D; however, it cannot predict the small rates of q_o and q_{bs} consistently. These small rates are associated with the mean water depth on the berm of the order of 0.1 cm. Figure 5.16 compares the measured and computed average q_o and q_{bs} for series R and B. No overtopping and overwash occurred in both series during t = 0 – 8,000 s. CSHORE predicts no overtopping and overwash during t = 0 – 4,000 s in series R and B, during t = 12,000 – 18,000 s in series R, and during t = 8,000 – 12,000 s in series B. These discrepancies arise from the disagreement between the measured and computed bottom elevations in the vicinity of the seawall. The reasonable prediction of q_o and q_{bs} requires an adequate prediction of the bottom elevation change including the seawall settlement.

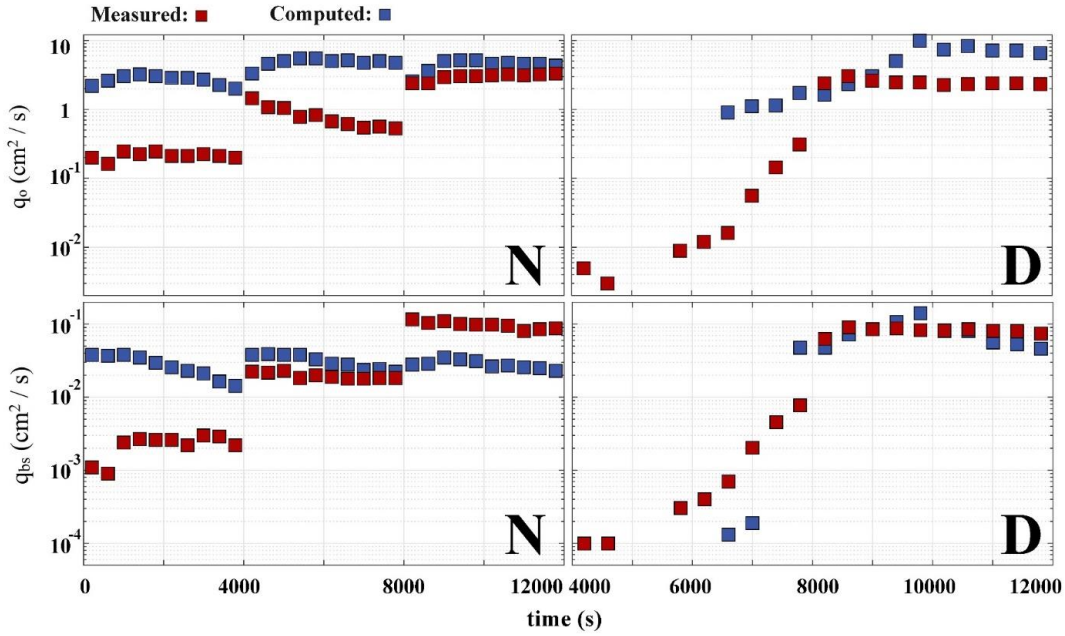

Figure 5.15: Comparison of measured and computed q_o and q_{bs} for series N and D

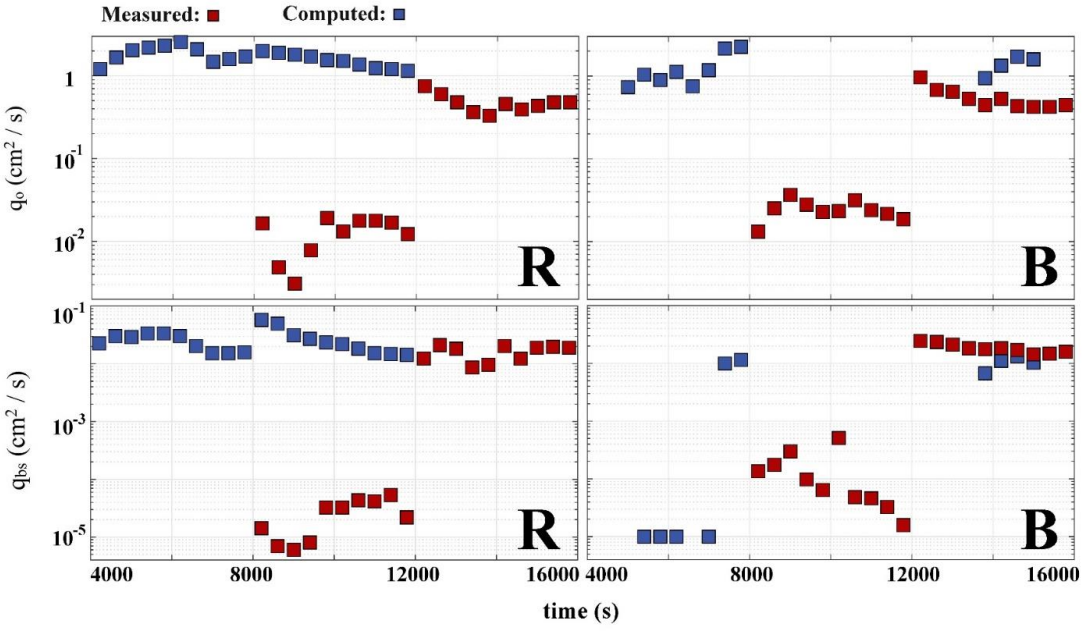

Figure 5.16: Comparison of measured and computed q_o and q_{bs} for series R and B

5.3 Beach Profile Evolution

The measured and computed profiles at t = 4,000, 8,000, and 12,000 s for series N and D are compared in Figure 5.17 where the initial profile at t = 0 is plotted to indicate the degree of the profile change at the given time. CSHORE predicts foreshore erosion but cannot predict sand deposition on the berm at t = 4,000 and 8,000 s in series N. The sequence of dune erosion, crest lowering, and dune destruction in series D is reproduced by CSHORE but the detailed features are not predicted well.

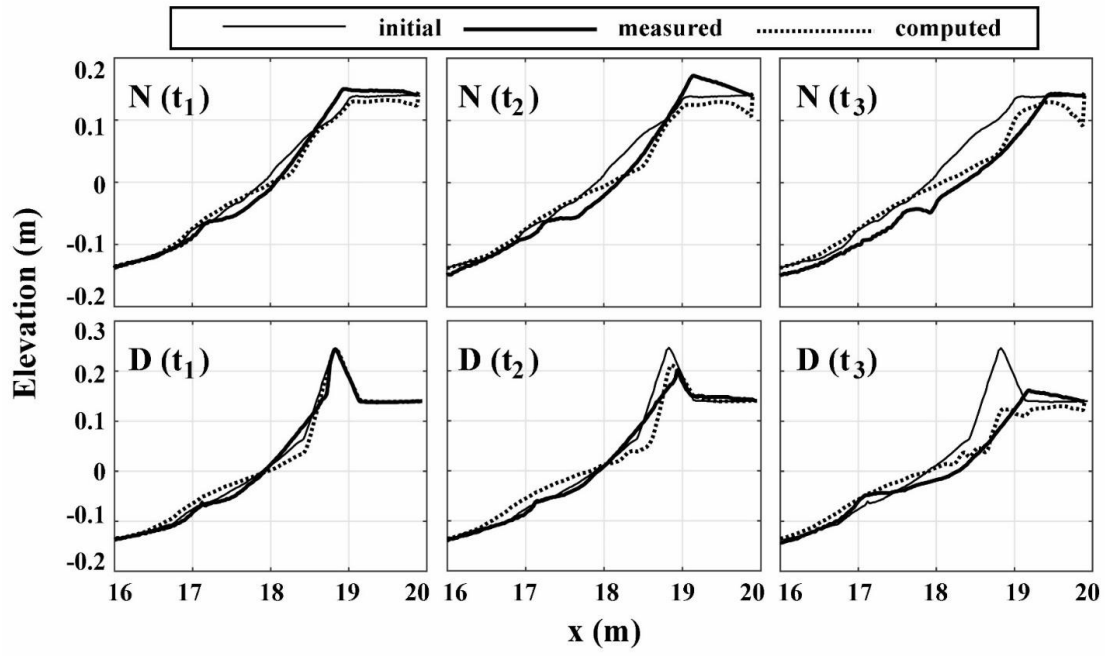

Figure 5.17: Measured and computed profiles at time t_1 = 4,000 s, t_2 = 8,000 s, and t_3 = 12,000 s for series N and D

Comparison of the measured and computed profiles for series R is shown in Figure 5.18. CSHORE predicts too much erosion in the vicinity of the seawall toe and no sand deposition on the berm. The simple reduction factor assumed in Eq. (4.1) is inadequate in predicting the cross-shore sand transport in the vicinity of the seawall with no sand cover. The horizontal shift between the measured and computed profiles at t = 16,000 s is related to the assumption of the fixed seawall with no settlement. Foreshore erosion in front of the seawall might have caused sand undermining below the filter (Figure 3.29), resulting in the rapid increase of damage from t = 12,000 to t = 16,000 s (Figure 3.28). The computed sand height V_d given by Eqs. (4.2) and (4.3) is less than 0.07 mm throughout series R, whereas the measured average sand height was 0.6 mm at the end of series R. Sand inside the porous structure was more mobile than expected.

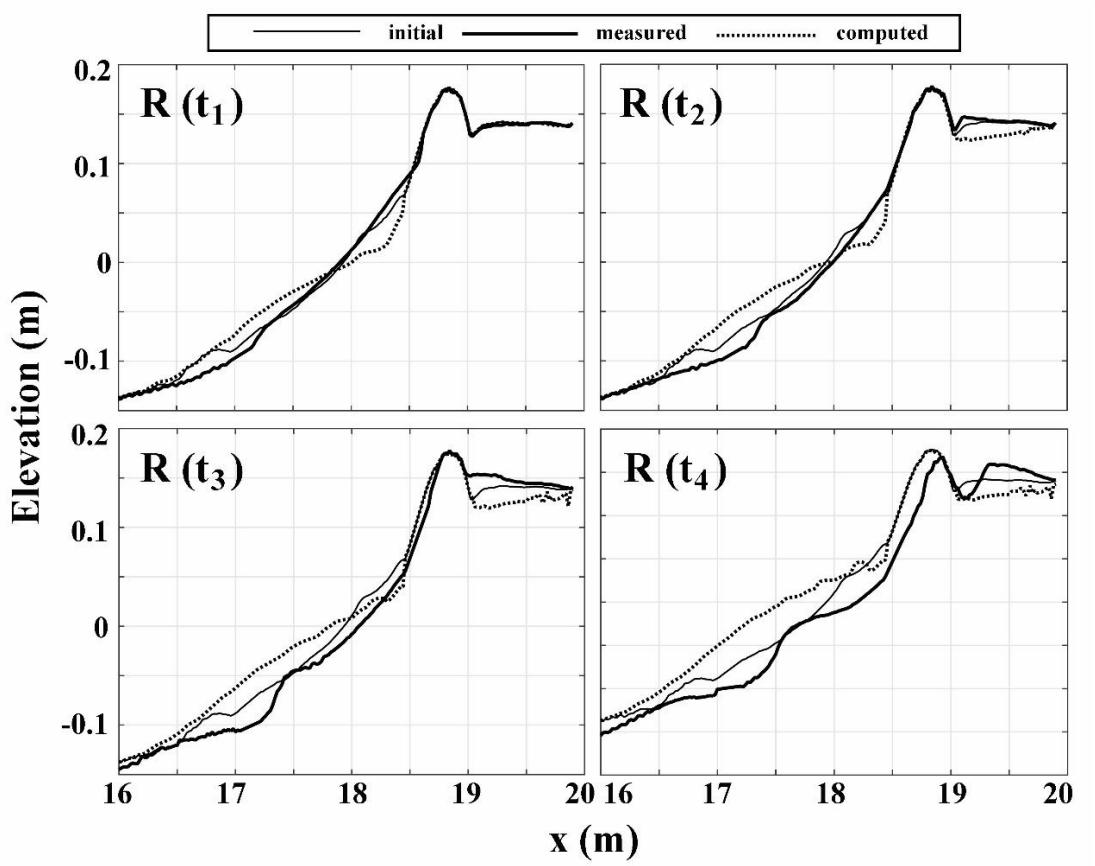

Figure 5.18: Measured and computed profiles at time t_1 = 4,000 s, t_2 = 8,000 s, t_3 = 12,000 s, and t_4 = 16,000 s for series R

Figure 5.19 shows the measured and computed profiles for series B. The overall agreement for the seawall with sand cover is better partly because the seawall settlement was reduced by sand supply from the sand-filled seawall. Nevertheless, the profile change seaward of the seawall is not predicted well by CSHORE. The computed sand height V_d at t = 0, 4,000, 8,000, 12,000, and 16,000 s is plotted in Figure 5.20. The computed erosion of sand on and inside the seawall progresses from the seaward side and downward. The computed erosion does not progress to the landward end of the seawall. The remaining sand height averaged over the entire stone

zone width is about 1 cm in comparison to the measured average sand height of 1 mm at the end of series B. The extended CSHORE for sand transport in the vicinity of the stone structure may not be accurate but sheds some light on the complex sand transport processes on and inside the porous structure.

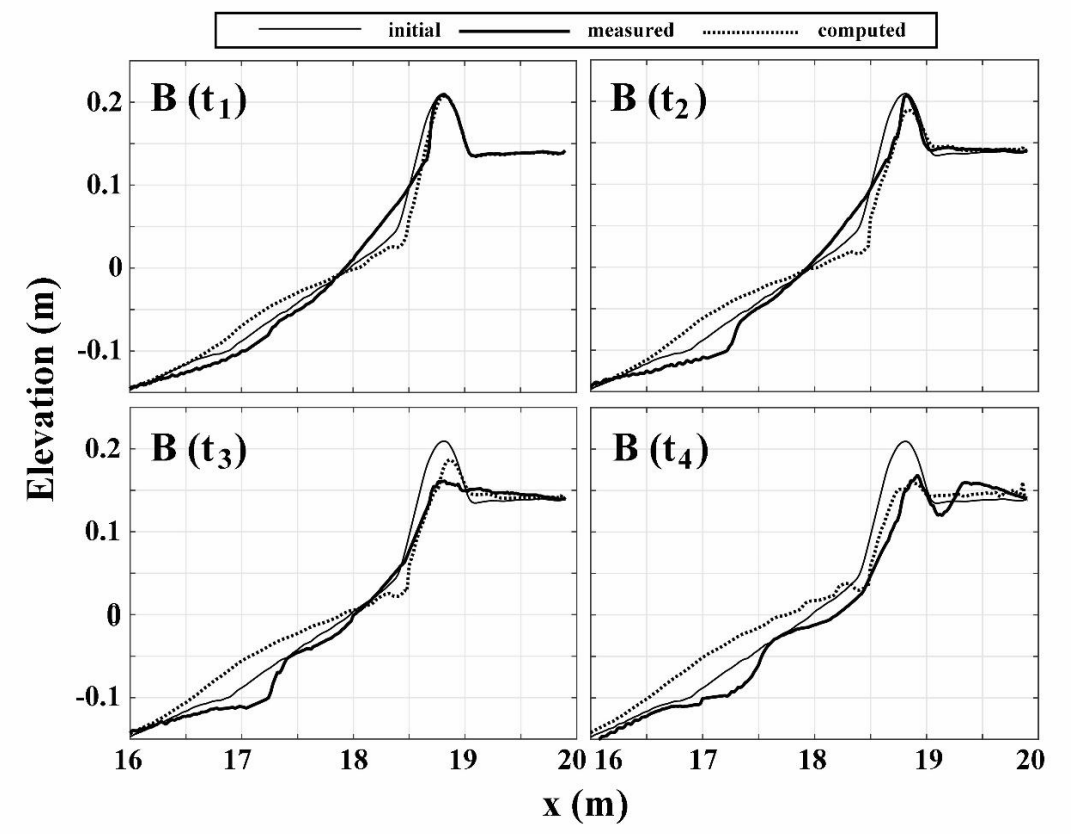

Figure 5.19: Measured and computed profiles at time t_1 = 4,000 s, t_2 = 8,000 s, t_3 = 12,000 s, and t_4 = 16,000 s for series B

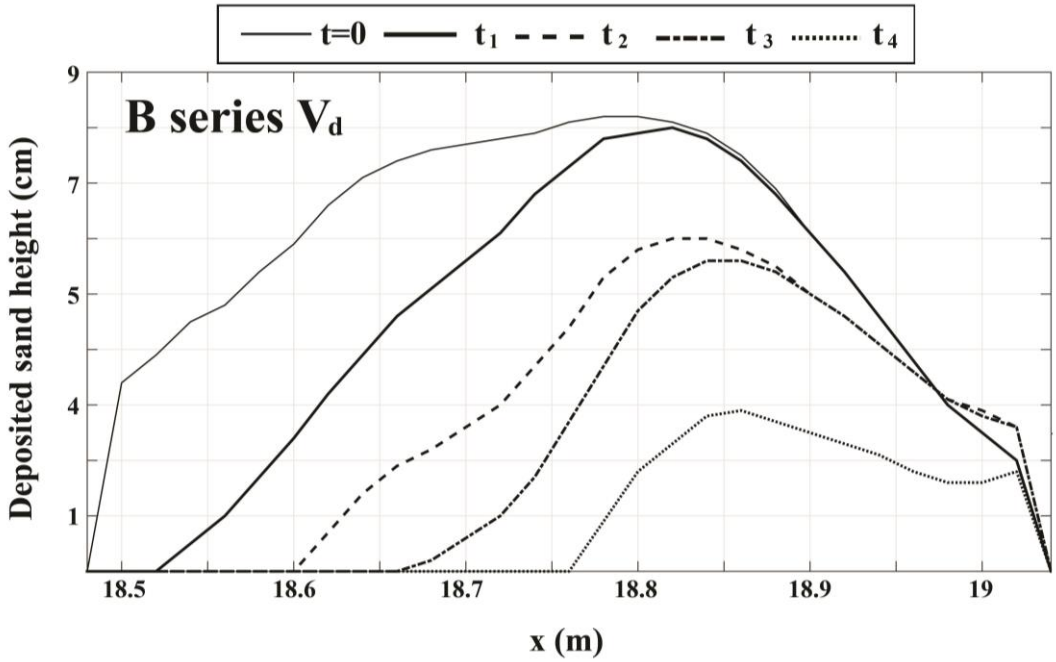

Figure 5.20: Deposited sand height V_d at time t = 0, t_1 = 4,000 s, t_2 = 8,000 s, t_3 = 12,000 s, and t_4 = 16,000 s for series B

Chapter 6

CONCLUSIONS

6.1 Experimental Findings

A laboratory experiment consisting of four test series: N, D, R and B with 140 runs in total (each run lasted 400 s) was conducted in a wave flume with a sand beach and a berm in order to compare the effectiveness of a dune (D), a stone seawall (R), and a seawall buried inside a dune (B) on a foreshore in reducing wave overtopping and sand overwash of the berm with no protection (N). The still water level was increased with an increment of 2 cm to create accretion and erosional profile changes on the foreshore and berm. The incident irregular waves were kept approximately the same for all the runs. The effectiveness of the narrow dune in comparison to the berm only was limited to the condition of no wave overtopping. The stone seawall was effective in reducing wave overtopping and overwash even after settlement (damage) of the stone in series R. The sand cover in series B acted like the narrow dune before it was removed by swash action. The exposed seawall in series B became similar to the seawall in series R. The sand cover reduced roughness and porosity of the seawall, resulting in slight increase of wave overtopping and overwash. The sand cover supplied sand and reduced the stone seawall settlement. The findings of this small-scale experiment will need to be confirmed in large- scale experiments and using field data. In order to reduce the stone settlement, different types of filter layers should be evaluated in addition to polyester fabric mesh used in the experiment.

6.2 Numerical Modeling

The cross-shore numerical model CSHORE is used to examine the findings of the experiment. The colored stones used in the experiment are computed to be stable against wave uprush and downrush in the swash zone if the experiment had been conducted on a fixed bottom. For series N and D with no seawall, CSHORE predicts the measured wave transformation, wave overtopping and overwash rates, and beach profile evolution with accuracy expected from previous comparisons. For series R and B with the seawall, CSHORE is extended to predict sand transport on and inside the porous structure on a fixed filter layer. The extended CSHORE predicts little sand deposition inside the seawall with no initial sand cover as well as extensive sand removal from the buried seawall. However, the agreement with the data in the vicinity of the seawall is marginal partly because of the assumption of no settlement of the seawall. In order to simulate the complicated interactions of sand, stone, and filter in the swash zone more realistically, it will be necessary to conduct detailed sand transport measurements in the vicinity of the seawall.

REFERENCES

Figlus, J., Kobayashi, N., Gralher, C., and Iranzo, V. (2011). "Wave overtopping and overwash of dunes." J. Waterway, Port, Coastal, Ocean Eng., 10.1061/ (ASCE) WW.1943-5460.0000060, 26-33.

Garcia, R., and Kobayashi, N. (2015). "Trunk and head damage on a low-crested breakwater." J. Waterway, Port, Coastal, Ocean Eng., 10.1061/ (ASCE) WW.1943.5460.0000276, 04014037.

Irish, J.L., Lynett, P.J., Weiss, R., Smallegan, S.M., and Cheng, W. (2013). "Buried relic seawall mitigates Hurricane Sandy's impacts." Coastal Eng., 80, 79-82.

Japan Society of Civil Engineers, Committee on Coastal Engineering (1994). "Japanese Coasts and Ports" Japan Society of Civil Engineers, Tokyo, Japan.

Kim, H.D., Kobayashi, N., and Chávez Cárdenas, X. (2016). "Comparison of rock seawall and dune for storm damage reduction." Coastal Eng. Proc., 35 (2016), 1-13.

Kobayashi, N. (2016). "Coastal sediment transport modeling for engineering applications." J. Waterway, Port, Coastal, Ocean Eng., 10.1061/ (ASCE) WW.1943-5460.0000347, 03116001.

Kobayashi, N., Farhadzadeh, A., and Melby, J. (2010). "Wave overtopping and damage progression of stone armor layer." J. Waterway, Port, Coastal, Ocean Eng., 10.1061/(ASCE)WW.1943-5460.0000047, 257-265.

Melby, J.A., and Kobayashi, N. (2011). "Stone armor damage initiation and progression based on the maximum wave momentum flux." J. Coastal Res., 27 (1), 110-119.

Walling, K., Herrington, T.O., and Miller, J.K. (2016). "Hurricane Sandy damage comparison: Ocean front houses protected by a beach and dune system with vs. without a rock seawall." Shore & Beach, 84 (3), 35-41.

Walling, K., Miller, J.K., Herrington, T.O., and Eble, A. (2014). "Comparison of Hurricane Sandy impacts in three New Jersey coastal communities." Coastal Eng. Proc. 34 (2014). 1-14.

Wolters, G., and van Gent, M.R.A. (2012). "Granular open filters on a horizontal bed under wave and current loading." Coastal Eng. Proc. 33(2012), 1-10.

Wolters, G., and van Gent, M.R.A., Olthof, J., and Smith, G.M (2014). “Sloped granular open filters under wave loading.” Coastal Eng. Proc. 34 (2014), 1-14.

Sea Grant
Delaware